ISSN 1000-9620

Marine Science Bulletin

Volume 4 · Number 1 2002

ISSN 1000-9620

9 771000 962001 01>

NATIONAL MARINE DATA AND
INFORMATION SERVICE OF CHINA

LIBRARY
Pacific Islands Fisheries Science Center
NOAA Fisheries
Honolulu, Hawai'i

CIENCE BULLETIN

May, 2002

LIBRARY
WITHDRAWN
AUG 2 2002
National Oceanic &
Atmospheric Administration
U.S. Dept. of Commerce

CONTENTS

Variability of the Continental Water Boundary near the Prydz Bay ···*Pu Shuzhen*（浦书箴）*et al.*（1）

Underway Measurement of Sea Surface Temperature and Salinity in the Taiwan Straits in August, 1999 ····· *Cheng Hua*（陈　华）*et al.*（11）

Vertical Sound Velocity Transition in the Coral Reef Core and its Significance of Indicating Facies ····· *Li Ganxian*（李赶先）*et al.*（19）

Underwater Acoustic Image Transmission System Based on DSP ·····*Ceng En*（程　恩）*et al.*（27）

Nitrogen and Phosphorus Diffusive Fluxes Across the Sediment-Water Interface in Estuarine and Coastal Tidal Flat ·····*Liu Min*（刘　敏）*et al.*（34）

Seasonal Cycle Analysis of the Nitrate Nitrogen and Nitrite Nitrogen in the Bohai Sea ·····*Shi Qiang*（石　强）*et al.*（42）

Study of Adsorption Isotherm Curves of Amino Acids on the Kaolinite ····· *Liu Xiaolan*（刘效兰）*et al.*（52）

Sediment Load of Asian Rivers Fllowing into the Oceans and Their Regional Variation····· Liu Shuguang（刘曙光）*et al.*（61）

Study and Application of Toxicity Test Method Using *Neomysis awatschensis* in Toxicity Evaluation of Drilling fluid····· *Yan Tian*（颜　天）*et al.*（71）

Effect of Salinity on the Growth, and Agar Yield and Composition of *Gracilaria tenuistipitata* var *liui* Zhang *et* Xia ····· *He Lihong*（贺丽虹）*et al.*（76）

Studies on the Technology for Mass Production of Abalone Breeding ····· *Chen Quanzhen*（陈全震）*et al.*（82）

Effect of Nitrogen Sources on the Growth and Docosahexaenoic Acid Accumulation in *Crypthecodinium cohnii* ·····*Wang Jufang*（王菊芳）*et al.*（87）

Effects of Lanthanum-Amino Acid Complexes on Egg Hatching and Nauplius Metamorphosis of *Penaeus chinensis* ·····*Xin Fuyan*（辛福言）*et al.*（93）

Variability of the Continental Water Boundary near the Prydz Bay*

LIBR

Pu Shuzhen (蒲书箴)[1], Dong Zhaoqian (董兆乾)[2], Hu Xiaomin (胡筱敏)[1],
Yu Fei (于 非)[1], Zhao Xin (赵 新)[1]
1 *First Institute of Oceanography, SOA, Qingdao* 266061
2 *Polar Research Institute of China, Shanghai* 200129

AUG 2 2002
National Oceanographic
U.S. Department of

Abstract Based on the data obtained during the 15th Antarctic Expedition of China between November 1998 and February 1999, the paper discusses the water masses distributed on both sides of the Continental Water Boundary (CWB) as well as the spacial variability of the physical characteristics of the central location, the frontal width, the frontal strength, the vertical depth, and the vertical thickness for CWB. The above results are compared with the results from the data obtained during the 9th Antarctic Expedition of China between December 1992 and February 1993, and the temporal variability of those characteristics is discussed. In addition, the inhomogeneity of the kinematic characteristics and the patterns of the dynamic heights for those water masses located on both sides of CWB are illustrated. As it is pointed out in the paper, the trough in the dynamic height field is identified with the frontal location of CWB and the oceanic current shear. Furthermore, the dynamic reason for the upwelling of the circumpolar deep water can be understood by the explanation described in the paper.

Keywords Pryze Bay, oceanic front, Continental Water Boundary, variability

Introduction

Oceanic front is one of the most remarkable phenomena in physical oceanography of the Southern Ocean. The continental water boundary (CWB) is a circumpolar front which is the closest to and the most effected by the Antarctic continent among all the fronts[1)][1]. Because of the irregularity of the coastline trend of the Antarctic and the irregular distribution in the coastal area of the glaciers which come from the Antarctic land covered with ice and slowly displace toward the Southern Ocean, their effects on the salinity of the continental water depend upon the irregularity. Therefore the continental water and its boundary to the north are not distributed in a regular zone parallel to the latitudinal circle. CWB is situated between the continental shelf water near the Prydz Bay and the circumpolar deep water in the Southern Ocean. It is usually located in the subsurface layer around 65°S and away from the shelf break. It can reach the 1500 m isobath at its deepest, becoming deeper from the north to the south in a longitudinal section and closer to the continental slope.

When it is the southern summer the surface water becomes warmer because of the solar radiation in the polar day light for as long as half a year, and it becomes freshened because of the freshening effect by the melting sea ice. The summer suface water is formed with higher temperature, lower salinity, less density, and stable structure in the Prydz Bay. In addition, stronger thermocline appears between this

Received on February 4, 2000
* Supported by National Science Foundation of China. The contract number is 49836010.
1) Continental water boundary (CWB) is also called Antarctic Slope Front in some literature.

surface water and the shelf water in the lower layer (See Fig.1). Therefore, CWB can not be found in the surface layer above the thermocline. However it is easy to determine its geographic location and frontal strength by means of the horizontal gradient of the water temperature in the subsurface layer.

Generally speaking, frontogenesis and frontolysis of an oceanic front is closely related to the fact that the water masses which exist on both sides of the front extend to or shrink back from the front, and the features of the water movement such as convergence, shear flows near the front etc. Therefore the variability of the frontal location and strength depend upon the movement of the water masses which are distributed near the front. In the Prydz Bay and its adjacent sea area, the water movement near CWB has some special features, which depends upon the longitudinal location of the front. It is the longitudinal dependence of the water movement features that causes the variability of spacial distribution and frontal strength of CWB, which is interjacent between the two water masses. This paper is intended for learning and understanding the CWB variability because it is not only an important subject in physical oceanography of the polar ocean, but it also provides the scientific background for explaining and understanding the features of the spacial distribution of the marine species, the relevant carbon chemical constituents, and the dynamic mechanism for the distribution of the water masses on both sides of the front.

Based on the full depth CTD data obtained during the 15th Antarctic Expedition of China between November 1998 and February 1999 and the data during the 9th Antarctic Expedition of China between November 1992 and February 1993, the features of the frontal strength, and the spacial and temporal variability of CWB at the Prydz Bay and its adjacent sea area are described in the paper by means of the scientific methods of classic oceanography. The dynamic mechanism for the variability is discussed as well.

1 The Location and Strength of CWB

In order to describe the geographic location and the frontal strength of CWB at the Prydz Bay and the adjacent sea area, first of all, it is necessary to learn the physical features of the water masses on both sides of CWB and their spreading extents. The shelf water near the Prydz Bay is located in the subsurface layer (from the 100 m depth to the bottom on the shelf) south of CWB, approximately to the south of 65°S. It is a water mass with temperature lower than −1.8℃, salinity between 34.40 and 34.50, and density (σ_t) more than 27.7 kg/m^3[2]. It is formed in the southern autumn and winter, when the atmosphere cools the sea surface and strong wind disturbs the sea water in the polar night for as long as half a year so that the cooled water moves downward to form the water mass with lower temperature and greater density in the subsurface layer. After the sea surface has become frozen and the salt has been separated out from sea ice, the salinity and density of the water beneath sea ice is increased, and the downward movement is continued and strengthened. The so formed shelf water near the Prydz Bay keeps stable and its characteristics do not change much even though solar radiation in the polar day light of the Antarctic ocean continues for half a year in the southern summer. Why does it remain unchanged in the subsurface layer? The reason for the remaining shelf water is that the marginal area on the Prydz Bay shelf is shallower than the inner area of the Bay, raising in the bottom topography (See Fig.1). Therefore the water can remain stable on the shelf. In addition, as it is described in the above, solar radiation in the polar day light of the southern summer for as long as half a year warms up the surface

layer to form very strong thermocline and stable temperature structure with the warm water sitting above the cold water. It is the stable structure that plays a role like a "barrier" for retaining the water, which has been formed with low temperature, high salinity and dense density in autumn and winter. This is another reason why the Prydz Bay shelf water keeps stable and unchanged.

The circumpolar deep water is located north of CWB, i.e. in the depth deeper than 200m approximately north of 64°S. Its temperature is about 1.8 ℃, the salinity is equal to or greater than 34.6 and the density is about 27.7 kg / m^3. In the studied area between 70° E and 75° E, it is distributed between 250m and 700m[2].

It is between the two water masses mentioned above that CWB lies in the southern ocean north of the Prydz Bay (See Fig.1 and Fig.2). For example, it can be seen from Fig.1 (b) that the longitudinal temperature gradient becomes increased in the subsurface layer from 100 m to 1500 m between 64°S and 65°S, having a maximum of about 0.023 ℃/km at the 100 m depth. If the 1.0 ℃ isotherm and the −1.0 ℃ isotherm are chosen as the measurement for the frontal width (because the horizontal temperature gradient becomes the greatest in between), the horizontal extent of CWB is from 64°8'56.8" S to 65°6' 18.9"S with its central position at 64°42'37.9"S.

The analysis and the result described above are based on the data from the full depth CTD measurements conducted during the 15th Antarctic Expedition of China between November 1998 and February 1999. As the water movement on both sides of CWB has temporal and spacial variability, the location and strength of CWB are different from one year to the other and from one longitudinal location to the other. The difference will be further discussed in the following.

2 Spacial Variability of CWB

The spacial variability of CWB will be first analysed here in order to discuss the variability of the front location, longitudinal width, frontal strength, and the vertical thickness, in the 70°E section, the 73°E section, and the 75° E section in the 1998/1999 southern summer. Fig.2 is the plots enlarged from the part above the 300 m depth of Fig.1. More details can be found from Fig.2. It is learnt from both Fig. 1 and Fig.2 that the frontal strength reaches its strongest in the 73° E section and CWB vertically spreads from the 100 m depth to the 1 500 m depth. The thickness is about 1 400 m. It is the thickest among those three sections. Second comes the frontal strength and vertical thickness of the 75° E section. The frontal strength becomes the weakest and the vertical thickness the least in the 70° E section (See Fig, 1 and Fig.2). More details of the statistical results from the 15th Antarctic Expedition of China are listed in Table 1.

It is learnt from Table 1 that the longitudinal width of CWB has a value between 0.79 × 60 n.m. and 2.25 × 60 n.m. with the central position between 64°42'37.9"S and 65°31'34.3"S. The average strength has a value between 0.004 ℃/km and 0.0195 ℃/km, with the vertical extent between 650 m and 1 400 m. Obviously in the 73°E section CWB reaches its narrowest in the frontal width, its strongest in the frontal strength, and its thickest in its vertical extent.

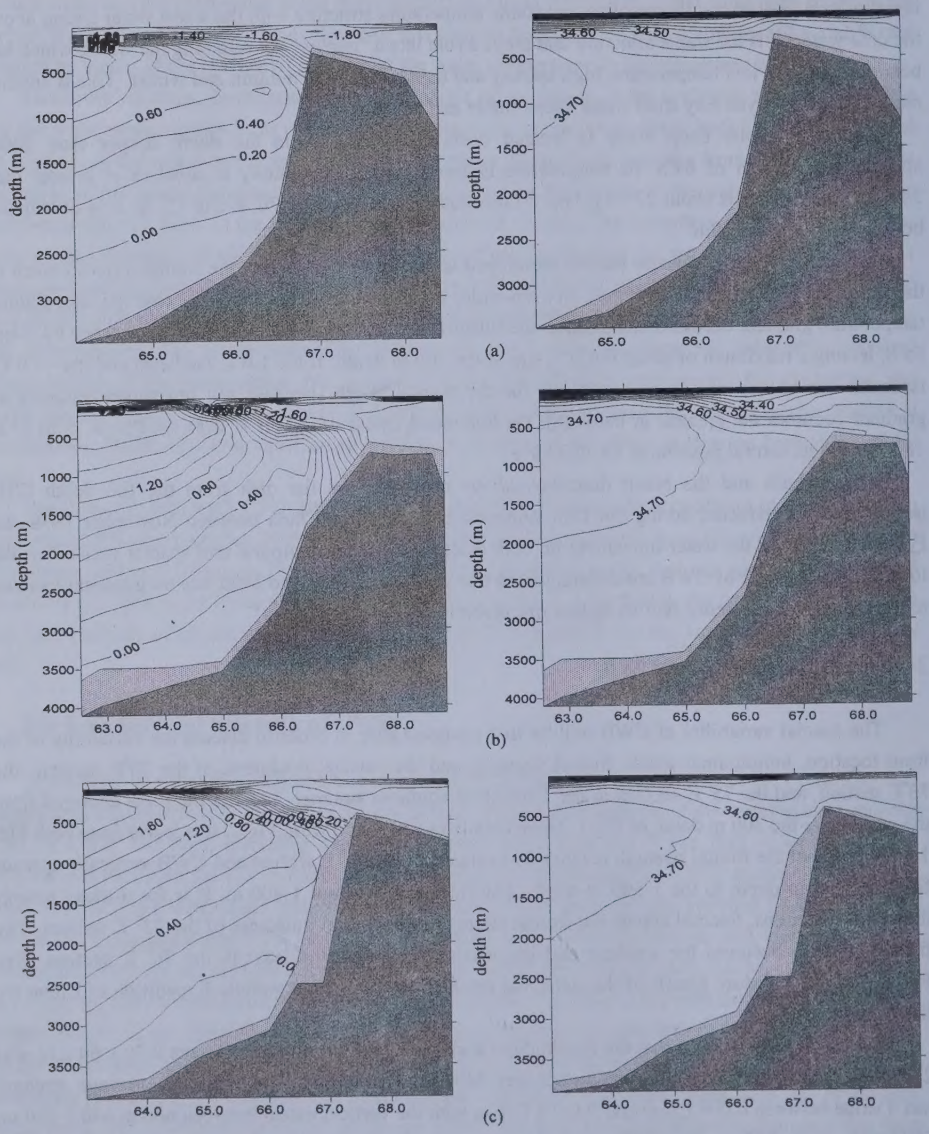

Fig. 1 Temperature section (left) and salinity section (right) plotted from the full depth CTD data obtained during the 15 th Antarctic Expedition of China

(a) 70° E section, (b) 78° E section, (c) 75° E section. The ordinate is for depth and the abscissa is for latitude. The part in the dark grey is the sea bottom and the area in light grey above the bottom is the maximum depth for CTD profiling.

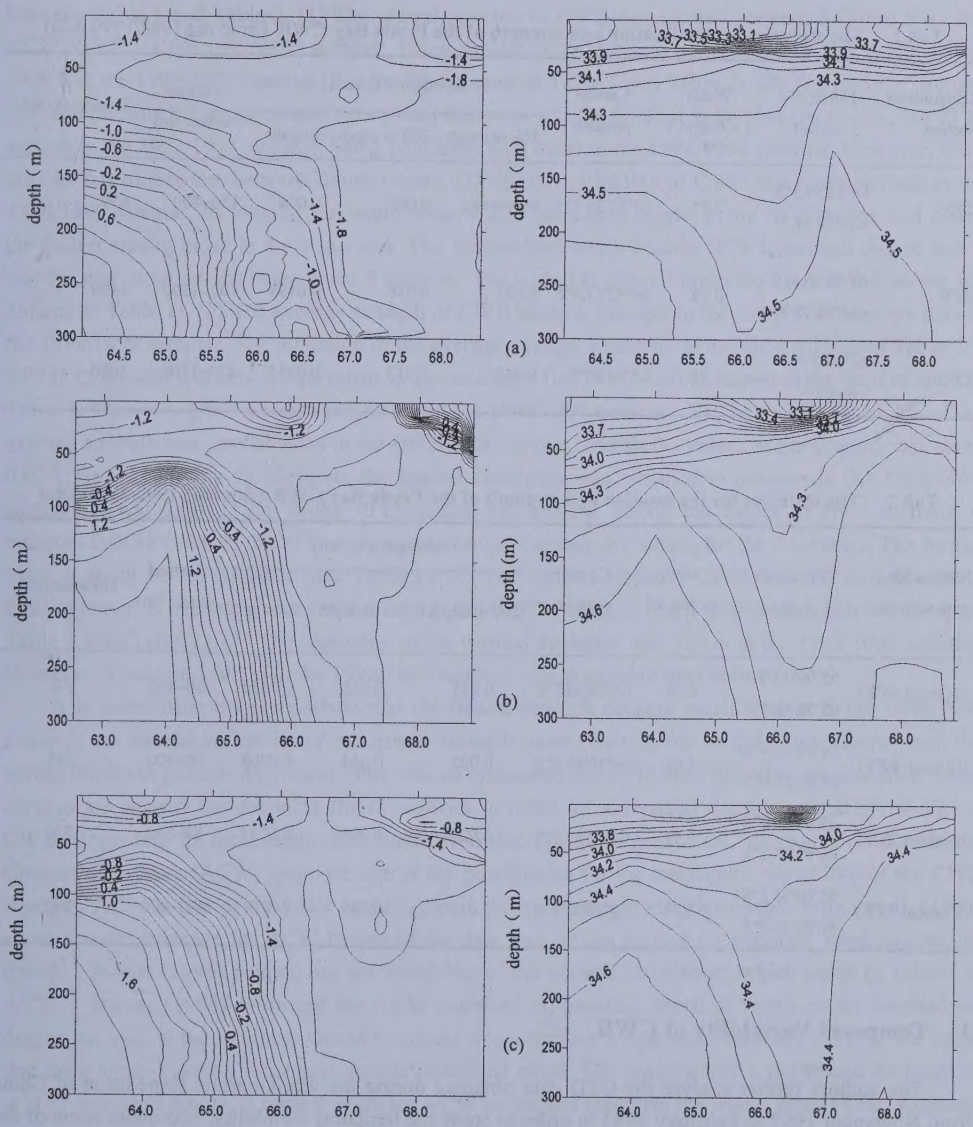

Fig. 2 Temperature section (left) and salinity section above the 300 m depth.
(a) 70° E section, (b) 73° E section, (c) 75° E section.

Tab 1. The statistics for the location and strength of the Prydz Bay CWB (from the 1998/1999 data)

Longtudinal section	Horizontal extent	Width (×60n.m.)	Central position	Strength (℃/km)			Vertical extent (m)	Thickness (m)
				100 m depth	200 m depth	average		
70°E	64°23'34.3"S ~66°38'34.3"	2.25	65°31'34.3"S	very weak	0.008	0.004	150~800	650
73°E	64°18'56.8"S ~65°06'18.9"	0.79	64°42'37.9"S	0.023	0.016	0.0195	100~1500	1400
75°E	64°03'0"S ~66°0'0"	1.95	65°01'30"S	0.012	0.017	0.0145	120~1200	1080

Tab 2. The statistics for the location and strength of the Prydz Bay CWB (from the 1992/1993 data)

Section No. with latitude	Horizontal extent	Width (×60n.m.)	Central position	Strength (℃/km)			Vertical extent (m)	Thickness(m)
				100 m depth	200 m depth	average		
II (about 63°E)	65°00'00"S~ 65°58'41.4"S	0.98	65°29'20.7"S	0.015	0.022	0.0185	60~400	340
III(about 68°E)	64°00'11.4"S~ 65°01'21.6"S	1.02	64°30'46.5"S	0.027	0.014	0.0205	30~300	240
IV(about 73°E)	65°02'28.2"S~ 66°02'25.2"S	0.99	65°32'26.7"S	0.022	0.025	0.0235	80~600	520
V (about 78°E)	65°00'04.2"S~ 66°01'39.6"S	1.03	65°30'51.9"S	0.019	0.019	0.019	100~400	300

3 Temporal Variability of CWB

The authors further analyze the CTD data obtained during the 9th Antarctic Expedition of China from November 1992 to February 1993 in order to study the temporal variability, and quote some of the results from Yu *et al.* (1996)[3] but leave out Section No. I (about 58°E) and Section No. VI(about 83°E) because there are only 3 stations in each of the sections without much data and the both sections can not be compared with the sections listed in Table 1. In order to take the same form as Table 1, the authors do some additional computing by use of the data obtained during the 9th Antarctic Expedition of China (1992/1993). The computed results are shown in Table 2.

It is learnt from Table 2 that the longitudinal width of CWB is 0.98~1.03 × 60n.m., its central position is 64° 30' 46.55" S ~ 65° 32' 26.7" S, its average strength is 0.0185~0.023 ℃/km, and its vertical

thickness is 240~520m in the 1992/1993 southern summer. It is obvious that there is some similarity between Table 1 and Table 2. (1) The central position of CWB was located between 64°30'46.5"S and 65°32'26.7"S in the 1992/1993 summer, being similar to the position between 64°42'37.9"S and 65°31'34.3"S in the 1998/1999 summer (See the 4th columns in Table 1 and Table 2). (2) The average strength of CWB became the strongest and the vertical thickness was the thickest in Section No.Ⅳ, i.e., the 73°E section in the 1992/1993 summer, being consistent with those in the 1998/1999 summer. However, there are obvious differences between the two cases. (1) Spacial variability of CWB was more obvious in the 1998/1999 summer. Its longitudinal width became 2.25 latitudinal degree in the 70°E section and it was the widest among those in the 3 sections. The longitudinal width became 0.79 latitudinal degree and it was the narrowest among those in the 3 sections. The widest is about 3 times the narrowest (See the 3rd column in Table 1). (2) The average strength of CWB became stronger in the 1992/1993 summer than in the 1998/1999 summer. The minimum of the average strength as shown in the third column of Table 2 is 0.0185℃/km and it is almost equivalent to the maximum (0.0195℃/km) as shown in the third column of Table 1. Therefore CWB became less strong in the 1998/1999 summer. (3) The spacial variability of the average strength was less obvious in the 1992/1993 summer, and all the values of the strength was about 0.02℃/km (See Table 2). However the spacial variability was remarkably obvious in the 1998/1999 summer. It was 0.004℃/km in the 70°E section, the weakest among the values of the 3 sections. It becames 0.0195℃/km in the 73°E section, the strongest among the values for the 3 sections. The former value is about 1/5 of the latter (See Table 1). (4) The vertical extent of CWB was 600 m in the 1992/1993 summer. It became about 1500 m in the 1998/1999 summer, much deeper than before (Compare Table 1 with Table 2). (5) The maximum of the vertical thickness was 520 m in the 1992/1993 summer. However, it became 1400 m in the 1998/1999 summer, one time more than before.

It is learnt from the comparison that the frontal strength became much weaker in the 1998/1999 summer, the spacial variability of the frontal strength more obvious, the vertial extent deeper, and the vertial thickness greater. At present, little data of systematic survey in the Prydz Bay are available. More surveys are needed for obtaining the time series in order to understand the interannual variability of CWB. Regarding its mechanism, it is considered that the development and propagation of Antarctic Circumpolar Wave (ACW) could be one of the possibilities for the interannual variability of the CWB strength. ACW is one of the polar oceanographic phenomena recently discovered. White et al. (1996) showed some evidence for ACW by use of the data such as sea surface air pressure, wind and sea ice extent[4]. Jacobs (1996) pointed out the variability of the oceanic circulation, which could be related to ACW[5]. Baines (1998) estimated the ACW eastward propagating speed at 9cm/s or 40 longitudinal degree per year in the Southern Ocean by means of sea surface temperature anomaly (SSTA). He found that there are 2~3 waves in the circumpolar latitudinal circle. The positive SSTA is 1℃ and the negative is -1℃ in a wave length. It takes 9 years for ACW to run and complete the whole zonal circle. Although some explanations have been presented for the ACW mechanism, we are far from fully understanding it. At present, two kinds of explanations have been given for ACW. (1) Low frequency variability of the sea surface temperature (SST) could be the response to the atmospheric forcing with relatively high frequency. The amplitude of the SSTA responding to the forcing is limited if it is the case[7]. (2) β effect plays an important role for ACW in the air-sea coupling processes in the Southern Ocean. Obviously those two kinds of mechanism are associated with the air-sea interaction of the Southern Ocean. As ACW is a kind of fluctuation in a long period and large scale, the oceanic variability caused by ACW

should be a long-term behavior such as the interannual—the decadal.

4 Characteristics of Water Mass Movement on Both Sides of CWB

In general, characteristics of water mass movement on one side of an oceanic front are different from those on the other side. The movement of the water masses separated by CWB near the Prydz Bay has features as follows. First of all, the Prydz Bay shelf water south of CWB obviously tends to extend northward. It can be seen from Fig.2 that the −1.6℃ isotherm becomes northward extended from 67°S to form a cold water wedge protruding between the surface layer and the thermocline. The further northward extention can be clearly seen in the 70°E section (See Fig.2 (a)), showing that the tendency of the northward extension is more remarkable in the western Prydz Bay. In addition, the circumpolar deep water (CDW) north of CWB obviously has upwelling features at 64°S (See Fig. 2(b)).

All the 1.2℃, 1.4℃, 1.6℃ isotherms become raised at 64 °S, showing the upwelling tendency of CDW. It is because the cold shelf water extends northward from the Prydz Bay and the warm CDW gets upwelling from the deeper layer that the temperature gradient of CWB becomes obviously increased at the 100 m depth. The frontal strength is 0.023℃/km there, reaching the strongest (See Table (1) and Fig. 2 (b)). Therefore the inhomogeneity of the movements of the water masses on both sides of CWB is the main dynamic element which causes the spacial variability of CWB.

Furthermore, the temperature inversion happens where the water temperature gets inereased with the depth, because the shelf water extends northward from the Prydz Bay to form the cold water wedge which protrudes over the warm water of CDW (See Fig.3). The profiles of temperature (Fig 3(a)), salinity (Fig.3(b)), and density (Fig.3(c)) for the station at 62° 53.70' S, 73° 06.53' E are shown in Fig.3. It is learnt from Fig.3 that the inversion layer is located in the depths between 100 m and 200 m, where the temperature become increased with depth. The inversion is caused also by the inhomogeneity of the movements of the water masses on both sides of CWB.

5 Dynamic Height near CWB

It is common knowledge that the oceanic currents in large scale depend upon the dynamic height distribution. The dymamic height pattern is governed by the spacial variability of water temperature and salinity. Since the spacial variability is remarkble in the ocean near CWB, the dynamic height distribution near CWB is different from that in other areas without any front. The dynamic height distributions for the sea surface, 5 000 hPa, 10 000hPa, and 20 000 hPa depths are shown in Fig.4 (a)-(b). It is learnt from Fig.4 that a dynamic height trough is situated at 65°S. Dynamic height becomes obviously increased either north or south of the trough. The trough lies from 70°E to 75°E along 65°S. The dynamic height along the trough line becomes lower and its maximum is 0.342 m^2/s^2. As the isopleths of the dynamic height are consistent with the streamlines of the large scale movement, it is understood that there is a cyclonic shear flow near the dynamic height trough. The current corresponding to the pattern in Fig.4 flows eastward to the north of the trough and westward to the south. The trough line, CWB, and the shear are consistent with each other. In addition, it is also learnt from Fig.4 that the Ekman pumping effect can be given by the cyclonic shear along the trough line and causes upwelling there. Therefore the mechanism for the upwelling is reasonably explained.

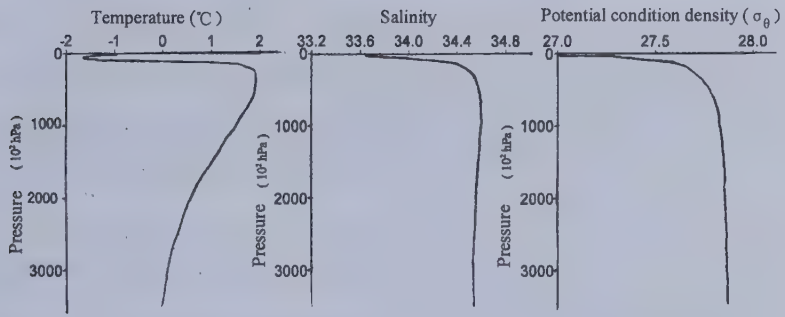

Fig.3 Vertical distribution of temperature, salinity and density in the measuring station at CWB (62°53.70'S, 73°6.53'E)

(a) Temperature (b) Salinity (c) Potential condition density

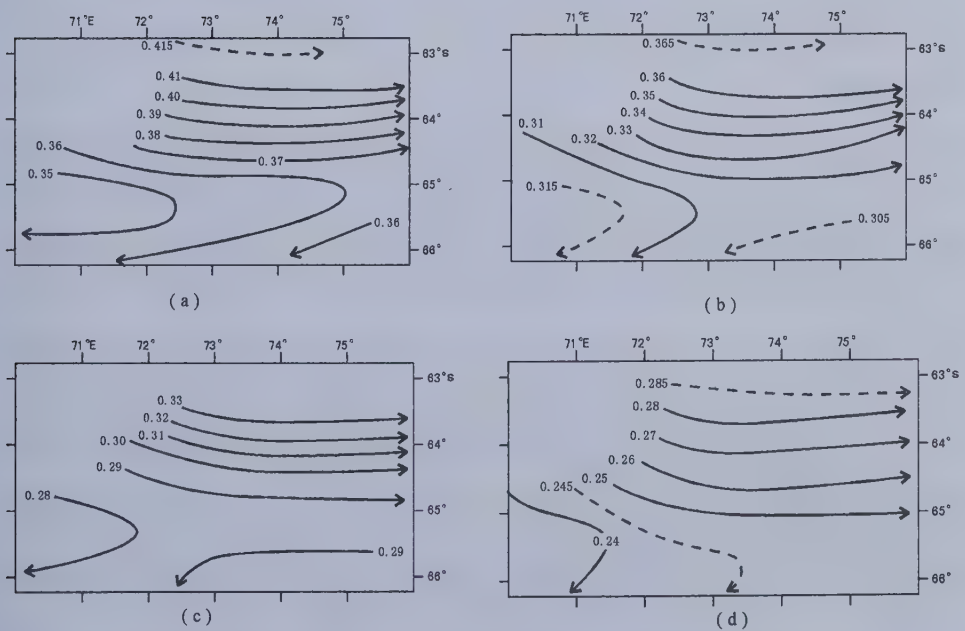

Fig.4 Distribution of dynamic depths (m^2/s^2) calculated from the data obtained during The 15th Antarctic expedition

(a)Sea surface (b)5 000hPa isobathic surface (c)10 000hPa isobathic surface (d)20 000hPa isobathic Surface. The arrow in the diagram denotes the direction of motion of currents.

6 Conclusions

Conclusions can be drawn from the above discussion.

(1) The frontal strength of CWB reaches the strongest and its vertical extent becomes the greatest in the 73° E section of the Southern Ocean near the Prydz Bay.

(2) The frontal width and the strength of CWB had the spacial variability more obviously in the 1998/1999 summer than in the 1992/1993 summer. All the average strength became weaker, the vertical extent and vertical thickness got increased than before.

(3) The shelf water south of CWB extends obviously northward from the Prydz Bay. Upwelling features can be found in CDW north of CWB. The inhomogeneity of the water movements on both sides of CWB results in the spacial variability of the front.

(4) The location of CWB, the trough line of the dynamic height, and the shear flows are consistent with each other. Westward current flows in the sea area north of CWB, and eastward current south of CWB.

(5) Cyclonic shear flow results in the upwelling near the trough line of the dynamic height pattern.

Acknowledgement

This study is completed on the basis of the field measurement on board R/V "Snow dragon" by the scientific team of the 15th Antarctic Expedition of China. Authors take this chance to make their sincere acknowledgement to the team.

References

[1] Liang Xiangsan and Su Jilan (1995) Progress in physical oceanographic studies related to some sea areas in the southern ocean, Progress in studies of the impact and interaction between Antarctica and global climatic environments (edited by Zhou Xiuji), Beijing: Science Press, 55-73(in Chinese).

[2] Pu Shuzhen, Dong Zhaoqian , Hu Xiaomin and Yu Fei (2000) Water masses and their northward extension in the upper ocean near the Prydz Bay of Antartica, *Chinese Journal of Polar Research*, **12** (3): 157-168 (in Chinese).

[3] Yu Honghua, Miao Yutian and Shi Maochong (1996) Structure and variability of the front in the southern Indian Ocean in summer, Studies of the impact and interaction between Antarctica and global climatic environments (edited by Zhou Xiuji and Lu Ronghua), Beijing: Meteorology Press, 156-158(in Chinese).

[4] White, W. B. and R. Peterson (1996) An Antarctic circumpolar wave in surface pressure, wind, temperature and sea-ice extent, *Nature*, 380: 699-702.

[5] Jacobs, G. A. and Mitchell, J. L. (1996) Ocean circulation variations associated with the Antarctic Circumpolar Wave. *Geophys. Res. Let.*, 23: 2974-2950.

[6] Baines, P. G. and W. Cai (1998) The Antarctic Circumpolar Wave. *International WOCE Newsletter*, (33): 35-36.

[7] Saravanan R, Mikolajewicz U., Sterl A. and Driffhout S. S. (1998) Advective atmosphere ocean interaction, an analytical stochastic model with implications for decadal variability. *J.Climate*, 11: 165-188.

[8] White, W B, Chen S-C and Peterson R G. (1998) The Antarctic circumpolar wave: a beta effect in ocean-atmosphere coupling over the southern ocean. *J.Geophys. Res.*, **28**(12): 2345-2361.

Underway Measurement of Sea Surface Temperature and Salinity in the Taiwan Straits in August, 1999*

Chen Hua (陈 华)[1], Hu Jianyu (胡建宇)[1], Pan Weiran (潘伟然)[1], Zeng Ganning (曾淦宁)[1], Chen Zhaozhang (陈照章)[1], He Zhigang (贺志刚)[1], Zhang Caiyun (张彩云)[1] and Li Hong (李虹)[2]

1 *Institute of Subtropical Oceanography, Xiamen University, Xiamen* 361005

2 *Fujian Institute of Oceanology, Xiamen* 361012

Abstract The distributional features of sea surface temperature and salinity (SST and SSS) in the Taiwan Straits have been analyzed using the SST and SSS underway measurements in August, 1999. The characteristics of SST and SSS are summarized as follows: There are several upwellings and diluted water in the Taiwan Straits. The upwellings are divided into two kinds: those along the western coast of the Taiwan Straits and those around the Taiwan Shoal. There are three sources of diluted water: diluted water of the Jiulongjiang River, diluted water of the Zhujiang River and diluted water of the Minjiang River.

Keywords Taiwan Straits, upwelling, diluted water

Located between China's mainland and Taiwan Island, the Taiwan Straits is an important channel connecting the East China Sea with the South China Sea. Most of the straits is shallow with an average depth of 60m or so. The Taiwan Shoal, whose 30m depth contour is shown in dash line in Fig.1, lies in the middle part of the southern Taiwan Straits.

The particular geographical location of the Taiwan Straits attracts many oceanographers. Many oceanography-related institutions, such as Xiamen University, Fujian Institute of Oceanology, Fujian Institute of Fishery, South China Sea Institute of Oceanology and Taiwan University, have conducted many surveys and obtained a lot of field data in the Taiwan Straits. Many researches have focused on the distributions of temperature and salinity, but underway measurement of sea surface has not been conducted so much.

The Xiamen University and Fujian Institute of Oceanology conducted a comprehensive survey in the Taiwan Straits in August 12~18,1999. The SBE21 Thermosalgraph was used in this survey. During the underway measurement, the seawater was pumped up and the sea surface temperature and salinity (SST and SSS) were measured by the respective sensor with the sampling time of 30s, while the longitude and latitude were positioned by the GPS. Because of the wave-induced salinity perturbation, the raw data were first processed by the sectional F test (Chen and Ma, 1991), which can filter the distinguished anomaly caused by wave during underway measurement. Then upwelling and diluted water in the surveyed region are analyzed using the obtained SST and SSS distributions along the sailing tracks.

Received on December 30, 2001

* This projecy was supported by Project (98-Z-179) of Fujian Province and Project (49636220) of the NSFC

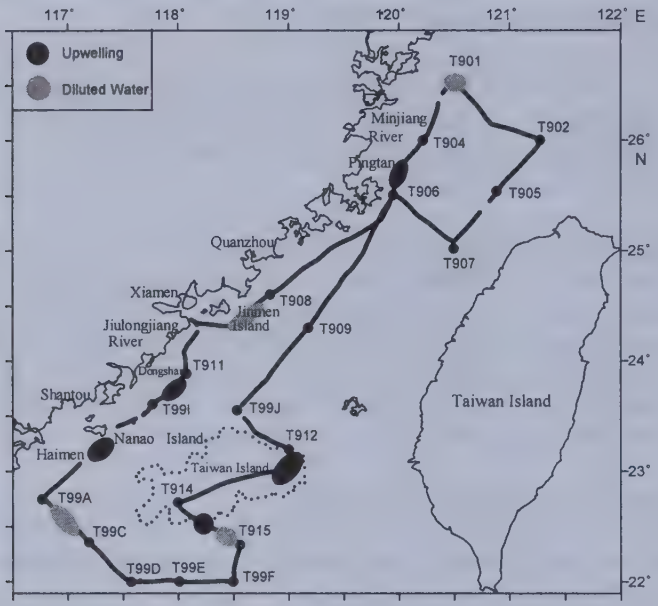

Fig. 1 Survey stations and the sailing tracks (1999-08-12~18)

1 Upwelling Regions in the Taiwan Straits during the Surveying Period

1.1 Upwelling regions along the western coast of the Taiwan Straits

1.1.1 Pingtan upwelling region

Figure 2 shows the SST and SSS distributions along Section T908-T901, which is located along the coast between the Minjiang River mouth and Quanzhou. It is indicated that there is an obvious low SST and high SSS zone at Station T906 (near Pingtan). The cold core SST is 25.2℃, about 2.2℃ lower than that in its surroundings. The high core SSS is 34 and its position is the same as that of the cold core SST. Figure 2 also shows that the width of the low SST and high SSS zone is about 20km. Many previous investigations have indicated that SST and SSS near Pingtan bear such similar characters in August. It is suggested that the low SST and high SSS is caused by upwelling but not by heat budget, horizontal currents and runoff in summer. Xiao (1988) pointed out that one of the strongest summertime upwelling regions along the western Taiwan Straits is located near Pintan. He considered the upwelling as being induced by uplifting of bottom topography from southeast to northwest, the climbing of the water flowing northeastward in summer and Ekman transport caused by the southwest monsoon.

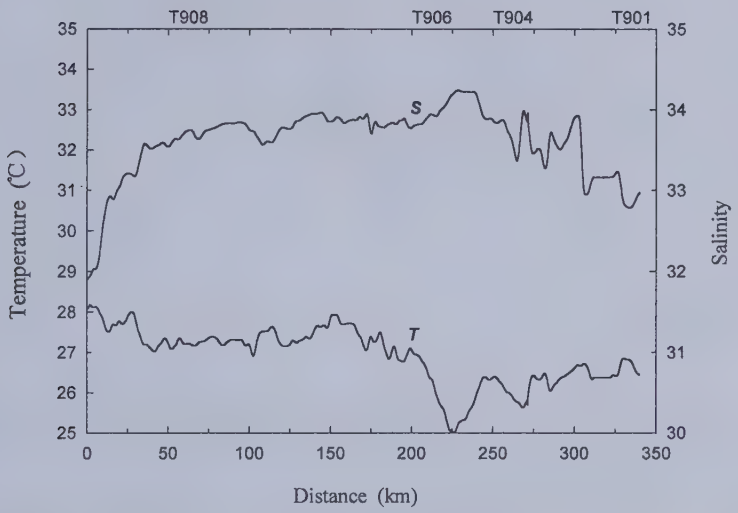

Fig. 2 Sea Surface Temperature and Salinity (SST and SSS) distributions along Section T908–T901

1.1.2 Dongshan upwelling region

Section T99A–T911 is located along the coast between Haimen and Dongshan. The SST and SSS distributions between T99I–T911 are shown on the right of Fig. 3. It is indicated that a low SST (less than 25.5 ℃) and high SSS (greater than 33) zone appears near Dongshan, which may be caused by upwelling. Many previous researches evidenced the upwelling to the east of Dongshan. For example, Xiao (1988) indicated a strong upwelling to the east of Dongshan. Hu et al. (1997, 2000) pointed out an upwelling-related low SST and high SSS zone along the coast between Dongshan and Shantou. Obviously, these previous resultes are further confirmed by the present underway measurements.

1.1.3 Nan' ao upwelling region

It can be seen from Fig. 3 that the lowest SST is at Station T913 near Nan' ao. This phenomenon may be caused by the upwelling near Nan' ao as mentioned by some researches before. Chen *et al.* (1982) indicated that one of two low SST regions in the southern Taiwan Straits lied near Nan' ao and possessed obvious low SST and high SSS caused by upwelling. Zeng *et al.* (2001) and Chen *et al.* (2001) drew similar conclusions according to the CTD data in the same cruise (August, 1999). Li Li and Li Da (1989) showed that the low SST and high SSS near Nan' ao may be affected by either upwelling along the coast of southern Fujian or eastern Guangdong. The upwelling near Nan' ao is regarded as being driven by the southwest monsoon.

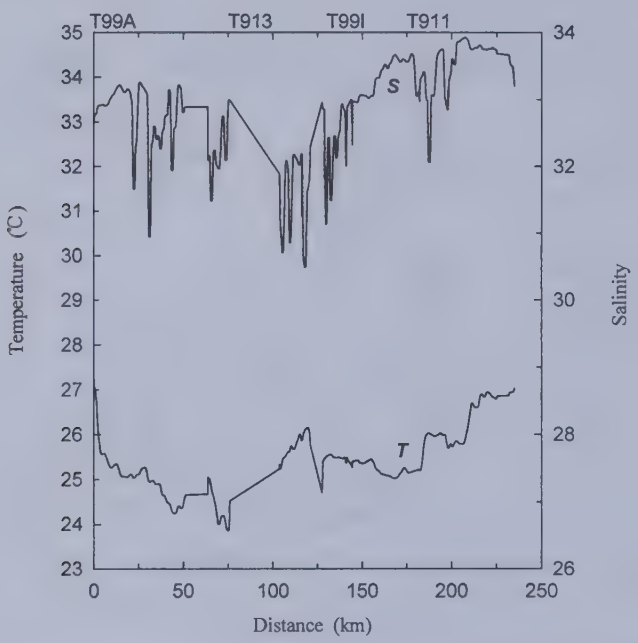

Fig. 3 Sea Surface Temperature and Salinity (SST and SSS) distributions along Section T99A–T911

1.2 Upwelling regions around the Taiwan Shoal

Fig. 4 is the SST and SSS distributions along Section T914–T912, which is located over the Taiwan Shoal. It is indicated that there is a 20km scale zone with obvious low SST of 25℃ and high SSS of 34.2 to the south of Station T912.

Fig. 5 is the SST and SSS distributions along Section T914–T915, which is located in the southern Taiwan Shoal. It can be seen from Fig. 5 that there is a narrow zone with the low SST of 25.5℃ and high SSS of 33.9, which may be caused by the upwelling in August. Since this zone is in the middle of the Taiwan Straits, summertime southwest monsoon wind doesn't contribute much to this upwelling. However, strong northward current flows around the Taiwan Shoal so as to induce an anticyclonic eddy there, which may be a reasonable explanation for the upwelling around the Taiwan Shoal. Furthermore, the climbing of current flowing northward due to the uplifting of bottom topography from south to north is another factor contributing to upwelling formation around the Taiwan Shoal.

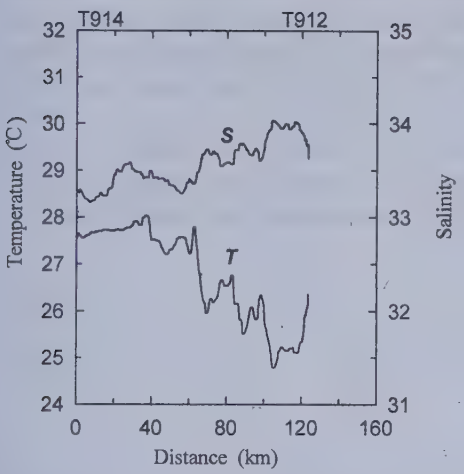

Fig. 4 Sea Surface Temperature and Salinity (SST and SSS) distributions along Section T914-T912

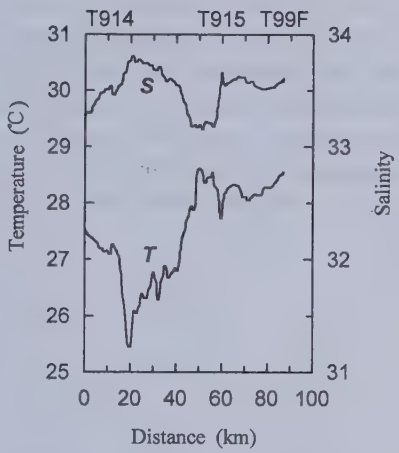

Fig. 5 Sea Surface Temperature and Salinity (SST and SSS) distributions along Section T914-T99F

2 Diluted Water

2.1 Diluted water of the Jiulongjiang River

It can be seen from Fig.2 that the SSS is less than 32 while the SST is up to 28 ℃ near Jinmen Island, which is to the southwest of Station T908. This may be influenced by the diluted water of the Jiulongjiang River because the SSS rises to 33.6 rapidly while the SST falls to 27 ℃ at Station T908. The Jiulongjiang River, whose area is about 11 909km^2 and annual runoff is about 117.46×10^8m^3 (Wang *et al.*,1986), is the second largest river in Fujian Province. It's reported that an outward low SSS and high SST water tongue usually forms in the estuarine region of the Jiulongjiang River. So it can be concluded that the low SSS and high SST to the southeast of Station T908 is caused by the runoff of the Jiulongjiang River.

2.2 Diluted water of the Zhujiang River

It can be seen from Fig.5 that there is a 20km scale zone with high SST (up to 28.6℃) and low SSS (about 33) near Station T915. This phenomenon is rather interesting because Station T915 is to the south of the Taiwan Shoal far from the coast. Since the affected region of the diluted water is about several hundred miles away from the river, the runoff must be from the big river along the western coast of the Taiwan Straits. Wu (1989) showed that the Zhujiang River was the main runoff source along the eastern coast of Guangdong. The Zhujiang River, with weak tide, has a strong runoff of 6×10^{10}m^3. In summer, the runoff of the Zhujiang River may result in an eastward branch while its main axis deflects westward, so the water at Station T915 is influenced by this branch of the diluted water from the Zhujiang River.

2.3 Diluted water of the Minjiang River

Figure 6 is the SST and SSS distributions along Section T901-T902, which lies in the north of the

Taiwan Straits. Both Fig.6 and Fig.2 indicate a high SST and low SSS zone at Station T901. It can be seen from Fig.1 that Station T904 is near the estuary and Station T901 is to the northeast of the Minjiang River. The feature of high SST and low SSS at Station T904 is less obvious than that at Station T901. Minjiang River, whose length is about 541km and drainage area is 60 992km^2, is the biggest river in Fujian Province with an average annual runoff of $620 \times 10^8 m^3$ (Li *et al.*, 1997). Since the southwest monsoon prevails in the Taiwan Straits in summer, the diluted water of the Minjiang River flows northward along the western coast of the Taiwan Straits. So the diluted water affects Station T901 much.

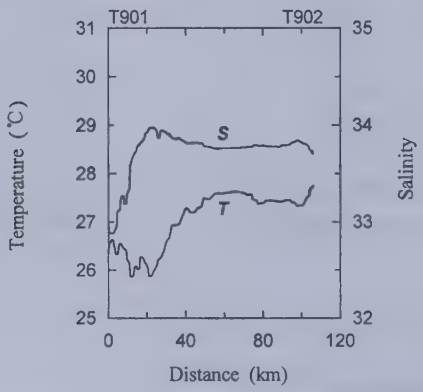

Fig.6 Sea Surface Temperature and Salinity (SST and SSS) distributions along Section T901-T902

3 Coastal Water in the Eastern Guangdong

Figure 7 is the SST and SSS distributions along Section T99A-T99F, which lies to the southwest of the Taiwan Shoal. It is indicated that Station T99A with the SST of 26.8℃ and SSS of 32.8 is near shore and Station T99C with the SST of 29.8℃ and SSS of 32 is far from the shore. The lowest SSS (31.5) zone is between Station T99A and Station T99C. This SST and SSS characteristic is difficult to be interpreted because the diluted water generally affects more the nearshore station than the offshore station. But it can be seen that the SSS between Station T99D and Station T99F is much higher than that of T99C, so we can conclude that Station T99C may be affected by the coastal water of Guangdong. Many researchers, such as Hong and Li (1989) and Han and Ma (1988), pointed out that there exist coastal upwelling regions along the coast of Guangdong, and, therefore, the coastal water shifts outward under the effect of the coastal upwelling.

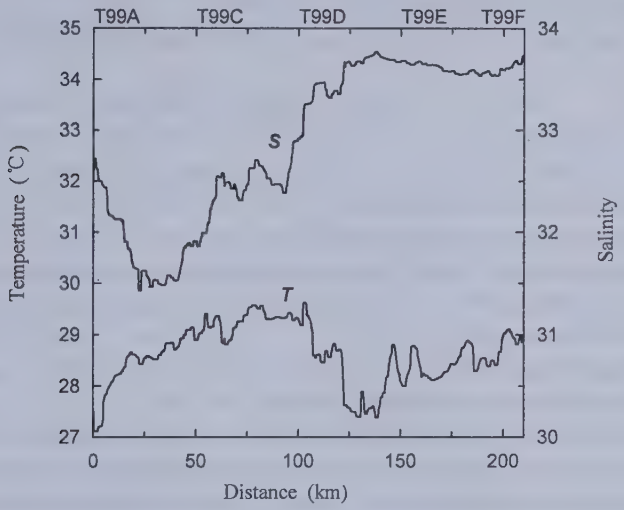

Fig. 7 Sea Surface Temperature and Salinity (SST and SSS) distributions along Section T99A-T99F

4 Conclusions

According to the above descriptions, we draw the conclusions as follows: there are several upwelling regions and diluted water in the Taiwan Straits in August (Fig.1).

(1) There are three upwelling regions along the western coast of the Taiwan Straits: the upwelling near Pingtan is caused by the southwestern monsoon and the uplifting of topography; the upwelling regions to the east of Dongshan and around Nan' ao Island are driven by southwestern monsoon. Two upwelling regions near the Taiwan Shoal are generated by the current-induced anticyclonic eddy and the current climbing.

(2) There are three kinds of diluted water in the surveyed area: diluted water of the Jiulongjiang River, diluted water of the Zhujiang River and diluted water of the Minjiang River. The tracks of diluted water of the Jiulongjiang River and Minjiang River are both close to the western coast, but the diluted water of the Zhujiang River has a branch extending eastward because the Zhujiang River has a big runoff and speed. Furthermore, the coastal water exists along the coast of the eastern Guangdong, but it stays offshore under the influence of coastal upwelling.

References

[1] Chen Jinquan, Fu Zilang, Li Faxi (1982) A Study on Upwelling in Minnan-Taiwan Shoal Fishing Ground. *Taiwan Straits*, **1** (2):5-13.

[2] Chen Shangji, Ma Jirui (1991) The Analyzing Methods of Ocean Data Processing and Application. China Ocean Press.

[3] Chen Zhaozhang, Hu Jianyu, Pan Weiran *et al.* (2001) Sectional Features of Density during August 1999. *J. Xiamen Univ. (Nat. Sci.)*, **40** (3):679-683.

[4] Han Wuying, Ma Kemei, (1988) A Study of Coastal Upwelling off Eastern Guangdong. *Acta Oceanography Sinica*, **10** (1): 52-59.

[5] Hong Qiming, Li Li (1989) Summer Hydrographic Features of Shelf Waters East to Guangdong. *Taiwan Straits*, **8** (8): 350-359.

[6] Hu Jianyu, Hong Huasheng, He Zhigang *et al.* (2000) An Analysis on Temperature and Salinity of Surface Water in August 1998. **19** (4): 15-22.

[7] Hu Jianyu, Liang Hongxing, Zhang Xuebin (1997) Distributional Features of Temperature and Salinity in the Southern Taiwan Straits and its Adjacent Sea Areas in Late Summer. *Oceanography in China*, (7):72-80.

[8] Li Li, Li Da (1989) Summer Hydrographic Features of Channel West of Taiwan Shoals and the Coastal Upwelling. *Taiwan Straits*, **8** (4):353-359.

[9] Li Li, Li Da, Hong Qiming (1990) Multi-dimension Fuzzy Analysis of Water Mass Around the Taiwan Shoals in Summer, 1984. *Acta Oceanography Sinica*, **12** (5):562-570.

[10] Li Rongguan, Jiang Jinxiang, Wu Qiquan *et al.* (1997) The Ecological Research of Macrobenthos in the Minjiang River Mouth and its Adjacent Waters. *Acta Oceanography Sinica.* **19** (5): 116-123.

[11] Wang Weiqiang, Huang Shanggao, Gu Deyu, (1986) Mixing Characters of Fresh Water with Sea Water in the Jiulongjiang Estuary, Fujian.*Taiwan Straits*, **5** (1):10-16.

[12] Wu Boyu (1989) The Study of Circulation in the Shelf Area in the West of Zhu River. *Taiwan Straits*, **8** (4): 360-365.

[13] Xiao Hui (1988) Studies of Coastal Upwelling in the Western Taiwan Strait. *Taiwan Straits*, **7** (2):135-142.

[14] Zeng Ganning, Hu Jianyu, Pan Weiran *et al.* (2001) Analysis on Temperature, Salinity and Density in the Southern Taiwan Straits in August 1999. *J. Xiamen Univ. (Nat. Sci)*, **40** (3):675-678.

Vertical Sound Velocity Transition in the Coral Reef Core and its Significance of Indicating Facies*

Li Ganxian（李赶先), Lu Bo（卢 博）
South China Sea Institute of Oceanology, Chinese Academy of Sciences, Guangzhou 510301

Abstract On the basis of the sound velocity measurements of the coral reef core from Nanyong No. 1 Well of Yongshu Reef in the Nansha Islands, the paper studies the relations between the vertical sound velocity transition features in the coral reef core and the corresponding stratigraphic depositional facies change as well as stratigraphic gap of erosion, analyses the cause of the sound velocity transition, expounds the concrete process of the sea level change resulting in the stratigraphic gap of erosion and facies change in the coral reef and explains the relations between the vertical sound velocity transition in the coral reef core and the corresponding stratigraphic paleoclimate and the sea level change. This study is of important practical value and theoretical significance to the island and reef engineering construction and the acoustic logging for oil exploration in the reef limestone area as well as the paleoceanographic study of the marginal sea in the western Pacific Ocean.

Keywords Coral reef, sound velocity, depositional facies, sea level change

In recent years, the physical research on marine sedimentary acoustics has penetrated into several domains of oceanography. As the acoustic properties are directly determined by the various characters of sedimentology and physicomechanics of sediment, they have become a sound way of inverting the various characteristics of sediment. On the basis of the sound velocity measurements from the coral reef core in Nanyong Well No. 1, the paper studies the relations between the sound velocity change in the coral reef core and its sedimentary facies as well as the corresponding stratigraphic paleoclimate and sea level change, and obtains results with theoretical and practical value.

1 Acoustic Properties of Reef Limestone

1.1 Sample measuring method and data

The Integrated Nansha Scientific Research Team of the Chinese Academy of Sciences drilled the Nanyong Well-1 with a depth of 152.07m on the reef flat of Yongshu Reef in the Nansha Islands of the South China Sea (Fig.1) and we have made sectional acoustic measurements of the core samples of the whole well. The upper part of the well between 0m and 17.3m is a loose biological gravel psammitic layer, which has not yet been cemented into rock, the middle part between 17.3m and 142m is the calcirudite and coral limestone, which has been cemented into rock and the lower part between 142m and 152.07m is the coral dolomite, which was formerly coral limestone, but has been dolomitized

Received on December 4, 2001

* This project was financially supported by Open Laboratory of Marginal Sea Geology and Paleoenvironment , South China Sea Institute of Oceanology, Chinese Academy of sciences, (No.6).

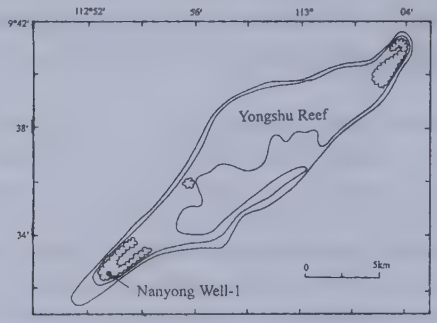

Fig. 1 Position of Nanyong Well-1

with a high level of diagenesis[1]. As the upper part is a loose sandy layer, acoustic measurement is made of the 28 representative core samples starting from beyond 17.3m and the samples appeared to be dry at the time of measurement. The instrument used for measurement is SYC-2 geotechnical acoustic parametron with a measuring frequency of 400kHz. The signal pulse is directly input into the CJ-1 data processing system in parallel connection with a computer for FFT transformation and spectral analysis. See Table 1 for the position, lithologic character, structure, depositional facies of the measured samples as well as the longitudinal wave sound velocity (V_p) and transverse wave sound velocity (V_s) values.

1.2 Acoustic properties of reef limestone in different facies belts

The coral reef facies may be divided in detail from outside to inside into the outer reef flat facies, inner reef flat facies, lagoonal slope facies and lagoonal basin facies, which may be simply lumped together into the reef flat facies and the lagoonal facies.The measurements of sound velocity in the cores from Nanyong Well-1 indicate that there exist vertical variations in sound velocity in the whole core and that the overall law is: the sound velocity increases with depth from above to below and the sound velocity value V_p ranges from about 3 800~4 900m/s, up to the maximum of 5 100~6 000m/s or so, which is caused by the higher level of cementation and diagenis and decrease of porosity with depth of the core strata under the long-term burial stress. Despite this general law, it may be found from a detialed study that there exist vertically some obvious sound velocity transitions in the core and that the law governing the longitudinal wave sound velocity transitions is: when the facies belt of the core stratum changes from the lagoonal facies to the reef flat facies from below, the sound velocity increases (at the well depths of 114m and 60m in Tab.1), when it changes from the reef flat facies to the lagoonal facies, the sound velocity decreases (at the well depths of 89.8m and 17.3m in Tab.1), while in the case of the transverse wave sound velocity, there is only exception (at the well depth of 114m) and there exists the same variation pattern as the longitudinal wave sound velocity in other positions of facies change. Both theory and practice indicate that there exists a relationship of positive correlation between the longitudinal and transverse wave sound velocities[2] , and it may be said that the above change law of longitudinal wave sound velocity represents the basic change pattern of sound velocity at the facies change of the coral reef core stratum, At the depth shallower than 17.3m in Nanyong Well-1 is a loose

coral psammitic stratum in the lagoonal facies.Although no measurement of sound velocity has been made there, by comparing it with the sound velocity in the same position of the YG3 well in Yongshu reef[3], it may be seen that there exist sound velocity transitions at the facies change with a well depth of about 17m and that there are also stratum facies changes around the well depth of 130~142m. But due to the karst cave in between, no core samples have been collected and it is impossible to measure the sound velocity at the facies change position.

Tab.1 Lithologic character, depositional facies and sound velocity of coral reef core samples from Nanyong Well-1

Samples No.	Position(m)	*Vp* (m/s)	*Vs* (m/s)	Lithologic character	Structure	Depositional facies	Cycle of sedimentation
YG3-12*	11.5~12.5	3566	1197	Loose arenite	Loose structure	Lagoonal facies	Cycle IV
1	16.8~18.4	4242	2003	Coral limestone	Block structure	Outer reef flat facies	Cycle III
2	18.4~20.1	4258	1756	Pebble limestone			
3	25.5~26.7	4630	1939	Coral limestone			
4	28.2~29.7	4918	1378				
5	29.7~32.2	4397	1711	Calcirudite			
6	32.2~33.4	4469	1469				
7	36.7~38.2	4946	1821				
8	39.2~40.1	3818	1441		Pebble structure		
9	44.6~46.3	4909	1213		Coated structure	Inner reef flat facies	
10	47.2~48.6	5587	1738				
11	54.9~57.7	5129	1842				
12	60.2~61.6	4756	1569	Calcarenite	Psammitic texture	Lagoonal facies	
13	71.1~74.1	4698	2011				
14	82.3~85.2	5218	2090				
15	89.0~90.1	4811	1680				
16	91.2~92.6	6163	2013	Coral limestone	Block structure	Outer reef flat facies	Cycle II
17	96.2~99.0	5773	1769				
18	99~101.5	5868	2285				
19	104~107.5	6020	2376	Pebble limestone		Inner reef flat facies	
20	107.5~111	5197	1777				
21	111.2~114	4598	1613				
22	114.2~118	4034	2365	Calcarenite	Psammitic texture	Lagoonal facies	
23	118~121.6	6067	1956				
24	121.6~125	6059	2045				
25	128.5~130	5576	2365				
	130~141.9	Karst Cave					
26	142~144.8	5418	2998	Dolomite	Block structure	Outer reef flat facies	Cycle I
27	144.8~146	4433	2308		Psammitic texture	Inner reef flat facies	
28	149.6~152	5234	2219				

Note: * Core sample from the well YG3 at a position of 12 m in Yongshu Reef.

The above-mentioned regularity of sound velocity transition at the facies change position in the core stratum is resulted from a number of factors, the decisive one of which is the difference in the varieties of primitively growing coral genera which comprise the reef limestones in the reef flat facies and the lagoonal facies while the varieties of coral genera growing in different facies belts are determined by such factors as hydrodynamic environment, water depth and nutrient supply at the time of stratigraphic sedimentation in different facies belts,. Generally speaking, the large block coral populations or those with thick branches like *Porites*, *Acropora* and crustose coral-algae, etc., mostly grow on the reef flat or the seaward slope of the reef flat front. This is because of the fact that these corals have the block and crustose appearance as a whole, possess stronger anti-wave capability and may grow densely on the reef flat and its seaward slope where the waves are strong and the nutrient supply is adequate. Block coral limestones in the reef flat facies are formed with small porosity (6%~8%) in the coral formation. In the lagoonal environment, the water is tranquil with less nutrient, so few corals are growing to form dense coral populations and there are only slenderly branched and lamelliform corals, such as *sinularia* and *parisis furiticosa verrill*, etc. Furthermore, in the lagoon, there are a large amount of coral detrituses transported from the breaking of reef flats, which form the calcarenite in the lagoonal facies with greater porosity (over 20%) in the formation[4]. Hamilton pointed out a long time ago that porosity is the primary factor determining the sound velocity in the submarine sediment[5]. The difference in the stratigraphical porosity decided by the different varieties of growing coral genera results in the sound velocity transition at the facies change position in the coral reef core formation.

2 The indicating Significance of Vertical Sound Velocity Transition to the Stratigraphical Erosion Discontinuity Surfaces

2.1 Formation of the erosion break in the core formation of the coral reef

Within the core depth of 152.07m in Nanyong Well-1 there are three stratigraphical erosion discontinuity surfaces at the well depths of 17.3m, 89.8m and 142m repectively. These three erosion discontinuity surfaces have an obvious general character: Below the erosion surface are coral limestones in the outer reef flat facies while above the erosion surface is the calcarenite in the lagoonal facies (In the depth shallower than 17.3 m are the loose sand cutting in the lagoonal facies, which becomes the calcarenite after being cemented into rock, and above the depth of 142 m is the 8 m karst cave, which, by inferrence, was originally also the calcarenite in the lagoonal facies and later corroded into the karst cave due to the larger porosity, loose texture and its location at the phreatic surface of the paleofresh water lens[6]).This general character of the three stratigraphical erosion surfaces is inevitably attributed to the shift of its coral reef facies belt with the rise or drop of sea level. When the sea level drops, the reef top relatively rises to the photic zone shallower than 70m below the sea surface, which is favourable for the growth of corals. As the reef top at this time has no ring reef flat in its periphery and is directly subjected to wave wash and receives nutrients brought by the waves from the open sea, it becomes the actual reef flat, on which are grown the anti-wave wash reef flat-type corals and in the core formation they become the coral limestones in the reef flat facies below the erosion break. In the course of the sea level dropping, the reef gradually emerges above the sea surface, the corals stop growing and the reef is subjected to denudation to become the erosion surface, with the constant dropping of sea level and the

relative rising of the reef, the plane of denudation enlarges increasingly. The reefs emerging from the sea surface have gone through a period of coral growth in the outer reef flat environment before their emergence, thus resulting in the coral limestone in the outer reef flat facies below the erosion surface of the core formation. When the sea level begins to rise and the reef relatively drops, atolls come into being around the reef. Charles Darwin observed and studied the formations of atolls as early as 1842[7]. When the sea level rises relatively, corals would first grow on the seaward slope around the reef shallower than 70m water depth, where the sunlight can penetrate and the waves from the open sea bring along with them adequate nutrients, thus forming a preferential growth zone for corals around the reefs. This ring growth zone of corals would get higher constantly with the increasing rise of sea level, (The rate of sea leve rise or drop is about equal to the growth rate of corals.) while its interior becomes a lagoon. In the course of the relative dropping of reefs, the original emerged denundation zone becomes a lagoonal environment surrounded by reef flats, thus forming the lagoonal facies sediment and resulting in the lagoonal facies calcarenite above the erosion disconlinuity surface in the core formation.

2.2 Indicating significance of Class -I sound velocity transition to the erosion discontinuity surface

For convenience' s sake, the transition of sound velocity decrease from below in the coral reef core is referred to as the Class-I sound velocity transition while that of sound velocity increase the Class-II sound velocity transition. It is obvious that the sound velocity in the coral limestone of the reef flat facies below the erosion discontinuity surface in the core formation of the coral reef is high while that in the calcarenite of the lagoonal facies above the erosion discontinuity surface is low. Therefore, the erosion discontinuity surface in the core formation must correspond to the Class-I sound velocity transition (Table 2). On the contrary, the existence of the vertical Class-I sound velocity transition in the core formation of coral reef directly has the indicating significanc to predicating the stratigraphic erosion discontinuity surface. This research is of specially important significance in the fields of oil exploration and acoustic logging in the reef limestone area.

Tab. 2 Relationship between the two kinds of sound velocity transition and the lithologic character, erosional surface, temperature and sea level change in the coral reef strata

Type of sound velociy	Position	Sound velocity	Lithologic character	Structure	Depositional facies	Erosion surface	Sedimentary cycle	Climatic temperature	Sea level	Glacial event
I	Upper	Low	Calcarente	Psammogenic texture	Lagoonal facies	Errosion surfaces of corresponding strata	Sedimentary cycle demarcation	Cool to warm	Drop to rise	Glacial period to interglacial stage
	Lower	High	Coral limestone	Block structure	Outer reef flat facies					
II	Upper	High	Gravel limestone	Gravel block	Inner reef flat facies	Corresponding facies change	Depositional facies demarcation	Warm to cool	Rise to drop	Interglacial stage to glacial period
	Lower	Low	Calcarenite	Psammogenic texture	Lagoonal facies texture					

3 Correspondence of Core Vertical Sound Velocity Transition with the Stratigraphical Sedimentary Cycle and Its Practical Value

The facies change in the coral reef core formation is determined by the eustatic change and the rate of coral growth in the geologic history. The reef coral can only grow in the photic zone with a water temperature >17℃ and a water depth < 70m. During the shift of cold and warm climates in geologic history, the water temperature in the tropical ocean in the last glaciation was only 3℃ less than the modern average of 28℃[1], so the tropical ocean duing the glacial stage was favourable for the growth of corals. The growth rate of reef coral was generally 5~10m/a. By comparison, when the sea level rises too quickly, the island and reef would be submerged while when the sea level rises too slowly, the growth of corals could only extend horizontally to expand the reef flat. Only when the rising speeds of the two are about the same, could the coral grow upwards constantly. In the course of the facies change in the core formation of Nanyong Well-1, there is also the facies change from the lagoon to the reef flat corresponding to the Class-Ⅱ sound velocity transition. This facies change is formed when the sea level changes from rising to stable relative to the island and reef. When the climate changes from warm to cold and the sea level from rising to stable, for the rising reef flat and lagoon originally formed on the island and reef, because the sea level is relatively stable, the coral stops growing upwards and the reef flat in the wave zone breaks, the coral grows hozizontally and the scope of reef flat expands to overlay the original sediment of the lagoonal facies, thus resulting in the facies change from the lagoon to the reef flat in the vertical core formation. Obviously, the Class-Ⅰ and-Ⅱ sound velocity transitions completely correspond with the process from the reef flat facies to the lagoonal facies and then again to the reef flat facies,i.e.,with the complete sedimentary cycle. The research on the sound velocity variations in the core formation of coral reef is of important value in many aspects. Lu Bo has studied the relations between the sound velocities in the core formation of coral reef and its various elastic parameters[8], finding that the compressibility coefficient β decreases with the increase of sound velocity V_p and that the bulk modulus K and the Lame constant λ increase with the sound velocity V_p. Therefore, the sound velocity variation in the core formation of coral reef directly indicates the difference in the engineering geological character in the reef limestone formation, which is of important value for reference in the island and reef engineering construction. In addition, as the strata of coral reef facies are often good oil reservoirs while the sound velocity is closely related to the stratigraphical porosity, this research is of practical guiding significance to the oil exploration in the reef limestone area.

4 Relations Between the Vertical Sound Velocity Transition in the Coral Reef Core and the Paleoclimate and Sea Level Change

It can be seen from the above analysis that when the sea level changes from falling to rising in relation to the island and reef, the facies change from the reef flat facies to the lagoonal facies corresponding to the Class-Ⅰ sound velocity transition is formed at the erosion discontinuity surface; while the sea level changes from rising to stable and dropping, the facies change from the lagoonal facies to the reef flat facies corresponding to the Class-Ⅱ sound velocity transition takes shape. These two kinds of sound velocity transition correspond to the complete sedimentary cycle, the shift cycle of cold

and warm climates and the repeated rising and falling of sea level and the ice age events. Since the Quaternary period, the global sea level has undergone the process of changing from falling to rising and then again falling and rising, which has resulted in the four sedimentary cycles in the coral reef core formation of Nanyong Well-1. Table 2 gaves the relationship between the two kinds of sound velocity transition and the lithologic character, erosional surface, depositional facies, ancient temperature and sea level change, in which the Class-I sound velocity transition indicates the existence of the stratigraphical erosion surface while the Class-II sound velocity transition indicates the existence of the facies change in the coral reef strata. Fig.2 plots the changing curve of the vertical longitudinal wave sound velocity in the coral reef strata of the Nanyong Well-1 and the corresponding paleoclimate and sea level change curves. It is clear from Fig.2 that the value of sound velocity V_p increases with depth and that two kinds of sound velocity transition exist, of which, the class-I sound velocity transition obviously corresponds with the process of the climate changing from cold to warm and the sea level from falling to rising while such correlation of the class-II sound velocity transition is not obvious, indicating that the shift of the coral reef facies from lagoon to reef flat has been subjected to the more complicated change in climatic temperature and sea level, its specific process of formaion pending further research.

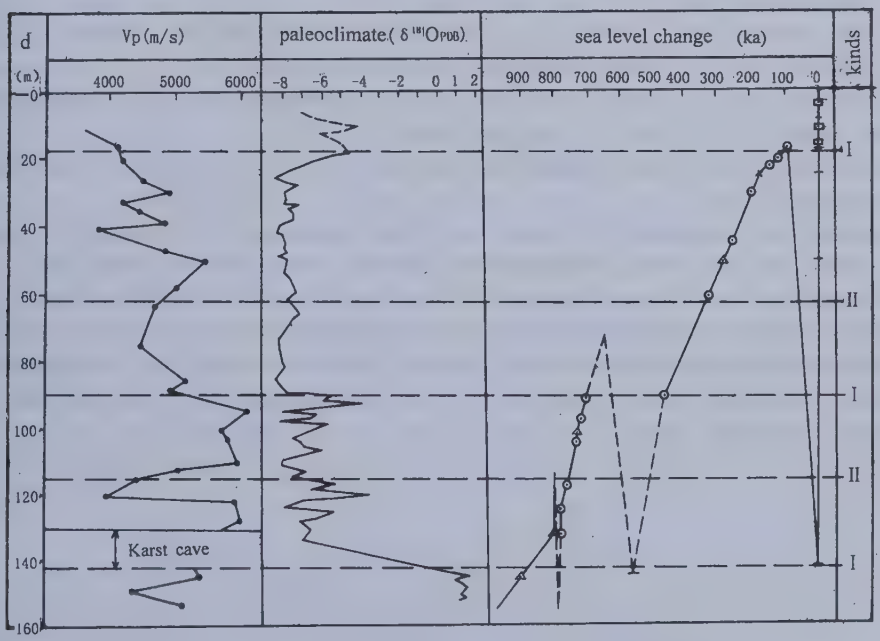

Fig. 2 Relations between the two kinds of sound velocity transition and the paleoclimate, sea level change in the coral reef core stata of Nanyong Well-1.

It is known from the above analysis that in the coral reef environment of the tropic ocean, the difference in the hydrodynamic conditions and nutrient supply in different facies belts results in the different varieties of genera growing on it, which determines the different porosity and sound velocity in the strata of different coral reef facies and thus results in the vertical sound velocity transition in the strata. When the coral reef core strata change from below from the lagoonal facies to the reef flat facies, the sound velocity increases while, conversely, the sound velocity decreases, which determines the existence of the sound velocity transition above and below the discontinuity surface of the strata and makes the sound velocity transition in the core closely correlated with the corresponding paleoclimatic temperature and sea level change in the strata.

References

[1] Zhao Huanting, Zhu Yuanzhi, Nie Baofu *et al.* (1992) Geologic Time of Yongshu Reef and Preliminary Division of strata in the Quaternary Period [J]. *Science Bulletin*, (23):2165-2168.

[2] Lu Bo, Sun Zongxun and Huang Shaojian (2000) Vertical Sound Velocity Variations and Geologic Events in the Coral Reef Core of Nanyong Well-1 in the Nansha Islands [J]. *South China Sea Reasarch and Development*, (1):22-25.

[3] Lu Bo and Huang Shaojian (1997) Acoustic Properties of Coral Reef and Reef Limestone, Coral Reef Engineering Geology of the Nansha Islands [M]. Beijing: Science Press, 107-119.

[4] Sun Zongxun and Lu Bo (1999) Research on the Properties of Elastic Waves in the Coral Reef Limestone of the Nansha Islands [J]. *Journal of Engineering Geology*, 7 (2): 175-185.

[5] Hamilton E.L. (1974) Physical and Engineering Properties of Deep-Sea Sediments [M]. New York: Plenum Press, 1-43.

[6] Integrated Nansha Islands Scientific Research Team of the Chinese Academy of Sciences (1992) Quaternary Coral Reef Geology of Yongshu Reef of the Nansha Islands [M]. Bejing: China Ocean Press, 47-83.

[7] J.Kennett (Translators: Cheng Guodong *et al.*) (1992) Marine Geology. Bejing: China Ocean Press, 151-152.

[8] Lu Bo and Huang Shaojian (1994) Elastic Properties of Coral Reef Limestone in the Yongshu Reef [A]. Integrated Nansha Islands Scientific Research Team of the Chinese Academy of Sciences, Collected Papers of Research on Geology, Geophysics and Reefs in the Nansha Islands and Their Adjacent Waters (II) [C]. Bejing: Science Press, 148-152.

Underwater Acoustic Image Transmission System Based on DSP*

Cheng En (程 恩), Xu Ru (许 茹)
Department of Electronic Engineering, Xiamen University, Xiamen 361005

Abstract The underwater acoustic image transmission system based on the high-speed DSP device TMS320C549 has been studied. We use Goertzel algorithm for source decoding and MFSK for modulation. Turbo code is used for channel coding and decoding. The purpose is to implement underwater video image data transmission.

Keywords underwater image transmission, MFSK, Goertzel algorithm, Turbo code

1 Introduction

The underwater acoustic image transmission system is a kind of observational device for underwater engineering. It can act as "eyes" of underwater robot and as a wireless telecontrol device of underwater auto-production system. It possesses clear graph and text information that is difficult to express in voice communication. According to communication technology, images have more data content than languages and texts. The development of modern communication technology has made communication easy and free in air and on land. But doing the same thing under water is still very difficult. Electromagnetic waves decline severely over long distances under water except at extremely low frequencies. Now the only method is to use acoustic signals. But in the ocean, the acoustic wave varies greatly with the frequency, the distance and other factors, thus resulting in a very limited transmitting bandwidth. Also, the signals reflection and scattering in the sea bring problems such as multi-path interference. These limit communications at high speed in the underwater acoustic channels. First introduced by Berrou in 1993, Turbo code is the most exciting and potentially important development in coding theory in recent years and offers near Shannon-limit error correction performance under certain circumstances. In this paper, it is applied to the underwater acoustic communication on poor channel conditions. The aim is to study how to realize miniaturization, lower power consumption and intellectualization of the underwater image communication device.

Fig.1 illustrates the functional diagram and the basic elements of an underwater image transmission system.

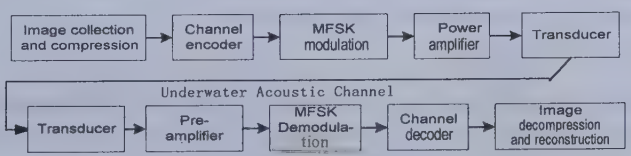

Fig. 1 Block diagram of underwater image transmission system

Received on November 21, 2001

* This project was supported by NFSC (No. 60172053) and Fujian Provincial Natural Science Foundation (No.A0110001)

2 MFSK Modulation and Transmission Control

In order to minimize the negative effect in the high-speed data transmission caused by the complex underwater acoustic channels, many research staffs of the world have tried different kinds of modulation projects: DPSK, MFSK, QPSK etc. The experiments show that most of the interference echo can be eliminated by lengthening the duration of each frequency in MFSK. Based on this unique characteristic of MFSK, our design adopts the MFSK modulation project to enhance the reliability of underwater acoustic transmission. Here, we use DSP chip to realize the pre-processing of encoded data, MFSK modulation and the corresponding transmission control , and the high speed, high precision and high stability of DSP chip are the most fundamental of all these functions.

2.1 Design of frequency synthesizer

Taylor Series Expansion is adopted to calculate values of Sine and Cosine, ranging from 0° to 45°, then calculate $\sin 2X = 2\sin X * \cos X$ to obtain the values of sin from 0° to 90°,and finally by duplicating, we can get the values of Sine, ranging from 0° to 359°. By consulting the table, outputting these sample values to I/O Ports, then putting them through a D/A converter and a low-pass filter, we can get the frequency output. The value of frequency is settled by the number of sample points in each period and the duration of intervals among sample points. The value of frequency can be expressed as:

$F=1/(T * N)$

Where

N— the number of sample points in each period

T— the duration of intervals among sample points

In our design, we choose 16 frequencies, ranging from 10kHz to 20kHz. Each frequency presents 4-bit data.

2.2 Mechanism of synchronous control

In our system we select another two frequencies besides the previous 16 frequencies as frame synchronization signal, and transmit this signal before each data frame. As the bit-oriented synchronization of the receiver is automatic, we don' t need additional bit-oriented synchronization signal. Moreover, the detection of frame synchronization signal can calibrate bit-oriented synchronization simultaneously. In addition, according to the scan mode of image display, we transmit row and field synchronization signals to minimize distortion and dislocation of image. The duration of synchronization signals is much longer than the that of each data bit and can be adjusted to real-time channel condition so as to insure the precision of synchronization.

2.3 Design of hardware and software

The basic hardware block diagram is shown in Fig.2. The system utilizes the buffered serial port (BSP) of TMS320C549 to receive encoded source data and realizes software modulation algorithm based on the high degree of operational flexibility and speed of DSP chip. External interrupts are utilized to realize parameter adjustment in real time. Software-programmable timer interrupts periodically to control precisely the duration of each frequency. Here, we choose the TLC7524 8-bit high-speed parallel digital-to-analog converter with 0.1 μs conversion time to insure the precision and continuity of data conversion.

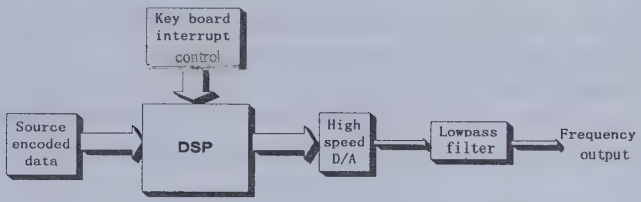

Fig. 2 MFSK modulation hardware block diagram

3 Demodulation of MFSK Signals with the Spectrum Analysis Method

Fig. 3 illustrates the diagram of the receiving systems.

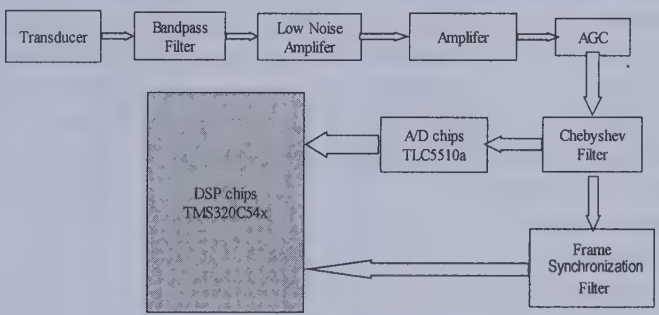

Fig. 3 The diagram of the receiving systems

Given the frequency distribution of the launching signal, the only thing we should do is to extract the corresponding frequency. Then spectrum analysis is made of the launching signal, the result of which is shown in Fig. 4 .

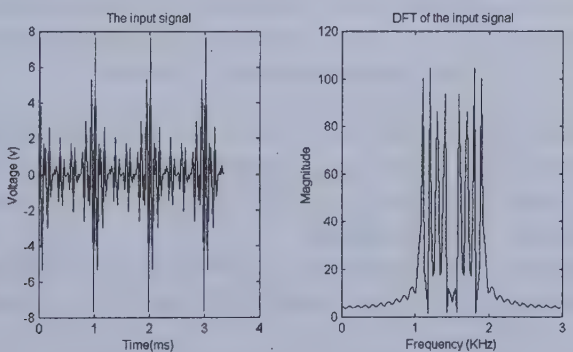

Fig. 4 (a) The launching signal (b) DFT of the launching signal

From Fig.4, we can conclude: if at the launching port the bit rate is 2kbit /s (also is 500 Baud /s), by just calculating DFT, we can extract the frequency accurately. The sampling frequency is $f_s = 4\ f_{max}$. The upper cut-off frequency is 1.5 f_{max}. in the anti-aliasing pre-filter.

Bit-oriented synchronizations apply the self-synchronization method. Because the sampling frequency f_s and the transmission velocity B_T have been determined, we can decide the sampling decision moment by using the number of the samples to get bit-oriented synchronization. Their relation is:

$$N = f_s / B_T$$

4 Core Algorithm of Signal Processing

4.1 Goertzel algorithm

The transmission process is by its nature a continuous one, meaning the decoding process is a real-time and continuous one. The decoder algorithm is Goertzel algorithm. This algorithm essentially utilizes two-pole IIR type filters to effectively compute DFT values. The Goertzel algorithm is much faster than the true FFT and it also does not need a big capacity of data memory. It is a recursive structure always operating on one incoming sample at a time. After a certain number of samples N (equivalent to a DFT block size) the Goertzel filter output converges towards a pseudo DFT value $v_k(n)$, which can then be used to determine the squared magnitude. Consult the following box for a short mathematical description of the algorithm.

Goertzel Algorithm in short:

1. Recursively compute for $n = 0, \cdots N$

$$v_k(n) = 2\cos(\tfrac{2\pi}{N}k)\cdot v_k(n-1) - v_k(n-2) + x(n)$$

where $v_k(-1) = 0 \qquad v_k(-2) = 0$

$$x(n) = input$$

2. Compute once every N

$$|X(k)|^2 = y_k(N)y_k^*(N)$$

$$= v_k^{\,2}(N) + v_k^{\,2}(N-1) - 2\cos(\tfrac{2\pi}{N}k)v_k^{\,2}(N)v_k^{\,2}(N-1)$$

The core part in the program (Fig. 5) is an interrupt service routine, RINT−ISR. When receiving one sample, it gives an interrupt request. Firstly, RINT−ISR filters the AWGN for the inputting signal by use of a seven-order Chebyshev I filter. RINT−ISR has two different tasks. Then according to the number of the samples, COUNT, we decide which task needs to process.

When COUNT< N, Task #1 performs the computation of the Goertzel filters for the first incoming N samples. At the end of its duration it will have the pseudo DFT values $v_k(n)$ computed.

When COUNT=N, Task #2 is then assigned to compute squared magnitude values, search for maximum, perform all validity checks and store detected digits into the result buffer. The result will be performed as the input of the Turbo Code Decoder.

Another interrupt service routine is the program, SYN−ISR. When the frame synchronization comes, it gives an interrupt request. Firstly initialize the frame buffer and rectify the bit-oriented synchronization.

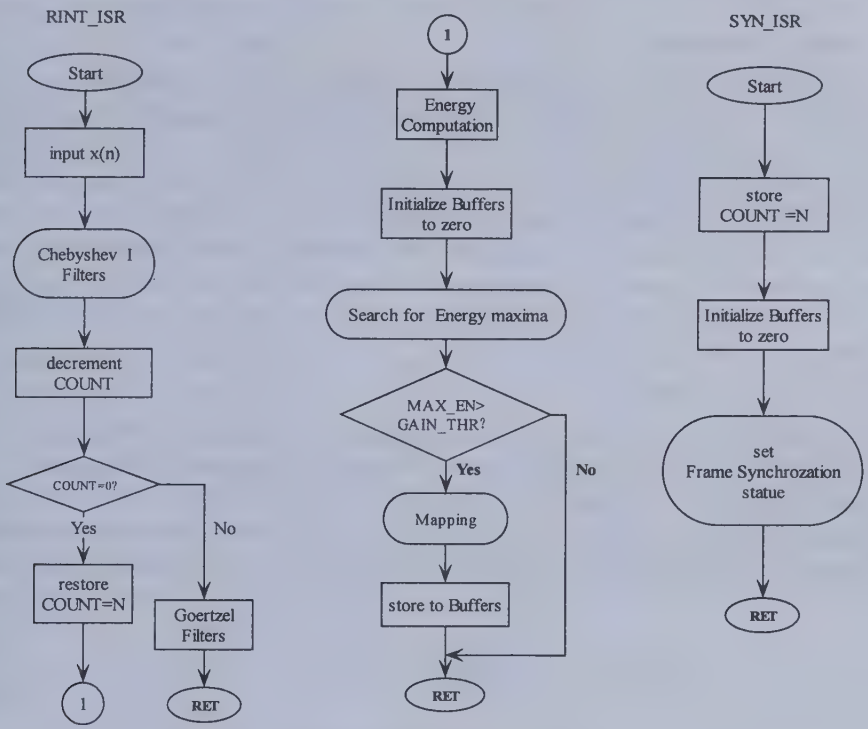

Fig. 5 Program flow description of the signal process

4.2 Turbo-code encoding and decoding

4.2.1 Turbo-code encoding

The encoder used in this paper consists of the parallel concatenation of two identical recursive systematic convolutional (RSC) component encoders with an interleaver between them. Fig.6 illustrates the structure of the turbo encoder we used. For an input bit sequence u, the RSC turbo-code encoder output is y, c_1 and c_2. By puncturing, the code rate will decrease from 1/2 to 1/3, which means the transmission time will be about 1/3 less.

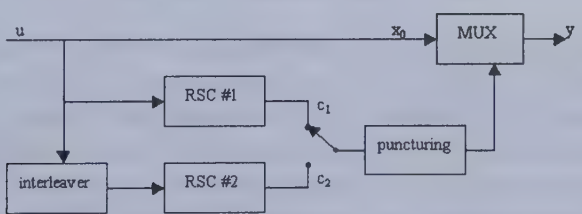

Fig . 6 The RSC turbo-code encoding scheme

4.2.2 Turbo-code interleaver

For Turbo codes, pseudorandom interleavers are preferable because they usually result in the best error-correcting performance, which also improves with interleaver size. Pseudorandom interleavers use a fixed but random-like pattern for shuffling the data. They're sometimes called uniform interleavers because, unlike rectangular interleavers, they spread the input data uniformly throughout the output. We use pseudorandom permutations (interleavers) by generating random integers i, $i = 1 \cdots N$, without replacement. We have designed a "S-random" permutation method as follows: Each randomly selected integer is compared to S previously selected integers. If the current selection is equal to any S previous selections within a distance of $\pm$S, then the current selection is rejected. This process is repeated until all N integers are selected.

4.2.3 Turbo-code decoding

A complete turbo-code decoder structure corresponding to one iteration of the algorithm includes two component decoders, implementing a-posteriori probability, and interleavers/ deinterleavers, which scramble the processed data according to the interleaving laws used in the encoder. The turbo decoding configuration used in this paper is shown in Fig.7. By depuncturing, the origin output bits are recovered first. Because Turbo codes use two constituent encoders on differently ordered blocks of data,

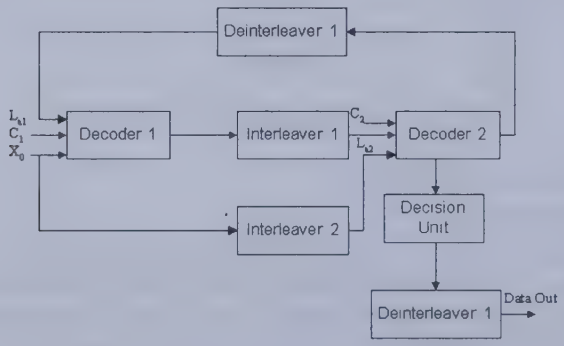

Fig. 7 The RSC turbo-code decoder structure

recovering the code directly from the received codewords is difficult. The Turbo-code decoder combines the parallel concatenated convolution codes (PCCC) with a two-stage iterative decoder block. The first stage performs a sequence detection using the received symbol and parity bit information from the first encoder, and calculates the maximum likelihood (ML) sequence of encoder states. From this sequence, the original symbol stream could be recovered with a deterministic function based on the encoder structure, but the important part of the decoder is that the first stage also passes along "soft" information, La_2, that specifies the confidence in that decision. The second stage performs the same ML detection on the interleaved data, but it now has the "extrinsic" data to help skew the results toward the

ML path from the first stage. If a symbol has been detected with high confidence in the first stage, the second stage is predisposed to make the same decision. Consider the case where the first stage has a low confidence and an incorrect symbol decision, and the second stage has a high confidence with the correct symbol. The second stage, with its high confidence, will reverse the first symbol decision, and since its "soft" information is passed back to the first stage, the iterative approach will converge to the ML path and the correct bit decisions. The Turbo code performance is not very high after the first iteration, but after several stages it converges to the low BER. If no further refinements are desired, a deinterleaver delivers the final output and passes it to the data sink.

5 Conclusion

Hydroacoustics provides the only way of underwater wireless communication. The condition that data communicate in the underwater acoustic channels is very bad. Its propagating carrier is the acoustic wave that has a low transmission velocity. So, for our modulation approach, error correction codes and source codes, it needs a special method. We use the high-speed DSP, introduce the mature MFSK way for modulation and utilize the latest Turbo Code for error-correcting codes. All of these methods prove to be practical in our experiments. Summarizing these research achievements, we find their common characteristic is to apply software for implementation as much as possible. Not only the Turbo Code, but also are MFSK modulation and demodulation implemented by software. They make our communication device as miniaturized and intelligent as possible.

Reference

[1] Texas Instruments (1997) TMS320C54X DSP Reference Set.

[2] John G. Proakis (1998) Digital Communications (Third Edition). WCB McGraw-Hill.

[3] Behrouz Forouzan (1998) Introduction to Data Communications and Networking. WCB McGraw-Hill.

[4] Daniel B, Kilifoyle, Arthur B.(2000) The state of the art in underwater acoustic telemetry. *IEEE Journal of Oceanic Engineering*, **25** (1):4-27.

[5] Proakis J G, Biglieri E, Shamai S.(1998) Fading channels: information-theoretic and communications aspects. *IEEE Trans. Information Theory* . 44:2619-2692.

[6] C Berrou, A Glavieux, and P Thitimajshima (1993) Near shannon limit error-correcting coding and decoding: turbo-codes. *Proceedings of ICC 93*, 5:1064-1070.

[7] Hagenauer J., Hoeher P. (1989) A Viterbi algorithm with soft-decision outputs and its applications, Proc IEEE Globecom Conf, 11:1680-1686.

[8] Benedetto S., Montorsi G., *et al.* (1996) Soft-output decoding algorithms in iterative decoding of turbo codes. TDA Progress Report, 2:63-87.

[9] Cheng En (2001) A method of coding and decoding in underwater image transmission. *Marine Science Bulletin.* **3** (2): 13-18.

Nitrogen and Phosphorus Diffusive Fluxes Across the Sediment-Water Interface in Estuarine and Coastal Tidal Flats

Liu Min (刘 敏), Hou Lijun (侯立军), Xu Shiyuan (许世远), Zhang Binliang (张斌亮), Ou Dongni (欧冬妮), Liu Qiaomei (刘巧梅)

Department of Geography, East China Normal University and Open Laboratory of Urban and Environmental Dynamic Process of the Ministry of Education, Shanghai 200062

Abstract Nitrogen and phosphorus contents are analyzed in the overlying waters and pore waters taken from the Changjiang Estuary and Shanghai coastal tidal flats in this study. In addition, the diffusion fluxes of nitrogen and phosphorus across the sediment-water interface in tidal flats are estimated according to the nutrient concentration gradients at the interface. It has been indicated that the concentrations of ammonium, nitrite, nitrate and dissolved phosphorus in overlying waters range from 0.0082~2.56, 0.03~0.58, 0.69~5.38 and 0.035~0.53 mg/L, respectively, while 0.0025~1.35 mg/L for NH_4^+-N, 0.0055~0.20mg/L for NO_2^--N, 0.61~1.14 mg/L for NO_3^--N and 0.11~0.53mg/L for DP insurface pore waters.The findings have revealed that ammonium, nitrite, nitrate and dissolved phosphorus diffusion fluxes across the sediment-water interface are between −0.024~0.99, −0.39~ −0.0019, −3.09~ −0.12 and −0.48~ 0.12 μg/ (cm^2·d) respectively, showing that the sediment in tidal flats is the source of phosphorus and an important sink for nitrogen in the waters.

Keywords Nitrogen and phosphorus, diffusion fluxes, pore waters, sediment-water interface, the Changjiang Estuary and coastal area

1 Introduction

N and P are essential to organisms in the aquatic ecosystem. Excessive nutrient inputs may cause water eutrophication. It is shown that parts of nutrient originate from the exchange between sediment and the overlying water[1,2]. The diffusive fluxes across the sediment-water interface play an important role in nutrient inputs. The estuarine and coastal zone as a land-ocean interactional region, is characterized by intense effects of natural and anthropogenic activities, where nutrient exchange and diffusion at the sediment-water interface have significant influences on the overlying quality[3].The present study is concerned with the concentrations of nitrogen and phosphorus at the sediment-water interface, and calculates the diffusion fluxes at the sediment-water interface.

Received on November 4, 2001

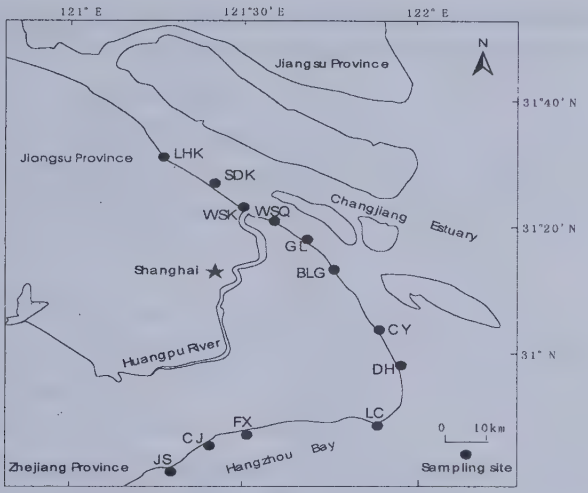

Fig. 1 Sampling sites along the Yangtze estuary and Shanghai coastal areas

2 Materials and Methods

2.1 Sample collection

The 13 sampling sites used to collect surface sediments and core samples from the Changjiang estuary and nearby coastal areas in August, 2000 are shown in Fig.1. And at the same time overlying water samples have been collected with high density polyethylene containers and filtered through 0.45 μg Millipore membrane filters in the laboratory. Pore water is extracted by centrifuging the sediment for 30 min at 4000rPm and 4℃.The pore water samples of surface sediments are then syringed and filtered through 0.45 μg filter membranes as above, acidified and stored at 4℃. The core sediments are extruded, sectioned at 1-cm intervals, and frozen. Pore water profile is derived from centrifuged core intervals. Sediment and pore water samples at sites LC, FX & CJ are not obtained because of storm condition, but overlying water at the coastal site is sampled.

2.2 Chemical analysis

The pore water samples for NH_4^+–N are immediately analyzed after sampling and extracting by the hypobromous oxidation method. The remaining samples are stored frozen at −20 ℃ and processed within 24h for NO_2^-–N and NO_3^-–N. NO_2^-–N is detected using the method of sulfanilamide and ethylene diamine hydrochloride solution, and NO_3^-–N with Zn–Cd reduction method. Inorganic nitrogen (IN) refers to the sum of the above three nitrogen components[4]. Dissolved phosphorus (DP) is detected spectrophotometrically as the phosphomolybdate blue complex[5] .The precision of these analyses is 10%. Dissolved oxygen (DO) of water is detected in situ with an oxygen electrode method.

Tab. 1 Nutrient contents in the overlying water from Changjiang Estuary and nearby coastal areas (mg/L)

Site	NH_4^+-N	NO_2^--N	NO_3^--N	IN	DP
LHK	0.28	0.030	0.86	1.17	0.28
LJ	0.031	0.041	2.03	2.10	0.18
SDK	0.077	0.076	0.71	0.87	0.071
WSK	0.45	0.58	5.38	6.41	0.53
WGQ	0.21	0.26	0.68	1.16	0.036
GL	0.16	0.31	1.71	2.18	0.071
BLG	0.38	0.12	2.77	3.28	0.18
CY	0.26	0.030	2.60	2.89	0.071
DH	0.0081	0.071	1.31	1.39	0.14
LC	0.29	0.11	3.25	3.64	0.11
FX	2.56	0.11	2.76	5.42	0.39
LJ	0.088	0.14	3.04	3.26	0.24
JS	0.34	0.041	4.09	4.47	0.18

Tab. 2 Nutrient contents in the surface pore water from Changjiang Estuary and Shanghai coast (mg/L)

Site	NH_4^+-N	NO_2^--N	NO_3^--N	IN	DP
LHK	1.35	0.027	1.03	2.41	0.53
LJ	0.0025	0.0055	1.14	1.15	0.11
SDK	0.0082	0.16	0.84	1.01	0.50
WSK	0.95	0.021	0.92	1.89	0.36
GL	0.95	0.0082	0.89	1.85	0.53
BLG	0.054	0.019	0.80	0.87	0.32
CY	0.43	0.20	0.86	1.50	0.30
DH	0.051	0.040	0.81	0.90	0.17
JS	1.71	0.033	0.61	2.36	0.36

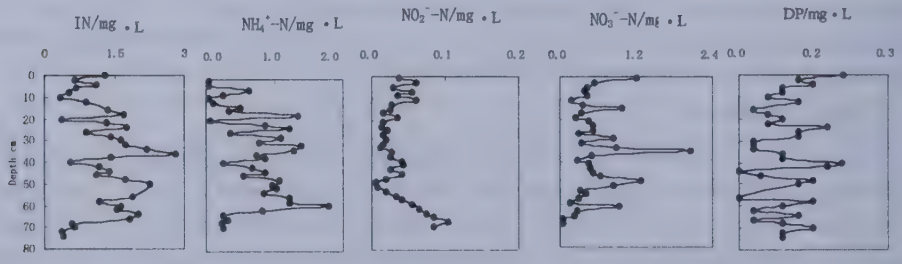

Fig. 2 Vertical distribution of nutrients in core pore water From the DH site with depth

(a: IN; b: NH_4^+-N; c : NO_2^--N; d : NO_3^--N; e: DP)

3 Results and Discussion

3.1 N and P concentrations in the overlying waters

The concentration of inorganic nitrogen in the overlying waters along coastal tidal flats from the Changjiang estuary range from 0.87~ 6.41 μg /mL with an average of 3.15 μg /mL given in Table 1.The distribution of inorganic nitrogen along the coastal areas reveals complex trends between sampling locations. Higher concentration levels are observed at sites LJ, WSK, BLG, FX and JS, and in particular 6.41 μg /mL at WSK.

NH_4^+-N concentrations vary between 0.0082 and 2.56 μg /mL, with a mean value of 0.39 μg /mL. Table1 indicates that the concentration of NH_4^+-N is typically low with the exception of only two sites, FX. and WSK. NO_2^--N, as an intermediate compound in nitrification (the oxidation of NH_4^+ to NO_3^-), is controlled by NH_4^+-N and NO_3^--N. The concentration of NO_2^--N varies from 0.030 to 0.58 μg /mL with elevated concentrations near WSK, suggesting active nitrification here. Nitrate concentrations of overlying waters range from 0.69~5.38 μg /mL with an average of 2.61 μg /mL, or occupying about 83% of the total nitrogen. The distribution pattern of nitrate for overlying water along coastal areas is similar to inorganic nitrogen with elevated values at sites LJ, WSK, BLG and JS.

The dissolved phosphorus (DP) of overlying waters varies from 0.035 to 0.53 μg /mL, with a mean value of 0.21 μg /mL. As with nitrogen species, the distribution of dissolved phosphorus is complex. Elevated concentrations are observed at LK, WSK, BLG and FX, with the highest value (0.53 μg /mL) at the site WSK.

3.2 N, P in pore waters

3.2.1 N, P in the interfacial pore waters

The distribution of N and P in interface pore waters near the sediment-water interface is listed in Table 2. Inorganic nitrogen ranges from 0.90~2.54 μg /mL, with a mean of 1.44 μg /mL, and is characterized by higher values at LHK, WSK, GL and JS. However, the range of concentrations for inorganic nitrogen is small compared to that in the overlying waters. The ammonia concentration in pore waters varies from 0.0025 to 1.35 μg /mL, with a mean of 0.51 μg /mL and similarly showing higher levels of concentrations at LHK, WSK, GL and JS. In contrast, nitrite concentration ranges from 0.0055 to 0.20 μg /mL, and the higher values are found at SDK and CY . Nitrate nitrogen ranges from 0.61~1.14 μg/ mL, averaged 0.87 μg /mL, and shows obvious spatial differences relative to the overlying waters.

The distribution of dissolved phosphorus in pore waters ranges from 0.11~0.53 μg /mL, with a mean of 0.32 μg /mL. Dissolved phosphorus concentration is elevated (e.g. at LHK, SDK and GL)

3.2.2 N and P in pore-water profiles

Nitrogen in pore water selected from the Donghai (DH) core profile, N and P concentrations in pore water profile have been analyzed (Fig.2). The concentration of inorganic nitrogen in the DH core ranges from 0.34~2.82 μg /mL, averaged 1.20 μg /mL. It shows that the total trend of inorganic nitrogen is characterized by decrease with depth. The reason could be that the inorganic nitrogen mainly originateds from mineralization of organic nitrogen. Thus the distribution pattern of inorganic nitrogen from the

pore water profile exhibits decrease with depth as above. Ammonia concentration ranges from 0.033~l. 79 μg /mL, averaged 0.66 μg /mL. The trend of ammonia shows increase with depth up to a depth of 64cm, and decrease with depth below 64cm. In general, the concentration level of ammonia nitrogen is mainly dependent on the sedimentary environment. Higher concentration levels occur under reduction environment[6]. The sedimentary environment in core profile shows relatively intensive reduction with depth. Thus the concentration of ammonia nitrogen is characterized by increase with depth. The significant finding is observed of a low concentration below the depth of 64cm. The reason may be the little amount of nitrogen input below the depth. The concentration of nitrate nitrogen ranges from 0.040~ 2.06 μg /mL, averaged 0.5l μg /mL. Fig.2 shows the distribution pattern of nitrate nitrogen in the pore water profile, suggesting decrease with depth. The concentration of nitrate nitrogen is closely related to the sedimentary environment. The oxidation environment is easily of nitrification production. The upper part of the core sediments has more intensive oxidation than the lower part. Therefore, the concentration of nitrate nitrogen in pore waters shows decrease with depth. The distribution of nitrite nitrogen ranges from 0.0054 ~ 0.10 μg / mL, averaged 0.035 μg /mL, showing decrease with depth in the core profile. Minimum nitrite concentration is at the depth of 50cm, only 0.0054 μg /mL. Below the depth, nitrite concentration shows again increase with depth. The characteristic feature of nitrite depth distribution is obviously controlled by nitrification-denitrification. Above the depth of 50cm the nitrite nitrogen in pore waters may originate from nitrification of ammonia nitrogen, while the nitrite nitrogen below the depth may result from denitrification of nitrate nitrogen.

The concentration of dissolved phosphorus in the pore water profile ranges from 0~0.21 μg /mL, averaged 0.088 μg /mL. It can be seen from Fig.2 that the concentration level is characterized by decrease with depth up to the depth of 50cm. Below this depth, its concentration shows increase with depth. This pattern of distribution could be related to the sedimentary environment, early diagenesis of organic phosphorus, and material exchange at the sediment-water interface[7].

3.3 N and P diffusive fluxes across the sediment-water interface

Nitrogen and phosphorus exchange in the sediment-water interface is an important process of material transport and accumulation in the aquatic ecosystem. The general exchange fluxes at the sediment-water interface is calculated with the following formula:

$F_{z=0} = F_d + F_a + F_s$

Where $F_{z=0}$ represents the net flux of a chemical species across the sediment-water interface, F_d is the flux due to molecular diffusion, $F_a + F_s$ is the flux due to advection of pore water. $F_a + F_s$ is small in comparison with the flux of molecular diffusion. Thus the above general flux equation can be expressed as Fick's first law listed below[8]:

$F_{z=0} \approx F_d = \phi \cdot D_s (dC/dZ)_{z=0}$

Where ϕ is porosity of sediment; D_s, is the whole-sediment molecular diffusion coefficient, and $(dC / dZ)_{z=0}$ is the concentration gradient across the sediment-water interface. Bulk sediment diffusion coefficients (D_s) are calculated from sea water values using $D_s = \phi \cdot D_0$ for $\phi < 0.7$, and $D_s = \phi^2 \cdot D_0$ for $\phi \geq 0.7$ where D_0 is diffusion coefficient in water at infinite dilution[8].

Tidal flat sediments in Changjiang estuarine and coastal areas consist of mainly silty mud, with the exception of LHK site composed of mud silt. Thus porosity at LHK site is given 0.65, and the remain given are 0.75. $(dC / dZ)_{z=0}$ is calculated with nutrient content difference between overlying water and

pore waters of surface sediments. Nutrient fluxes across the sediment-water interface in tidal flats are calculated with the first Fick's law (Table 3).

Tab.3 Nutrient fluxes across sediment-water interface in tidal flats($\mu g/cm^2 d$)

Site	NH_4^+-N	NO_2^--N	NO_3^--N	IN	DP
LHK	0.77	-0.0019	0.12	-0.44	-0.066
LJ	-0.02	-0.025	-0.62	-1.38	-0.019
SDK	-0.049	-0.057	-0.088	-0.26	0.11
WSK	0.36	-0.39	-3.09	-4.19	-0.48
GL	0.57	-0.21	-0.57	-1.14	0.12
BLG	-0.24	-0.073	-1.37	-2.05	0.038
CY	0.12	-0.12	-1.21	-1.80	0.061
DH	0.03	-0.022	-0.35	-0.84	0.0074
JS	0.99	-0.0057	2.41	-2.85	0.048

It has been shown from Table 3 that the flux of inorganic nitrogen ranges from $-4.19\sim -0.26\ \mu g/(cm^2 \cdot d)$, where negative fluxes represent diffusion direction from overlying water to sediments, reflecting that sediments are an important sink of inorganic nitrogen. Nitrate nitrogen is dominant in the diffusive fluxes of inorganic nitrogen, averagely occupying 62.84% of the total inorganic nitrogen. Most of ammonia nitrogen in tidal flats release from sediment into overlying water, while nitrate nitrogen diffuses from overlying water to sediment. The diffusive phosphorus diffusive flux varies from $-0.48\sim 0.12\ \mu g/(cm^2 \cdot d)$. Most fluxes show the diffusive direction from sediment to overlying water with the exception of LJ and WSK sites. The above shows that sediment is a sink for inorganic nitrogen and a source of phosphorus.

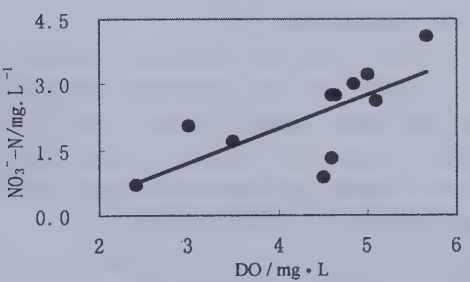

Fig. 3 The correlation between NO_3^--N and DO in overlying water

3.4 Discussion

Nitrogen and phosphorus external source inputs to the Changjiang estuary and Shanghai coastal zones are mainly from the Changiiang River runoff, coastal industrial and agricultural sewage discharges

etc. According to the distribution of overlying water inorganic nitrogen and total dissolved phosphorus, high N and P concentration levels at WSK site maybe result from the effects of the Huangpu River input. Higher N and P concentration at BLG site may be the influence of domestic sewage input from the Bailonggang sewage outlet. High N and P values are related to the local agricultural sewage discharge at FX site. The nearby coastal distribution of overlying water nitrate shows that the nitrate concentration is similar to the distribution of the local pollutant sources and related to environmental physical and chemical factors. Nitrate concentration has positive correlation coefficient with the dissolved oxygen level ($p = 0.05$). It is thus clear that the higher dissolved oxygen concentration facilitates the occurrence of nitrogen nitrification. In comparison, the sediment pore water changes in a more complex way, where N and P concentration levels are related to their inputs, and sedimentary environment and early diagenesis.

The exchange fluxes of inorganic nitrogen across the sediment-water interface show negative values, indicating that the sediment is a significant sink for nitrogen. The reason is probably the higher inputs in the flood season which result in a higher nitrogen concentration in the overlying water than in the pore water. Ammonium nitrogen concentration in most of the sampling sites diffuses from sediment into overlying water while from overlying water to sediment for nitrate due to the effects of sedimentary environment. The above result is similar to that in the previous report[2]. The phosphorus exchange flux at the sediment-water interface in tidal flats is of positive values. This maybe is because the higher temperature in summer is easy to produce for phosphorus early diagenesis. The diffusion for phosphorus from sediment to overlying water indicates that phosphorus release from sediments is an important phosphorus internal source.

4 Conclusions

The following conclusions may be drawn from this work:

(1) Nutrient spatial distribution is related to inputs and has differences between locations. Nitrate nitrogen is a dominant component in the dissolved inorganic nitrogen in the overlying waters, averagely occupying 82.61% of the total inorganic nitrogen.

(2) Dissolved inorganic nitrogen in pore water from surface sediments is characterized by nitrate and ammonia, averagely occupying 60.28% and 35.11% of the total inorganic nitrogen respectively. Percentage of nitrate nitrogen in pore water is smaller than that in overlying water, indicating that nitrate in pore water produces obvious denitrification. Ammonia in pore water profile increases, nitrate nitrogen decreases and dissolved phosphorus concentration increases with depth. It may be a result of the sedimentary environmental impact on the nutrient profile pattern.

(3) Nutrient fluxes (NH_4^+-N, NO_2^--N, NO_3^--N, DP) at the sediment-water interface in tidal flats are 0.28, −0.061, −1.04 and 0.043 μg /($cm^2 \cdot d$), respectively. It can thus be seen that NO_3^--N is the main component in exchanging across the sediment-water interface, and the second is NH_4^+-N. Nitrogen diffuses from overlying water to sediments, while dissolved phosphorus diffuses just in the opposite direction, showing that tidal flat sediments are an important pool for nitrogen and a significant source for phosphorus in the estuarine and nearby waters.

Acknowledgements

The work is supported by the National Natural Science Foundation of China (Grant Nos.430100203 and 49801018), and the Foundation for University Key Teachers by the Ministry of Education of China.

References

[1] Berner E K, Berner R A. (1987) The lake water cycle, geochemistry and environment. New Jersey, Engglewood Cliffs, Pretice Hall Inc, 190.

[2] Heinrich F K, Rodney A A, IANC B. (1985) Microbial nitrogen transformations in sediments and inorganic nitrogen fluxes across the sediment/water interface on the south island west coast, New Zealand. *Estuarine, Coastal and Shelf Science*, 21:245–255.

[3] Edward C, Douglas E.H. (1982) Nutrient exchange across the sediment-water interface in the Potomac river estuary. *Estuarine, Coastal and Shelf Science*, 15:395–413.

[4] Han Wuying, Rong Ronggui, Huang Xineng, *et al.* (1986) Handbook on investigation of seawater chemical elements. Beijing: China Ocean Press, 121–148.

[6] Xie Xianqun, Wang Lijun (1998) Determination and analysis of water environmental elements. China Standards Press, 56–57.

[7] Motimer R.J.G, Davey J.T, Krom M.D, *et.al.* (1999) The effect of macrofauna on pore water profiles and nutrient fluxes in the intertidal zone of the Humber Estuary. *Estuarine, Coastal and Shelf Science*, 48:683–699.

[8] Lerman A (1979) Geochemical process: water and sediment environments. John Wiley & Sons Inc.

Seasonal Cycle Analysis of the Nitrate Nitrogen and Nitrite Nitrogen in the Bohai Sea

Shi Qiang (石 强), Chen Jianglin (陈江麟), Li Chongde (李崇德)
North Sea Branch of SOA, Qingdao 266033

Abstract During 1985~1987, the concentration of nitrate nitrogen was higher in the Laizhou Bay and the Bohai Bay while that of nitrite nitrogen was higher in the Liaodong Bay and the Bohai Bay. The concentration of nitrate nitrogen was highest in winter and lowest in summer while that of nitrite nitrogen was highest in autumn and lowest in spring. The seasonal variation of the concentration of nitrate nitrogen was maximum in the Laizhou Bay and the Bohai Bay while that of the concentration of nitrite nitrogen was maximum in the Liaodong Bay. There was a great difference in the concentration of nitrate nitrogen between the surface and the bottom in autumn and in the concentration of nitrite nitrogen between the surface and the bottom in summer. The main reason for the seasonal variations of the concentration of nitrate nitrogen and nitrite nitrogen was the marine biochemical process. The nitrate nitrogen and nitrite nitrogen in the Bohai Sea basically maintained a quasi-equilibrium state seasonal cycle. The quasi-equilibrium state seasonal cycle of nitrate nitrogen and nitrite nitrogen at the bottom was stable while that at the surface was liable to variations caused by other factors.

Keywords Nitrate nitrogen, nitrite nitrogen, quasi-equilibrium state, seasonal cycle, Bohai Sea

Introduction

The inorganic nitrogen is an important nutrient substance in seawater and one of the basic nutrients for marine phytoplankton. Nitrate nitrogen and nitrite nitrogen are a non-conservitive matter, which may participate in the nutrient cycle in the marine ecosystem. Such chemical and biological processes as intake of marine organisms, nitrification, remineralization, excretion of zooplankton, decomposition of organic debris, photoreduction as well as burial and regeneration of inorganic nitrogen in the sediment, etc. all affect the change in the concentration of nitrate nitrogen and nitrite nitrogen. Therefore, the distribution of the concentration of nitrate nitrogen and nitrite nitrogen in the ocean is the result of the combined action of the biological, chemical and physical processes.

Based on the Bohai Sea sectional data during 1985~1987, this paper makes an analysis of the seasonal time and space distribution and cycle of the concentration of nitrate nitrogen and nitrite nitrogen in the sea water of the Bohai Sea. As the analysed data were taken in the period when the level of eutrophication in the Bohai Sea was relatively low, the analytical results are of significance for reference in studying the "normal" seasonal cycle process of nitrate nitrogen and nitrite nitrogen in the

Received on November 19, 2001

Bohai Sea, evaluating the level of eutrophication in the Bohai Sea and improving the eco-environment of the Bohai Sea.

1 Survey Data and Methods of Analysis

The analyzed data are taken from the surface and bottom observations of the concentration of nitrate nitrogen (NO_3-N) and nitrite nitrogen (NO_2-N) in the seawater of the surveyed sections in the Bohai and Huanghai Seas during 1985~1987. The survey months are February, April, May, June, August and November in 1985 and 1987 respectively, and January, April, May, June, August, September and November in 1986, totalling 19 months in 3 years. The instrument for analysis is the marine spectrophotometer and the methods of analysis follow the provisions in the Marine Survey Norms of the State Oceanic Administration. (See Fig.1 for the locations of survey stations). Although the survey stations are sparsely distributed in part of the sea area (for example, the Bohai Bay and Laizhou Bay waters) and can not reflect the variations of NO_3-N and NO_2-N in some littoral waters accurately, the survey data are still of significance to the discussion on the cycle process of NO_3-N and NO_2-N in the entire Bohai Sea waters.

We calculate the observations of concentration of NO_3 -N and NO_2 -N at each station site in every month to the grid points covering the studied sea area for analysis by applying the multi-conicoid method for objective analysis based on the radius base function.

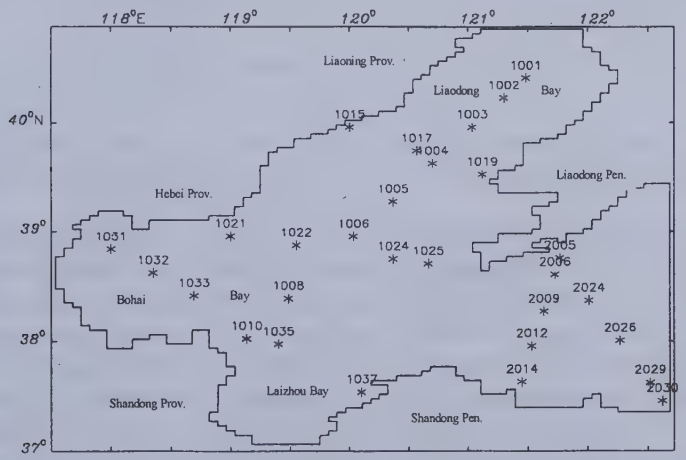

Fig. 1 Locations of observation stations in the Bohai Sea

2 Seasonally Mean Spatial Distribution of the Concentrations of Nitrate and Nitrite

2.1 NO_3-N

NO_3-N in the seawater is a stabilized form in the inorganic nitrogen of the compound (in thermodynamics). Without considering the input of NO_3-N from land, the variation of the NO_3-N

concentration in the seawater is mainly resulted from the biologically active reaction, so the space-time distribution of NO_3-N may be taken as a good index reflecting the distribution and variation of the biological activity[5].

The high-value area of the mean NO_3-N concentration in the Bohai Sea in spring is located along the coast of the Huanghe River delta and the low-value area in the middle of the Bohai Sea (Fig.2); In summer, the high-value area is from the Bohai Bay to the Huanghe River mouth (Fig.3); In autumn, the high-value area is found between the Bohai Bay and the Laizhou Bay and the secondary high-value zone near the Liaohe River mouth (Fig.4); In winter, the high-value area is located between the Bohai Bay and the Laizhou Bay (Fig.5).The mean NO_3-N concentration in the studied sea areas is highest in winter and lowest in summer (with the figure omitted).This seasonal feature of the horizontal distribution of NO_3-N concentration is related to the breeding and feeding of marine biota, the release of NO_3-N in the sediment to the waters and the discharge of land runoff into the sea.

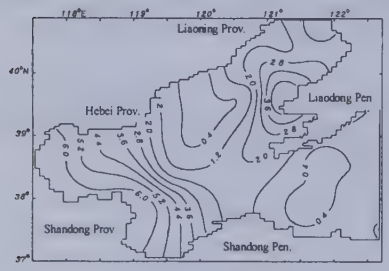

Fig. 2 Mean concemtrations of nitrate nitrogen at the bottom of the Bohai Sea in spring (μ mol/L)

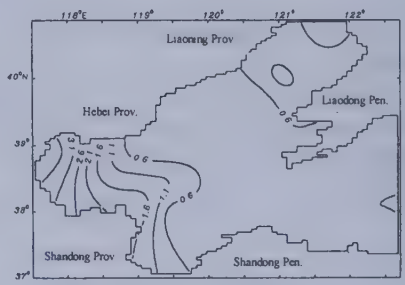

Fig. 3 Mean concentrations of nitrate nitrogen at the bottom of the Bohai Sea in summer (μ mol/L)

In the bottom of the shallower sea area, biocoenose is an important regeneration source of inorganic nitrogen [6]. In winter and spring, the vertical convection in the ocean is strong and the concentrations of NO_3-N at the surface and bottom layers are basically the same; In summer and autumn, the vertical stratification in the ocean water is obvious and the interior vertical in the ocean is checked. In the meantime, the solar radiation is intense and NO_3-N in the surface layer is subjected to the photo-reduction reaction, which results in NO_2-N [5]; The phytoplankton in the surface propagates and takes in NO_3-N in great amount, thus lowering the concentration of NO_3-N in the surface. In the bottom layer, due to the rising water temperature, the regeneration rate of NO_3-N in the bottom algae sediment as well as between the sediment water interface is accelerated and NO_3-N diffuses into the water body, as a result of which, the concentration of NO_3-N in the bottom of the Baohai Sea in summer and autumn is larger than that in the surface.

2.2 NO_2-N

The concentration of NO_2-N in seawater is usually lower than that of other forms of inorganic nitrogen compound. The horizontal distribution of the concentration of NO_2-N is somewhat different from that of NO_3-N: In spring and summer, the high-value area of the concentration of NO_2-N is in the waters of the Bohai, Laizhou and Liaodong Bays, in autumn, it is in the sea area of the Liaodong Bay

and in winter, it is near the east coast of the Laizhou Bay. The horizontal distribution of NO_2-N concentrations is also affected by the runoff into the sea, and the NO_2-N concentration in the Bohai in summer and that in the sea area of the Liaodong Bay in autumn are highest (Fig. 6~9).

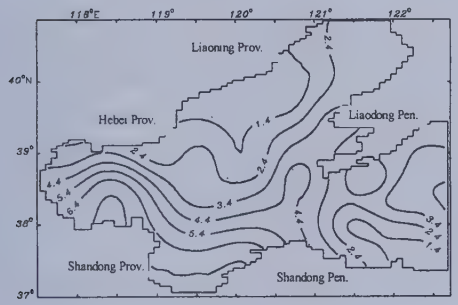

Fig. 4 Mean concentrations of nitrate nitrogen at the bottom of the Bohai Sea in autumn (μmol/L)

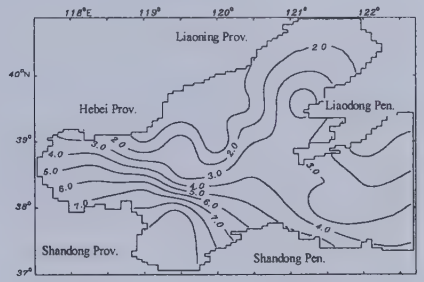

Fig. 5 Mean concentrations of nitrate nitrogen at the bottom of the Bohai Sea in winter (μmol/L)

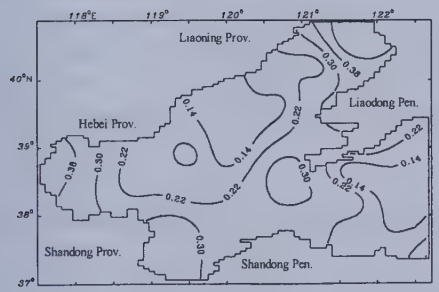

Fig. 6 Mean concentrations of nitrate nitrogen at the bottom of the Bohai Sea in spring (μmol/L)

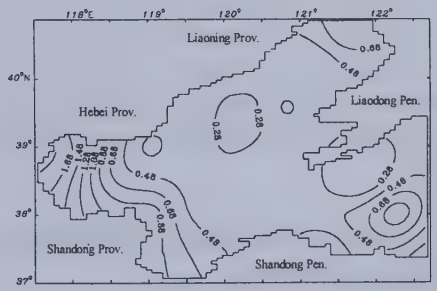

Fig. 7 Mean concentrations of nitrite nitrogen at the bottom of the Bohai Sea in summer (μmol/L)

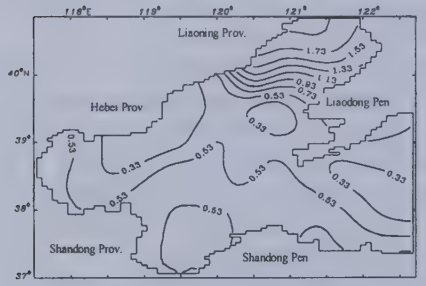

Fig. 8 Mean concentrations of nitrite nitrogenat the bottom of the Bohai Sea in autumn (μ mol/L)

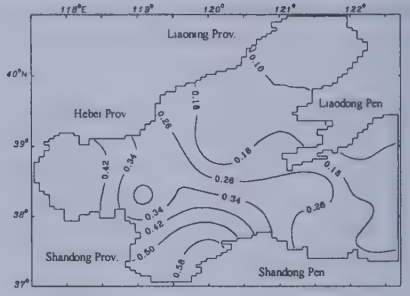

Fig. 9 Mean concentrations of nitrite nitrogen at the bottom of the Bohai Sea in winter (μ mol/L)

As an intermediate oxidation state between NH_4–N and NO_3–N, NO_2–N may be regarded as a transitional form of NH_4–N oxidation or NO_3–N reduction. In the ocean, these two reactions are mainly activated by the biological effect[5]. Therefore, the concentration of NO_2–N in seawater is higher in summer and autumn when the biological activity is exuberant while it is lower in winter and spring when the biological activity is not vigorous.

Under natural conditions, the NO_2–N in sea water seems not liable to further photoreduction[10], and in the sediment the exchange effect of NO_2–N with the water body is not significant[7]. Consequently, the vertical distribution of the NO_2–N concentration in seawater is mainly influenced by the activity of convections within the ocean. In spring and winter when the convective activity is strong, there is less difference in the concentration of NO_2–N between the surface and bottom layers while in summer and autumn when the convective activity weakens, there is greater difference between the surface and bottom layers.

3 Analysis of the Space-Time Characteristics of the Seasonal Cycle of Nitrate and Nitrite Concentrations.

The biological, chemical and physical processes affect the seasonal cycle of inorganic nitrogen in the Bohai Sea. To find out about the space-time characteristics of seasonal cycle of nitrogen in the Bohai Sea, we have made an analysis by applying the EOF method, which has found many applications in analyzing the annual and seasonal variations of primary productivity as well as in the field of ecology[2-4].

First of all, the analytical date which are evenly distributed over the 54 station locations of the analysed sea area are extracted according to the order of observations (with the figure omitted) to form 54 data sequences, for each of which the second-order Shapiro ideal low-pass filtration is carried out five times[8], to reduce the noise interference and finally to make the EOF analysis .We apply the N rule similar to that in Reference[10] to make the judgement: The first and second characteristic vectors

(EVE_1, EVE_2) and the principal components (PC_1, PC_2) of NO_3–N at the surface and bottom and NO_2–N at the bottom as well as the first eigenvector (EVE_1) and the principal component (PC_1) of NO_2–N at the surface are of geochemical significance. We now make an analysis of these eigenvectors.

3.1 NO_3–N

Fig.10 shows the first eigenvector of NO_3–N concentration (EVE_1) at the bottom of the Bohai Sea. The EVE_1 distribution of NO_3–N concentration at the surface is very similar to that at the bottom. It is known from analyzing Fig.10 that the concentration of NO_3–N in the Bohai Sea is in its entirety dominated mainly by the iso-phase seasonal variations, with the maximum variation in the central sea areas of the Laizhou Bay and Bohai Bay and the minimum variation in the middle of the Bohai Sea and along the coast of western Liaoning. The growth of phytoplankton, bacteria and algae needs to take in NO_3–N and Laizhou and Bohai bays in summer are the high-value sea areas in terms of the number and density of phytoplankton and the primary productivity[11-14], which indicates that the marine biochemical process is a main factor contributing to the seasonal variations of NO_3–N in the sea water.

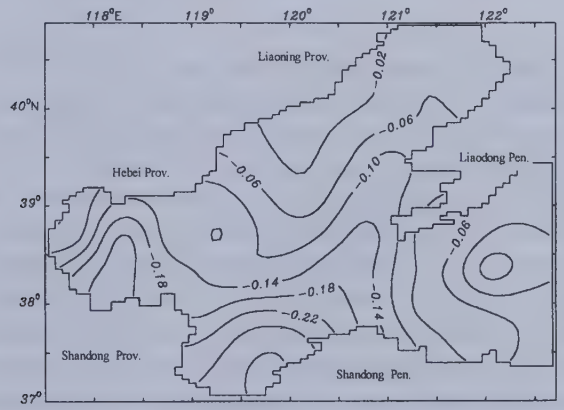

Fig. 10 First eigenvector (EVE_1) of NO_3–N concentration at the bottom of the Bohai Sea (62%)

Fig.11 shows the second eigenvector (EVE_2) of the NO_3–N concentration at the bottom of the Bohai Sea. Analysis of the figure indicates that there exists a process of the NO_3–N in the Bohai Sea exchanging with that in the Huanghai Sea, which affects the distribution of NO_3–N in the Bohai Bay and the middle of the Bohai Sea, with its main influence found in the Bohai Bay. Moreover, the variation of NO_3–N caused by the exchange process is in opposite phase with the variations in the Laizhou and Liaodong Bays. It is thus inferred that the water exchange between the Huanghai and Bohai Seas plays an important role in regulating the distribution of NO_3–N in the Bohai Bay and the middle of the Bohai Sea. The large amount of NO_3–N input by the Huanghe River runoff makes the seasonal variation of NO_3–N distinct off the Huanghe River mouth. The EVE_2 magnitude distribution of NO_3–N concentration at the surface is similar to that at the bottom (with the figure omitted), but the magnitude symbol is

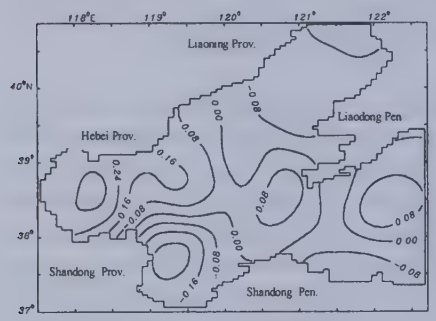

Fig.11 Secord eigenvector (EVE_2) of NO_3-N concentration at the bottom of the Bohai Sea (21%)

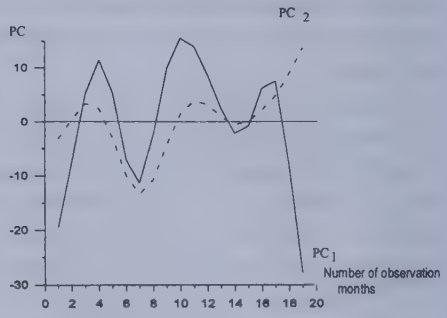

Fig. 12 Principal component of NO_3-N concentration at the bottom of the Bohai Sea

opposite to that at the bottom. This shows that the concentration of NO_3-N at the bottom contains the variation component in opposite phase, especially in the sea areas of the Laizhou, Bohai and Liaodong bays where the magnitude of NO_3-N variation is greater. The reason for this is that the stratification of seawater in summer weakens the vertical convection in the water body and that the intake of NO_3-N by the surface phytoplankton during its breeding causes the concentration of NO_3-N at the surface to drop. According to the Arrhenius equation, the regeneration rate of inorganic nitrogen in the sediment and between the sediment water interfaces increases with temperature at an exponential rate[7]. Due to the rising water temperature, the regeneration process of the bottom algae and the NO_3-N in the sediment and between the sediment water interfaces is active, thus causing the concentration of NO_3-N at the bottom to rise. In winter, the water temperature drops, which weakens the regeneration process of the bottom algae and the NO_3-N in the sediment and between the sediment water interfaces. The vertical convection in the water body strengthens the transport of NO_3-N at the bottom to the surface, thus resulting in the variations of NO_3-N at the surface and bottom in opposite phase.

As for the variations of principal components, in the first 17 months, PC_1 and PC_2 of NO_3-N at the bottom vary in phase, presenting the single peak variation each year while in the last two months, the variations are in opposite phase (Fig.12). PC_1 of NO_3-N at the surface and bottom and PC_2 of NO_3-N at the bottom present the in-phase single-peak variation annually. PC_2 of NO_3-N at the surface does not have the characteristic of single-peak variations annually (with the figure omitted), i.e., PC_1 of NO_3-N at the surface and PC_1 of NO_3-N at the bottom present the variation of the quasi-equilibrium state cycle. It is concluded from analysis of the above that, during 1985~1987, in the studied sea area, NO_3-N basically presented the variation of the quasi-equilibrium state seasonal cycle, the quasi-equilibrium state seasonal cycle at the bottom is stable and the seasonal cycle at the surface is liable to variation due to the influence of other factors. As eutrophication in the studied sea area was accelerated, in the last two months in the period of analysis, the sequence picked up speed in deviating from the equilibrium position and the quasi-equilibrium state seasonal cycle showed the sign of being disrupted.

3.2 NO_2–N

Fig.13 shows EVE_1 of NO_2–N concentration at the bottom of the Bohai Sea. The high-value area is in the Liaodong Bay and the magnitudes of EVE_1 are of the same symbol. Based on analysis of Fig.13, it is found that the NO_2–N concentration at the bottom of the Bohai Sea is dominated in its entirety by the in-phase seasonal variation and that the magnitude of variation is greatest in the Liaodong Bay and smaller in other sea areas. Compared with Fig.11, the sea area in Fig.13 with great change of NO_2–N is just the sea area in Fig.11 with small change of NO_3–N, which indicates that the sea area features for the NO_2–N variation in the studied sea area are not in conformity with those for NO_3–N.

Fig.14 shows EVE_2 of NO_2–N concentration at the bottom of the Bohai Sea. The high-value area is in the Laizhou Bay, and the magnitude of EVE_2 is negative in the Liaodong Bay while it is positive in the other sea areas of the Bohai Sea. Based on the analysis of Fig.14, it is concluded that the NO_2–N concentration in the Liaodong Bay fluctuates within a wide range mainly due to the effect of the discharge of coastal runoff. In the middle of the Bohai Sea, the feature of NO_2–N in the bottom water exchanging with that in the Huanghai Sea is more distinct.

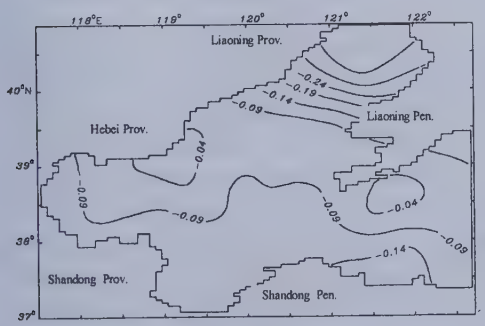

Fig.13 First eigenvector (EVE_1) of NO_2–N concentration at the bottom of the Bohai Sea (58%)

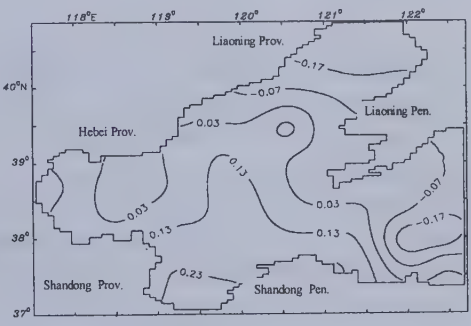

Fig.14 Second eigenvector (EVE_2) of NO_2–N concentration at the bottom of the Bohai Sea (24%)

For the variation of principal components, in the first 17 months of the period of analysis, PC_1 of NO_2–N at the surface and bottom presents the variation of the quasi-equilibrium state seasonal cycle with the single-peak variation within the year and, compared with PC_1 of NO_2–N at the surface and bottom, it presents a variation in opposite phase while PC_1 and PC_2 at the surface vary in opposite phase. In the last 2 months of analysis, PC_1 of NO_2–N at the surface and bottom showed the signs of quasi-equilibrium state cyclicvariation (Fig.15). To sum up, during the first 17 months of analysis,NO_2–N at the surface and bottom of the studied sea area basically presented the variation of the quasi-equilibrium state cycle. The main part (PC_1) of the variation is controlled by the reduction of NO_3–N (or NH_4–N oxidation) and the input of inorganic nitrogen in the land runoff only affects small part of the NO_2–N variation. In the last 2 months of the period of analysis, the quasi-equilibrium state cycle of NO_2–N at the surface and bottom showed the signs of variation. (The sequence has deviated from the equilibrium position).

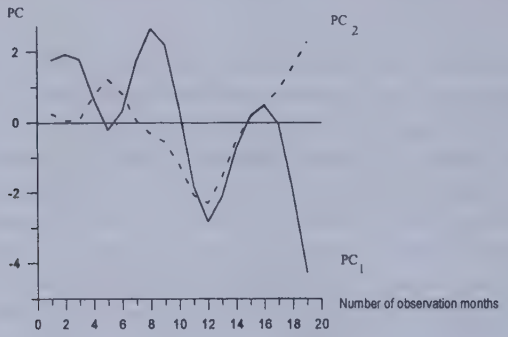

Fig. 15 Principal component of NO_2–N concentration at the bottom of the Bohai Sea

4 Conclusions

The Laizhou Bay and Bohai Bay are the sea areas with higher concentration of NO_3–N while the Liaodong Bay and Bohai Bay are the ones with higher concentration of NO_2–N. The seasonal variations of the nitrate nitrogen and nitrite nitrogen are distinct in the studied sea areas. The concentration of NO_3–N is highest in winter and lowest in summer; the concentration of NO_2–N is highest in autumn and lowest in spring. In the studied sea area, there is greatest difference in the mean concentration of NO_3–N between bottom and surface in autumn and greatest difference in the mean concentration of NO_2–N between bottom and surface in summer. The exchange of water bodies between the Huanghai Sea and the Bohai Sea exerts influence upon the distribution of NO_3–N concentrations in the Bohai Bay and the middle of the Bohai Sea. The seasonal variations of the NO_3–N concentration are maximum in the sea areas of the Laizhou Bay and the Bohai Bay and the seasonal variations of the NO_2–N concentration are maximum in the Liaodong Bay.

EOF analysis indicates that the marine biochemical process is the primary reason for the seasonal variation of the concentration of nitrate nitrogen and nitrite nitrogen in the Bohai Sea while the input of land runoff and the water exchange between the Huanghai and Bohai Seas are the secondary cause. Although in the early 1980s, there already occurred eutrophication in the Bohai Sea and the concentration of inorganic nitrogen increased gradually[1], for most time between 1985 and 1987, the nitrate nitrogen and nitrite nitrogen in the studied sea area basically maintained a quasi-equilibrium state seasonal cycle. Due to acceleration of eutrophication in the Bohai Sea, since September, 1987, the quasi-equilibrium state seasonal cycle of nitrate nitrogen and nitrite nitrogen has shown signs of being disrupted.

References

[1] WeiXiuhua Tong Jun'an and Li Yongqi (1993) Pollution condition in the Huanghai and Bohai Sea areas and its effect on ecology. *Huanghai and Bohai Seas Marine Science*, **11**(3): 76–82.

[2] Jassby A.D. and Powell T.M. (1990) Detecting changes in ecological time series. *Ecology*, 71: 2044–2052.

[3] Jassby A.D., Goldman C.R. and Powell T. M. (1992) Trend, seasonality, cycle, and irregular fluctuations in primary productivity at lake Tahoe. California Nevada, USA. *Hydrobiologia*, 246: 195–203.

[4] Jassby A.D. and Powell T.M. (1994) Hydrodynamic influences on interannual chlorophyll variability in an estuary: upper San Francisco Bay-Delta (California, USA). *Estuarine, Coastal and shelf Science*, 39: 595–618.

[5] Reilly J.P. and Skiro G. (1982) Chemical Oceanography, Vol. II , Beijing: Ching Ocean Press.

[6] Harrison W.G. (1980) Nutrient regeneration and primary production in the sea. In: Primary production in the sea (P.G. Falkowski, editor). Plenum Press, New York, 411–458.

[7] Valklump J. and Martens C.S. (1983) Benthic nitrogen regeneration. In: Nitrogen in the marine environment (D. Capone and E. Carpenter, editors). Academic Press, New York, 411– 458.

[8] Shapiro. R. (1970) Smoothing, filtering and boundary effects. *Rev. of Geophys and Space Phys.* 8: 359–387.

[9] Preisendorfer R. W. and Barnett T.P. (1977) Significance tests for empirical orthogonal functions. Fifth Conf. Probability and Statistics in Atmospheric Sciences. Las Vegas, Amer. Meteor. Soc., 169–172.

[10] Overland J.E. and Preisendorfer R.W. (1982) A significance test for principal components applied to a cyclone climatology. *Mon. Wea. Rev.* **110** (1): 1–4.

[11] Yu Jianluan and Li Ruixiang (1993) Research on phytoplanktonic ecology in the Bohai ad Huanghai Seas, *Huanghai and Bohai Seas Marine Science*, **11** (3): 52–59.

[12] Fei Zunle, Mao Xinghua, *et al.* (1991) Research on productivity in the Bohai Sea. *Marine Fisheries Research*, (12): 55–69.

[13] Kang Yuande (1991) Quantity distribution and seasonal variation of phytoplankton in the Bohai Sea. *Marine Fisheries Research*, (12): 31–54.

[14] Zhu Mingyuan, Mao Xinghua *et al.* (1993) Chlorophyla and primary productivity in the Huanghai Sea area. *Huanghai and Bohai Seas Marine Science*, **11** (3): 38–51.

Study of Adsorption Isotherm Curves of Amino Acids on the Kaolinite

Liu Xiaolan (刘效兰)[1], Zhang Zhengbin (张正斌)[2]

1 *College of Chemical and Environmental Engineering, Beijing Technology and Business University, Beijing* 100037

2 *Institute of Marine Chemistry, Ocean University of Qingdao, Qingdao* 266003

Abstract This paper studies the adsorption isotherm curves of four amino acids (glycine, aspartic acid, glutamic acid and lysine) and the effects of existences of different concentrations of Cu(Ⅱ) on them. Both the adsorption isotherm of the amino acids on the kaolinite and that when the copper ion Cu (Ⅱ) exists belong to the Langmuir type. The slopes of these adsorption isotherm increase with the increasing concentrations of Cu(Ⅱ) added. It can be explained in terms of formation of the type(Ⅰ) ternary surface complexes in these systems. The regular pattern of the effects of copper ion Cu(Ⅱ) on the adsorption isotherm of amino acids on the kaolinite is identical with that of its effects on the exchange and adsorption percentage E (%)–pH on the kaolinite in the same system.

Keywords amino acids, kaolinite, copper ion Cu(Ⅱ), adsorption isotherm

1 Introduction

The study on the adsorption of organic matter on the solid particles and its regular pattern is one of the important components in the research on the seawater chemical model as well as the liquid-solid interface theory and its application in seawater chemistry[1~3]; and closely related to some researches in the fields of marine biology and marine environment. The research in this aspect is now far from adequate mainly due to the two major difficulties: ①Analysis of the organic matter in the natural water is more complicated and especially the detection of trace organic matter is rather difficult; ② The research on the interaction between the organic matter and the solid particles has fallen short of a complete description due to the numerous factors affecting adsorption and the greater variety of marine organic matters. The past researches mainly involved those on the organic matter of biological significance, such as organic acid, amino acid, saccharide, humic matter, etc. as well as that on the organic matter in the environmental pollutants[4] in recent years, among which the most typical is the research on amino acids. However, few researches have been made on the adsorption of amino acids and the effects of metal ions on the adsorption[2,3,5], especially the research on the isotherm. Therefore, this paper has chosen one of the main components of solid particle and sediment in the ocean—the kaolinite and made a preliminary study on the adsorption isotherm of amino acids on the kaolinite and the effects of copper ion Cu(Ⅱ).

Received on November 8, 2001

2 Experimental Part

2.1 Instrument

Model 985 pH meter; Model D/Mex/ γ B X-ray diffractometer; large-scale reciprocating thermostatic oscillator; Model M850 fluorospectro-photometer.

2.2 Materials and formula for processing

The materials include the glycine biochemical reagent and the chemically clean phthalic formaldehyde, and the water used for compounding the reagent is the secondary distilled deionized water. The glass apparatuses for use in the experiment need to be immersed in the dilute alkal liquor (0.1N NaOH) for 12 hours before use, after which they are cleaned with the running water and the distilled water respectively, and then oven-dried for use. The water for use in the experiment is taken from the sea water in the Lushun Park of Qingdao at the flood time and, after aging, is filtered with a 0.45 μm membrane filfer and then sterilized with the ultraviolet lamp before use. The salinity of the water is 31.85. Taken from the natural kaolinite ore of Suzhou, the clay kaolinite is purified and modified according to the methods in the References, and then 40～80 mesh are taken to be used. The analytical result of the purified clay upon α-ray diffraction is that the kaolinite accounts for 77% and the quartz 23%.

2.3 Experimental methods

2.3.1 Isotherm

Weigh 0.1000 ± 0.0002g solid adsorbent with an andlytical balance and put it in a 250 mL ground V-beaker and add into it a certain amount of filtered seawater and solution so that the organic compounding concentration may increase in seriation and the total volume of solution reach 100 mL. Use sodium hydroxide and hydrochloric acid solution to accurately control the pH value and metal ion concentration of the solution. Under 25.0 ± 0.5 ℃ the thermostat oscillation reaches the equilibrium. Measure the concentration of the amino acid in the balance solution upon filtration, calculate the adsorbance and plot the isotherm.

2.3.2 Analytical method

The phthalic formaldehyde fluorescence method is applied to measure the concentration of amino acid.

2.3.2.1 Solvent compounding

A. Buffer solution: 0.4M boric acid buffer solution. 24.7g analytically pure boric acid is weighed and dissolved in the distilled water. The solution is adjusted to pH=9.50 ± 0.02 by using 1 N NaOH and diluted to 1 litre.

B. Buffer reagent: 0.4000g phthalic formaldehyde is weighed and dissolved in 4 mL anhydrous ethyl alcohol. Add the buffer solution and 0.5mL analytically pure 2-sulfhydryl ethyl alcohol ($HSCH_2CH_2OH$) and use this buffer solution to the constant volume of 200mL. This buffer reagent may be available for use one hour after its compounding.

2.3.2.2 Measurement of amino acid

Take 5.0mL sample solution and put it into a 25 mL colorimetric cylinder and add 5.0mL buffer

reagent as prepared above and oscillate it for full hybrid reaction. Measure its fluorescent intensity (F_s) during the maximum fluorescence generating time at the optimum excitation wave length (E_x) and the optimum emission wave length (E_m). Measurement of the blank value of the reagent refers to the measurement of fluorescent intensity under identical conditions by using the seawater sample without the addition of amino acid reagent.

2.3.2.3 Working curve and adsorption curve

Working curve:

Take treated seawater to compound the standard solutions of glycine, aspartic acid, glutamic acid and lysine at different concentrations, measure their maximum fluorescent intensities within their respective fluorescent intensity stablizing time according to the above-mentioned methods, and plot their calibrated working curves respectively.

The results of calculation:

Amino acid concentration in the water sample

$C\ (\mu mol/L)=(F_S - F_B)\ F$

The E_x, E_m values of the four amino acids may be obtained respectively through wavelength scanning; F is the calibrated working curve slope, which may be calculated with the least square method.

Adsorption curve:

Add a certain amount of amino acid and the treated seawater to several V-beakers with clay which has been weighed, put them in the oscillator for thermostat oscillation, take samples for filtration at different time, measure the content of amino acid in the balance solution and then plot Fig.1 and Fig.2.

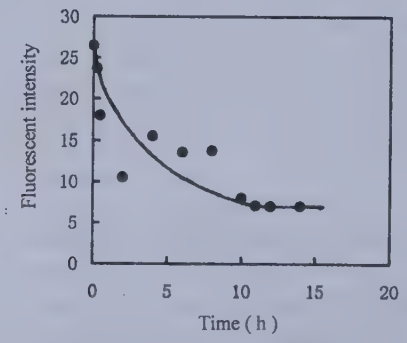

Fig. 1 Adsorption curve of Gly. with time on kaolinite

It may be known from the above adsorption curve that after 11 and 12 hours' oscillation for glycine and aspartic acid, respectively, their adsorption may reach equilibrium. For the same reason it may be found that glutamic acid and lysine may reach their adsorption equilibriam after 10 hours' oscillation.

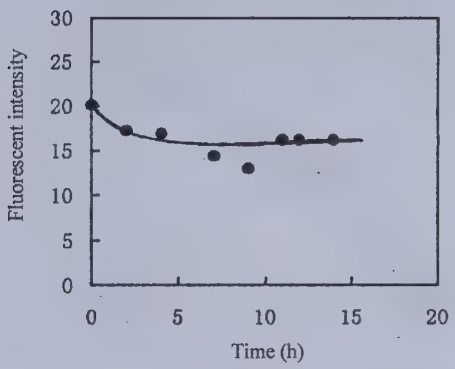

Fig. 2 Adsorption curve of Asp. with time on kaolinite

3 Experimental Results and Discussion

3.1 Experimental results

The adsorption isotherms of glycine, aspartic acid, glutamic acid and lysine in sea water on the kaolinite and the effects of metal copper ion on their isotherms are as shown in Figs. 3, 4, 5and 6 respectively.

It can be seen from the figures that the adsorption isotherms of various amino acids on the kaolinite are basically linear; After the copper ions have been added, with the increase of copper ion concentrations, the corresponding isotherm slope also increases and so does the adsorbance, and the various isotherms are basically also the linear-type ones.

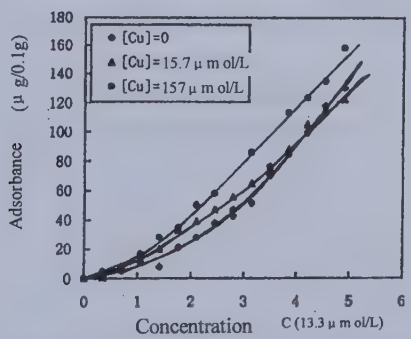

Fig. 3 Adsorption isotherm of Gly. on kaolinite

pH=7.89 ±0.05

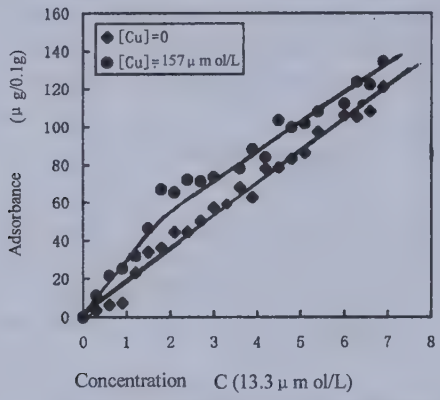

Fig. 4 Adsorption isotherm of Asp. acid on kaolinite

pH=7.70 ±0.05

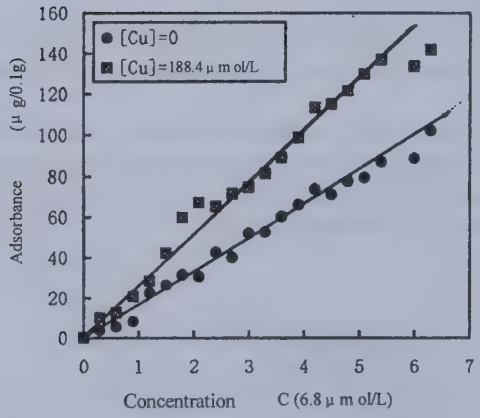

Fig. 5 Adsorption isotherm of Glu. acid on kaolinite

pH =7.70 ±0.05

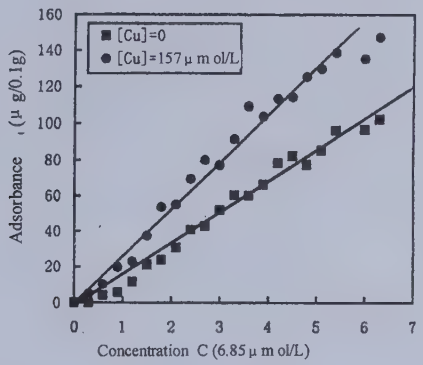

Fig. 6 Adsorption isotherm of Lys. on kaolinite

pH =8.00 ±0.05

3.2 Discussion

kaolinite is a natural clay mineral containing aluminosilicate, with a double layered structure and without sandwich ions. In the water solution its surface hydroxyl radical is amphiprotic, having the following balance (═ *S* is the solid surface).

$$\text{═ } SOH_2^+ \xrightleftharpoons{Ka1} \text{═ } SOH + H^+ \xrightleftharpoons{Ka2} \text{═ } SO^- + 2H^+$$

The property of the solid surface is correlated with the pH of the solution. The solid surface has the zero charge pHpzc. When pH＞pHpzc, the solid surface carries the net negative charge and the clay is at the same time the exchange agent of anion and cation. The main properties of kaolinite are: the intrinsic acid constant pK_{a1}=4.66, pK_{a2} =9.28; pHpzc =6.82; pH range of exchange with Cu^{2+} 5.0~9.0.

See Table 1 for the amino acid complex stability constants.

It can be seen from the distribution diagram of the amino acid complex stability constants and the major forms of existence for amino acids that in experimenting on pH, the major forms of existence for

Tab. 1 Amino Acid Complex Stability Constants

Ion and balance \ Amino acids(molecular waight)		Glycine (75)	Aspartic acid (133)	Glutamic acid (147)	Lysine (146)
H^+	HL/L • H	9.75	9.63	9.67	10.53
	H_2L/HL • H	2.36	3.70	4.25	8.95
	H_3L/H_2L • H		1.93	2.19	2.18
Cu^{2+}	ML/M • L	8.15	8.57	7.87	
	$ML_2/M \cdot L_2$	15.03	15.35	14.16	

various amino acids are, respectively:

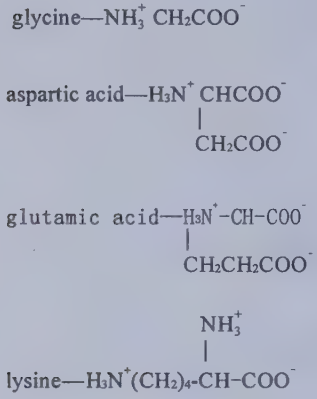

They may be subjected to exchange–adsorption on the clay surface in the patterns of hydrogen bond, electrostatic action, coordination and ion exchange. The adsorption of glycine and aspartic acid, for example, may be expressed as follows:

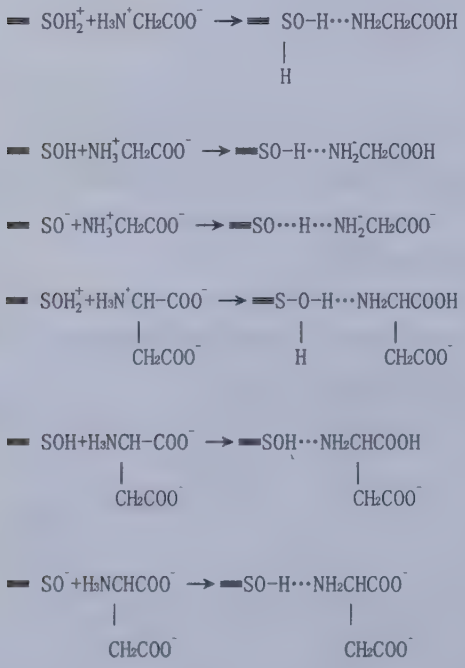

The adsorption of glutamic acid and lysine may be expressed in a similar way.

After addition of the copper ion, in the experiment on the pH value, the clay kaolinite surface obviously adsorbs the metal copper ion. Apart from adsorption on the solid surface in the above-mentined way of action, the free amino acid also adsorbs the copper ion through complexation with the copper ion adsorbed on the solid surface. With the addition of the copper ion and the increase of concentration, the adsorbance of amino acid increases and so does the adsorption isotherm slope. The process of complexation may be expressed as follows:

$\equiv$SOH+Cu+HL $\rightarrow$ $\equiv$SOCuHL+H (electric charge omitted)

$\equiv$SOCuHL means Type (I) ternary surface complex.

According to the experimental results and the above analysis, it may be concluded that the Type (I) ternary surface complexes have formed in these systems[1,3].When the copper ion is added, it is absorbed through ion exchange and the adsorbance of amino acid increases through the combination of the copper ion with the amino acid to form complexes. The adsorbance increases with the concentration of copper ion and so does the isotherm slope,but not in proportion; There are differences in the variation of the isotherm spopes under the identical or similar concentrations between different amino acids and copper ions. Comparatively speaking, the degree of promotion of the amino acids by the addition of identical or similar concentrations of copper ions is manifested in the following: lysine $>$ aspartic acid $\approx$ glutamic acid $>$ glycine.

Obviously, the amino acids and the adsorption after addition of the copper ion are necessarily subjected to the combined effect of many actions: ion exchange, coordination, hydrogen bond, Coulomb action, the combination of copper ion with the amino acid in the solution after its addition (desorption) and the combination of the adsorbed copper ion with the free amino acid (promoting adsorption) etc. Of course, there is difference in the adsorption and combination capacities among various amino acids. Judging from the experimental results, under the current experimental conditions, the increase of amino acid adsorption through the formation of Type (I) ternary surface complex is the primary effect. When the copper ion concentration in the solution is not too high, the complexion of amino acid and copper ion on the solid surface is strong, which is favourable for the formation of the Type (I) ternary surface complex,thus resulting in the increase of the adsorbance and the isotherm slope.

Jadging from the shape of the adsorption isotherm obtained from the experiment, within the given range of concentrations, the adsorption isotherm of amino acid on the clay kaolinite bascially belongs to the Langmuir type.

Summary

The researches on the isotherms of glycine,aspartic acid, glutamic acid and lysine on the clay kaolinite and the effect of copper ion on the isotherms indicate that the adsorption isotherms of amino acid should belong to the langmuir type and that the existence of copper ion and the increase of concentrations may contribute to or increase the adsorbance of varions amino acids on the surface of kaolinite mainly through the formation of the type(I) ternary surface complex, which increases the adsorption. The results of this experiment are consistent with the variation pattern about the effect of copper ion on the exchange—adsorption percentage E (%)and the pH curve of amino acid on the kaolinite[7].

References

[1] Zhang Zhengbin and Liu Liansheng (1991) Marine Physical Chemistry, Beijing: Science Press, 410–449.

[2] E. K demarce; R • dawson (chief editors); Translated by Ji Minghou, Qian Zuoguo, *et al.* (1992) Marine Organic Chemistry, Beijing: China Ocean Press, 576–594.

[3] Zhang Zhengbin, Liu Liansheng, Liu Guosheng and Yu Zhiming (1996) The determination of the stability constant of ternary surface complexes at liquid-solid interface in natural water. *J. Colloid & Interface sci*, **182** (2) :492–500.

[4] Yang, G. -P., Zhang, Z.-B., Zhang, J.-W., Liu L.-S. (1997) Analysis and distribution features of benzothiophene in sediments of Nansha Islands sea area, China. *J. Oceanol. Limnol.* **15** (3): 198–203.

[5] Lauro, T. Kubota *et al.* (1996) Study of the adsorption of some amino acids by silica chemically modified aminobenzenesulfonic and phosphate groups. *J. Colloid & Interface Sci.*, 183: 453–457.

[6] Martell, A. E. and Smith, R. M. (1974) Critical Stability Constants Vol. 1, Amino Acid, Plenum Press, p. 469.

[7] Zhang Zhengbin and Liu Xiaolan (1999) Effect of copper Ion in seawater on the amino acid–clay system liquid –solid interfacial action, *Journal of Ocean University of Qingdao*, **29** (2) : 325–331.

Sediment Load of Asian Rivers flowing into the Oceans and their Regional Variation*

Liu Shuguang (刘曙光)[1, 2], Zheng Yonglai(郑永来)[2], Zhuge Zhengji (诸葛正技)[2],
Li Congxian (李从先)[1]

1 *Key Laboratory of Marine Geology, Tongji University, Shanghai* 200092

2 *Department of Geotechnical Engineering, Tongji University, Shanghai* 200092

Abstract Study of the major Asian rivers discharge to the ocean reveals variations of their water discharges and sediment loads, and local characteristics of river sediment concentrations. On the basis of this, the Asian rivers fall into three regions, including Eurasia Arctic, East Asia, Southeast and South Asia Regions. The Eurasia Arctic Region is characterized by the lowest sediment concentration and load, while the East Asia Region is of the highest sediment concentration and higher sediment load, and the South-East and South Asia Region yields higher sediment concentration and highest sediment load.

The sediment loads of these regions are mainly controlled by climate, geomorphology and tectonic activity. The Eurasia Arctic rivers with large basin areas and water discharge, drain low relief which consists of tundra sediment, thus causing the lowest sediment load. The East Asia rivers with small basin areas and lowest water discharges, drain extensive loess plateau, and transport most erodible loess material, which results in highest sediment concentration. The SE and South Asia rivers originating from the Tibet Plateau have large basin areas and the largest water discharges because of the Summer Monsoon and high rainfall influence, causing the highest sediment load.

In Asia, tectonic motion of the Tibet Plateau plays an important role. Those large rivers originating from the Tibet Plateau transport about 50% of the world river sediment load to ocean annually, forming large estuaries and deltas, and consequently exerting a great influence on sedimentation in the coastal zone and shelves.

Keywords Asia, river flowing into the ocean, sediment load, water discharge

Introduction

River is one of the most important and active components in the Earth system. It plays an important role in surface migration, geomorphic portray and interaction of land and ocean. Asia is the largest continent and has the most complex physical geographical condition in the world. Asia extends across the frigid, temperate and tropical zones, and has many large rivers flowing into the ocean. While these rivers transport plentiful water discharge into the ocean, they carry a huge amount of sediment into the ocean, thus forming an important characteristic of Asian rivers. At the same time, Asia is a region with

Received on December 3, 1999

* The Project is sponsored by the Chinese National Nature Science Foundation (49676288), Scientific Research Foundation for the Returned Overseas Chinese Scholars of the Ministry of Education of China and the Russian Foundation for Fundamental Research (Project N00-05-64690)

the highest population density and the fastest economical development and human activities directly or indirectly influence rivers, coastal zone and paralic environment, resulting in difference of water discharge and sediment load and the particularity of effect on coastal zone. Therefore, study on regional variation of the sediment load of Asian rivers flowing into the ocean contributes to a better understanding of the global change and the particularity of interaction of land and ocean in Asia.

According to the hydrological and sediment data and the field measuremeuts in some large rivers of North and East Asia, the authors have made a comparative study on the deltas in some large rivers of Russia and China, and discussed regional variation of sediment load of large rivers in Russia and China[1-5]. On the basis of this, we have collected new data of water discharge, sediment load and concentration of major rivers flowing into the ocean in Southeast and South Asia, and studied characteristics of water and sediment discharges of Asian rivers in different natural zones, indicated regional variation of sediment load in different latitudes, and discussed the relationship between river sediment formation, transportation and deposition and physical geographic condition of drainage basin.

1 Total Sediment Load of Major Asian Rivers Flowing into the Ocean

Rivers, draining the Asian continent, mainly flow to the Arctic, Pacific and Indian Oceans. Table 1 shows the water discharge and sediment load. Rivers from the Asian continent transport a total water discharge of 6362.4km^3, and contribute a total sediment load of 4145.2×10^6t into the oceans (Table 2).

Tab. 1 Drainage area, water and suspended sediment discharges for the major rivers of Asia[1-8,10-13,15-17]

Ocean	River	Drainage area ($\times10^3$km^2)	Water discharge (km^3/a)	Sediment discharge (10^6t/a)	Sediment concentration (kg/m^3)	Ocean	River	Drainage area ($\times10^3$km^2)	Water discharge (km^3/a)	Sediment discharge (10^6t/a)	Sediment concentration (kg/m^3)
India Ocean	Tigris-Euphrates	3800	46	100	2.17	Arctic Ocean	Ob'	2500	430	16	0.037
	Indus	969	175	435	2.49		Nadym	64	18	0.4	0.022
	Narmada	49	5.2	6.9	1.327		Taz	150	44	0.9	0.02
	Krishna	250	32	4	0.125		Pyr	110	34	0.6	0.018
	Brahmani	28	16	20	1.25		Yenisei	2600	620	13	0.021
	Ganges	980	590	520	0.881		Pyasina	180	86	3.4	0.04
	Brahmaputra	580	630	540	0.857		Khatanga	360	85	1.7	0.02
	Irawaddy	430	430	260	0.61		Anabar	100	17	0.4	0.024
Pacific Ocean	Mekong	790	470	160	0.34		Olenjok	220	36	1.1	0.031
	Hongho	160	120	130	1.08		Lena	2500	520	18	0.035
	Zhujiang	329.7	227	71.8	0.34		Omoloy	39	7	0.13	0.019
	Hanjiang	30.1	25.9	7.2	0.28		Yana	320	34	3.5	0.093
	Jiulongjiang	15	15	3.1	0.21		Indigirka	360	61	13	0.213
	Minjiang	61	58	7.5	0.13		Alazeya	68	8.8	0.7	0.08
	Qiantangjiang	41.5	34.2	4.4	0.13		Kolyma	660	130	16	0.046
	Yangtze	1900	930	480	0.52		Amgyem	30	9.2	0.85	0.092
	Yellow river	770	59	1100	27.8						
	Yongdinghe	50.8	1.4	81	60.8						
	Luanhe	44.9	4.9	22.7	4.63						
	Dalinghe	23.2	2.1	36	21.9						
	Liaohe	166.3	5.6	41	6.86						
	Yalujiang	63.8	25.1	1.9	0.08						
	Amur	1800	320	23	0.072						

Water discharge into the Arctic Ocean, the Pacific Ocean and the Indian Ocean is about 30% of the total water discharge apart. Water discharge into the Arctic Ocean is more than that into the other oceans. Sediment load into the Pacific Ocean is the most. In contrast, sediment load into the Arctic Ocean is the least, only about 2.2% of the total sediment load. The water discharge from Ganges-Brahmaputra Rivers is the most, and the second largest in Asia in terms of water discharge is the Yangtze River. The water discharge of Yellow River is only about 1/20 of the Yangtze River, while its sediment load is far greater than that of the Yangtze and any other large river in the world. Water discharge of the Yenisei River flowing into the Arctic is about 1/2 of the Yangtze River, while sediment load is only 1/25 of the Yangtze River. About 70% of this total sediment load in the world is derived from Asia[6].Asian rivers have an important place in the world rivers.

Tab. 2 Distribution of water discharge and sediment load of Asian rivers flowing into the ocean

Ocean	Drainage area		Water discharge		Sediment load	
	10^3km^2	% of total drainage area	km^3	% of total water discharge	10^6t	% of total sediment load
Indian	7086	30	1924.2	30.2	1885.9	45.5
Pacific	6246.3	26.5	2298.2	36.1	2169.6	52.3
Arctic	10261	43.5	2140	33.7	89.68	2.2
Total	23593.3		6362.4		4145.18	

2 Spatial Distribution of Sediment Load of Asian Rivers Flowing into the Ocean

The sediment load of major Asian rivers is affected by climate, terrain, vegetation, soil and so on, and has distinct regional and seasonal difference.

Distribution of sediment load in Asia continent is nonuniform. Sediment load in the rivers of the Southeastern Asia is larger than that in the Northwestern Asia. Sediment load in the rivers of lower latitudes is larger than that in the higher latitudes. Sediment load in the rivers that originate from the Qinghai-Tibet Plateau is more than that in the rivers rising in other regions.

Variation of sediment concentration of Asian rivers is very clear (Fig. 1). Rivers of North China, locating in the latitudes 34~39°N, drain in the Loess Plateau, transporting the most easily erodible material available to moving water. As a result, sediment loads are huge and concentrations are tremendous. The Yellow River carries 11×10^8t of sediment annually into the sea. The average yearly sediment concentration in the Yongding River is as great as $60.8kg/m^3$. These concentrations, as shown in Fig.1, are far greater than those for any other large river in Asia. Sediment concentration in the rivers of Southeast and South China is less than $0.5kg/m^3$. Rivers originating from the Qinghai-Tibet Plateau into Southeast Asia are large and have large fall. Sediment concentration of those rivers is in excess of $0.5kg/m^3$. In the Indian River it is the highest[5], up to $2.49kg/m^3$. Although concentration of those rivers is less than that in the Yellow River, uplift of Qinghai-Tibet Plateau, summer monsoon, large runoff and water discharge cause tremendous sediment load. Compared with that in the above-mentioned rivers, sediment concentration in the rivers of North Asia appears very small. These rivers drain low-lying

terrain in tundra and taiga regions, and are less than 0.05kg/m^3 concentration, which is the lowest in Asia.

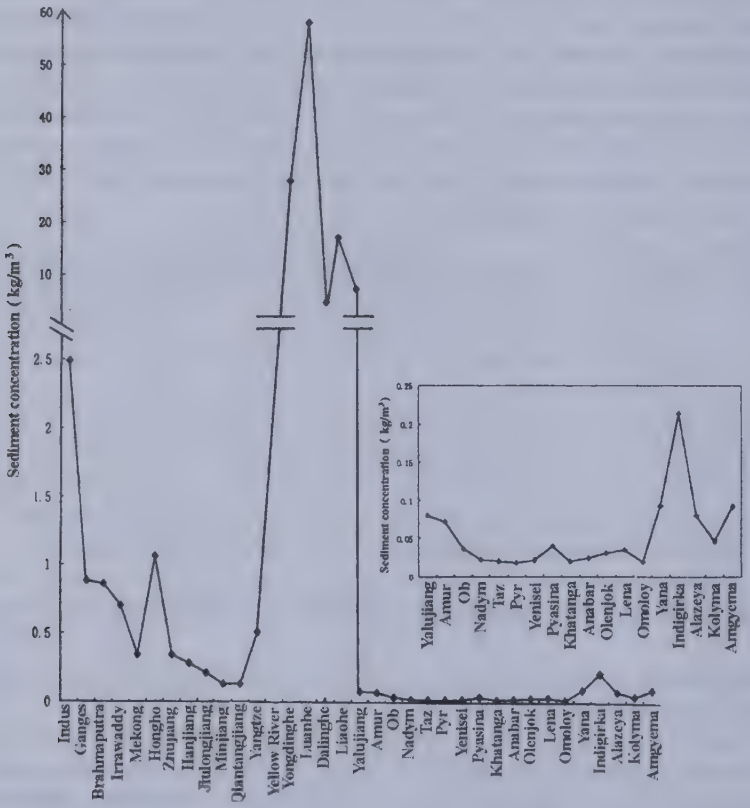

Fig. 1 Variation of sediment concentration in the Asian rivers flowing into the ocean

3 Temporal Distribution of Sediment Load of Asian Rivers Flowing into the Ocean

A majority of regions of Asia continent is controlled by monsoon. Seasonal distribution of water discharge and sediment load to a great extent depends on the variation of runoff, and, therefore, secular and seasonal variations have a large change rate.

3.1 Secular variation

Yearly variations of precipitation, runoff and sediment load are usually shown by the variability coefficient C_V. The larger the value C_V, the larger the variation. The value C_V of water discharge in the rivers of North Asia is 0.15~0.30, and the value C_V in the rivers of Southeast Asia is 0.2~0.4. In latitudes 34~39°N, the value attaches the largest C_V = 0.6~1.0[12].

Variability coefficient C_V of sediment load in the rivers of North Asia is the lowest, C_V = 0.13. Coefficient C_V in the rivers of North China such as the Yellow River, Haihe River and Liaohe River is the largest, C_V= 0.77~1.87.

3.2 Seasonal variation

Annual distributions of runoff, water discharge and sediment load are not uniform, basically characterized by plentiful water in summer, and low water in winter. Usually the period from May to October is flood period. In the flood period the water discharge is 70% of the average annual total and the sediment load is 75~90% of the average annual total. In the low water period the water discharge and sediment load are very low.

Sediment hydrograph is similar to discharge hydrograph. The peaks of sediment concentration and discharge of the majority of rivers appear in the flood period, when the peak of flood appears (Fig. 2). Fig.2(1) shows that appearance of peaks of flood and sediment is basically synchronous in the Lena River. In striking contrast with Lena, Fig.2(2) shows that the flood in the Yellow River rapidly rises and falls, and, therefore, the peaks of flood and sediment are generally synchronous. In many cases, the maximum sediment peak appears ahead of the maximum flood peak. Fig.2(3) shows that appearance of peaks of flood and sediment is basically synchronous in the Yangtze River.

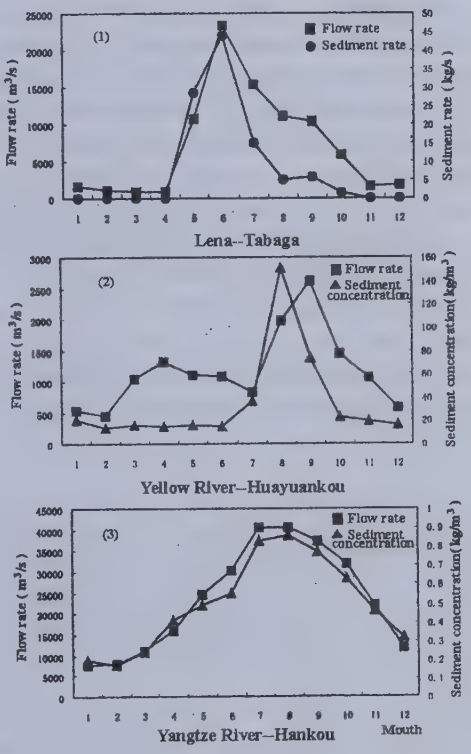

Fig. 2 Seasonal variations of water and sediment discharge in different regions

4 Regional Distribution and Controlling Factors of Sediment Load

The sediment loads of Asian rivers are mainly controlled by climate, hydrology, vegetation, soil, geomorphology and tectonic activity. In different areas, these factors play a different role. The Asian rivers can be divided into the following three types in terms of their values of water and sediment discharges:

(1)Rivers that carry little sediment, but have large water discharge. These rivers include the Ob', Yenise and Lena Rivers, draining into the Arctic Ocean.

(2)Rivers that contribute tremendous sediment load, but are of low water discharge. These rivers

include the Yellow, Haihe, Liaohe and Luanhe Rivers, draining into the the Yellow Sea and Bohai Sea.

(3)Rivers that transport very large sediment load and have very large water discharge. These rivers include Yangtze and Zhujiang (Pearl), draining into the Pacific Ocean and Mekong River, Ganges, Brahmaputra, Indus River, draining into the Indian Ocean.

Distribution of sediment load of the above-mentioned three types is of distinct characteristics. On the one hand they depend on basic variation tendency of precipitation and runoff. On the other hand they relate to geological construction, terrain, soil and vegetation.

Rivers with very large sediment load are located in frigid, middle, and warm temperate zones and semi-humid and semiarid regions. Rivers with large sediment load are located in warm, middle and cool subtropical zones and broad-leaf and deciduous forest regions. Rivers with small sediment load are located in frigid, frigid-temperate zones and semi-humid and taiga regions.

According to the above analysis, the Asian continent can be divided into three regions in terms of sediment concentration (Fig.3), each characterized by a different general climate or terrain. Region I is located in North Asia, where rivers have low sediment concentration. Region II is located in East Asia, where rivers have very high sediment concentration. Region III is located in the southern part of East Asia, Southeast and South Asia, where rivers have middle-level sediment concentration. In our opinion, regions I and III can be divided into some subregions in terms of their value of sediment concentration.

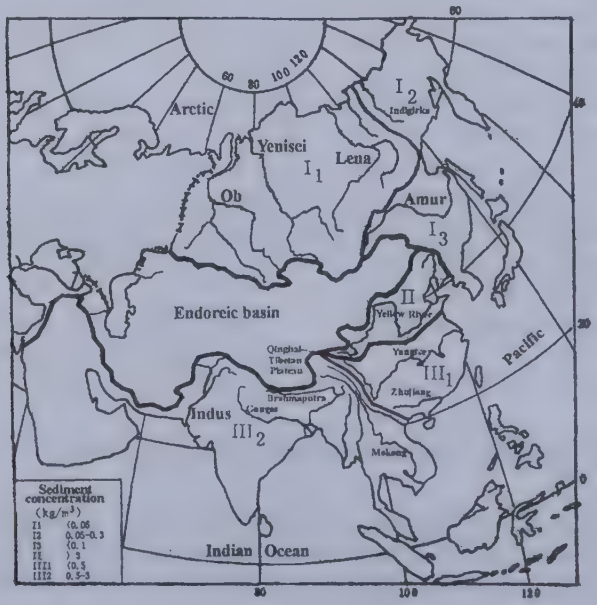

Fig. 3 Regional distribution of sediment concentration of Asian rivers flowing into the ocean

Table 3 shows the basic characteristics of water discharge and sediment concentration in the three regions.

Region I is characterized by large drainage area, plentiful water discharge, lowest sediment yield ($5\sim39 t/km^2 \cdot a$), low sediment concentration and flux, and accounts for about 51.4% of the total basin area draining into the oceans, drained by four large rivers (Ob', Yenisei, Lena and Amur).These rivers contribute about 39.1% of the Asian rivers' water discharge into the ocean annually, but sediment discharge is about $114.6 \times 10^6 t/a$, only about 2.8% of the Asian rivers' fluvial sediment flux into the ocean. The bed load in rivers is higher, 11~40% of the total sediment discharge. Different terrain and climate results in different sediment concentration, and, therefore, Region I can be divided into three subregions (Fig.3).

Tab. 3 Regional distribution of drainage area, water discharge and sediment load of major Asian rivers

Region		Drainage area		Water discharge		Sediment load		Sediment yield	Runoff depth	Sediment concentration
		$10^3 km^2$	%of total drainage area	km^3	% of total water discharge	$10^6 t \cdot a^{-1}$	% of total sediment load	$t \cdot km^{-2} a^{-1}$	$mm \cdot a^{-1}$	$kg \cdot m^{-3}$
I	I1	8 784		1 890		55		5—6	130—220	0.05
	I2	1 477		250		34		9—39	130—150	0.02—0.2
	I3	1 864		345		25		28	180	0.1
I Subtotal		12 125	51.4	2 485	39.1	114	2.8			
II	II	1 055	4.5	73	1.1	1281	30.9	240—2 800	35—80	6—60
III	III1	2 377		1290		574		130—250	450—700	0.1—0.5
	III2	8 036		2514		2 176		200—1 100	250—1 000	0.5—2.5
III Subtotal		10 413	44.1	3 804	59.8	2 750	66.3			
Total		23 593		6 362		4 145				

Subregions I 1 and I 2 are located in the frigid continent climate zone, widely distributed over the tundra belt and taiga. Sediment concentration is small and controlled by terrain and climate. Rivers in Subregion I 1 drain low plain, much swampland, causing low sediment concentration. Subregion I 2 has massif relief, with an elevation of about 600m. Just as the height of terrain and degree of vertical dissected topography gradually increase, and the rainfall gently reduces, from west to east, so the sediment concentration increases. Sediment concentration to the west of about 140° E (I 1 region) is different from that to the east of about 140° E (I 2 region). Rivers in this region are located in the frigid zone, where thaw weathering is strong, but chemical thaw is weak, so the sediment particles in the rivers are thick, and the bed load has a high proportion.

Most part of Subregion I 3 drains the tundra zone. The difference between it and the subregions I 1 and I 2 is that the rivers in Subregion I 3 are located in the sub-frigid and temperate zones, controlled by

monsoon. Runoff recharge originates from mainly the rainfall caused by summer monsoon. The annual precipitation is large, and therefore, sediment concentration in Subregion I 3 is higher than that in Subregion I 1.

Region II has small water discharge, highest sediment yield (240~2 800 t / km^2 · a), large sediment concentration and load. These rivers contribute only approximately 1.1% of the Asian river water discharge, but their total sediment flux is about 1 281 $\times 10^6$t · a, contributing more than about 30.9% of the Asian fluvial sediment discharge to the ocean. The bed load is less than 1% of the total sediment load. In this region, there are the Yellow, Liaohe, Haihe Rivers, etc.

There is little vegetation in Region II . Storm rainfall is concentrated in the flood period, and forms strong surface erosion and carries large amounts of sediment into the river channel, resulting in sediment deposit along the river and transport into the sea. Especially the Yellow River drains the Loess Plateau, so a huge amount of loess is scoured into the channel. The Yellow River is a river with the largest sediment load in the world.

Region III is characterized by large drainage area and water discharge, middle sediment yield (130 ~1 100t / km^2 · a), low sediment concentration, but large sediment discharge. The majority of the rivers in Region III originate from the Tibet Plateau, and drain in the sub-tropic and tropic monsoon zone. These rivers carry about 59.8% of the Asian rivers' water discharge into the ocean. Sediment concentration is smaller than that in Region II , but due to many large rivers and rich water discharge, sediment load is larger. These rivers have about 2 750$\times 10^6$ t / a of sediment discharge, contributing about 66.3% of the Asian fluvial sediment discharge to the ocean. Region III has the highest sediment load in the world. According to field measurement and calculation, the bed load is only about 1~5% of the total sediment load.

The subregion III 1 includes the Yangtze, Minjiang, Qiantangjiang, Zhujiang and Hanjiang Rivers. Sediment concentration and load in the Yangtze River, originating from the Qinghai-Tibet Plateau, are the most. Sediment load of the Yangtze River is mainly from the upper reaches, where there is much sandy shale. Low corrosion-resistance and impermeability of sandy shale results in a large sediment load. Sediment load of the Minjiang, Hanjiang and Qiantangjiang rivers is low, because the climate in these river basins are warm and humid, and their underlying surface consists of the corrosion-resistance igneous rock. The value of sediment concentration in the Zhujiang River is higher than those in the Minjiang, Hanjiang and Qiantangjiang rivers, because the mountainous region and hills account for about 90% of the Zhujiang River basin and the rich water discharge causes a large sediment load.

The subregion III 2 is drained by Hongho, Mekong, Ganges, Buramaputra and Indus Rivers. The majority of these rivers originate from the Qinghai-Tibet Plateau. Due to the Qinghai-Tibet Plateau uplift and the strong river undercutting, water fall is large and the erosion and transport action is very strong. The value of sediment concentration is higher than that in the subregion III1. As the rainfall originates from summer monsoon, and water discharge is large, sediment load is very large. It is the region with the highest sediment load and water discharge.

5 Conclusions

(1) Distribution of sediment load in the Asian rivers flowing into the ocean has clear regularity. Asian rivers can be divided into three regions in terms of sediment concentration. Rivers in North Asia

have large water discharge, but the lowest sediment concentration and load; Rivers in East Asia (34~39°E) have the highest sediment concentration and a large sediment load; Sediment load in Southeast and South Asia is the largest.

(2) Sediment load is controlled by climate, hydrology, terrain, geology, soil and vegetation. Rivers, originating from the Qinghai-Tibet Plateau, are influenced by uplift of Qinghai-Tibet Plateau. In this region, erosion action is strong and rainfall is large, and, therefore, sediment load is large. Sediment load in the rivers draining the Loess Plateau is large, mainly because of dry climate , small rainfall and strong physical weathering of loess. Sediment concentration in the rivers of North Asia is the lowest, because these rivers drain into the tundra and taiga zone, with gentle basin relief and a high covering rate of vegetation.

(3) In different natural zones, the composition of river sediment is different. The bed load in the rivers of North Asia occupies a high proportion, about 11~43% of the total sediment load, because these rivers drain into the frigid zone, where thaw weathering is very strong, and the particle in the river is very thick. Suspended sediment in the rivers draining the middle and low latitudes predominates over the bed load, which makes up only 1~5% of the total sediment value.

(4) The Asian rivers flowing into the ocean occupy an important position in the world. Every year they transport huge amounts of sediment into the ocean, and exert important influence on the ocean deposit and the land and ocean interaction.

Reference

[1] Liu Shuguang and Chalov R.S. (1998) Oriented Vertical Channel Deformation of Large Rivers of Russia and China., *Journal of Moscow State University, Ser. 5, Geography* (5): 35–40. (in Russian)

[2] Alekseevskii N.I., Liu Shuguang and Chalov R.S. (1999) Sediment Transport in Some Large Rivers of Russia and China. *Water Resources,* **26** (2): 170–178. (in Russian)

[3] Liu Shuguang and Chalov R.S. (2000) Morphodynamic types of the Lower Huanghe and Yangtze Channels and Conditions of Their Formation. *Geomorphology*, (1): 106–116. (in Russian)

[4] Chalov R.S., Liu Shuguang ang Alekseevskii N.I. (2000) *Sediment yield and Channel Processes on the Large Rivers of Russia and China*, Moscow: Moscow State University Press.(in Russian)

[5] Liu Suguang, Chalov R.S.(2000) Wu Dandan and Li Congxian, Sediment Load and Its Influence on Channel Processes of Some Large Rivers in Russia and China, *International Journal of Sediment Research*, **15** (3): 307 –302.

[6] Li Congxian and Zhang Guijia (1996) River sediment and Chinese Coastal Line Change. *The Quaternary Research*, (3): 277–282. (in Chinese)

[7] Milliman J.D. and Meade R.H. (1983) World-wild Delivery of River Sediment to the Oceans. *J. of Geology*, 91:1–21.

[8] Miliman J.D. Christine Rutkowski and Michel Meybeck (1995) *R iver Discharge to the Sea/ A Global River Index (GLORI)*, LOICZ REPORTS AND STUDIES, Texel, The Netherlands, LOICZ Core Project Office.

[9] Chalov R,S. (1994) *River Regime in North Eurasian.* Moscow: Moscow State University Press . (in Russian)

[10] Chalov R.S., Panchenko V.M. and Zernova S.Y. (1995) *Waterways in Basin Lena*, Moscow: MIKIS Press. (in Russian)

[11] *Surface water //Physical Geography of China* (1981) Beijing: Science Press. (in Chinese)

[12] Tang Qicheng and Xioang Yi *et al.* (1998) *River Hydrology of China*, Beijing: Science Press. (in Chinese)

[13] Liu Changming and Wei Zhongyi *et al.* (1989) *Agricultural Hydrology and Water Resources in the North China Plain*, Beijing: Science Press. (in Chinese)

[14] Qing Ning, Zhang Ren and Zhou Zhide (1987) *River Channel Processes*, Beijing: Science Press. (in Chinese)

[15] Liu Desheng *et al.* (1986) *Physical Geography of World*, Beijing: Higher Education Press. (in Chinese)

[16] Qian Yiying Te Qingchao and Zhou Wenhao (1993) *The changes of Water discharge and sediment load and channel Processes in Yellow River*, Beijing: China Construction Meterial Industry Press.(in Chinese)

[17] Mikhailov V.N. (1997) *River Mouths of Russia and Adjacent Contries: Past, Present and Future,* Moscow: GEOS Press.(in Russian)

[18] Chen Tianwen and Zhao Chunian (1985)The estimation of discharge and loads from the rivers flowing into littoral seas of China and their influence. *Acta oceanologica*, 17(4), 460–471. (in Chinese)

[19] Xu Jiongxin (1996) *Fluvial processes of natural zone in China*, Beijing: Science Press. (in Chinese)

Study and application of Toxicity Test Method Using *Neomysis awatschensis* in Toxicity Evaluation of Drilling Fluid*

Yan Tian (颜 天), Zhou Mingjiang (周名江), Tan Zhijun (谭志军),
Yu Rencheng (于仁诚), Li Jun (李 钧), Wang Yunfeng (王云峰)
Institute of Oceanology, Chinese Academy of Sciences, Qingdao, 266071

Abstract *Neomysis awatschensis* was collected on the west coast of Jiaozhou Bay, Qingdao in 1992 and acclimated in the laboratory conditions. The acute toxicity method using 4~6 day juvenile mysid of this species is studied. The species is compared with *M. bahia* in taxonomy, geographic distribution, morphology, as well as the sensitivity to reference toxins. Based on the results, we recommend *N. awatschensis* to be a standard marine organism for toxicity test in China and the method to be applied in toxicity evaluation of drilling fluids. In this paper, we report the results of the above studies and the application of the method in the evaluation of several drilling fluid products.

Keywords *Neomysis awatschensis*, toxicity evaluation, standard organism, drilling fluid

More and more attention has been paid to the pollution caused by the drilling fluid discharging along the Chinese coast with the development of oil industry in China. The method for its toxicity evaluation is mostly based on the bioassay method developed by API(American Petroleum Institute)[1], and ASMT(American Society for Testing and Materials)[2]. Crustacean *Mysidopsis bahia* is suggested as a standard test organism in the API procedure. However, the species does not distribute along the Chinese coast. Therefore, we have chosen *Neomysis awatschensis*, which has a wide distribution in China's coastal waters[3], and acclimated it in laboratory conditions for years, using it as the standard test organism in the toxicity assessment of drilling fluid. We will report our study on the acute toxicity method using *Neomysis awatschensis*, and the results of its application in some drilling fluid and its additives product.

1 Materials and Methods

1.1 Collection and culture maintaining

N. awatschensis has been collected from the west coast of Jiaozhou Bay, Qingdao and cultured in flow-through 100L glass tanks. Cultures are continuously supplied with sand-filtered seawater pumped from Huiquanjiao (a site out of Jiaozhou Bay without pollution history). 48h old *Artemia* naupliis and

Received on January 13, 2002

* The work is supported by National Basic Research Project No.2001CB409709, NNSFC project (49906007, 39950001, 20177023, 40076030), CAS Innovation Project (KZCX2-206), Direct Project of CAS and Project of the Commission of Science, Shandong Province.

artificial foodstuff are added twice a day. Healthy and active mysid juvenile of age 5 ± 1d are collected and used in the experiments.

1.2 Toxicants tested

SDS (sodium dodecyl sulfate), $CdCl_2$ and KCl have been purchased from the Shanghai Chemical Factory. Drilling fluid products are provided by the companies concerned and prepared by mixing with seawater at 1:10 (V/V) according to the USEPA method (ASMT, 1988; Weber, 1993). The SPP (Suspended Particle Portion) is removed and used for testing.

1.3 Acute toxicity test procedure

1L glass beakers are used for each toxicity test. For the acute 96h toxicity test, we use five different toxicant concentrations, and seawater is used as the control. Each concentration has three replicates. Twenty (5±1)d juveniles are selected and randomly distributed into each beaker. 48h old *Artemia* naupliis are added as food (100/day · juvenile). The survival of the juveniles is observed every 12h and dead organisms are removed. The medium is changed after 48h experiment.

1.4 Statistical analysis

The relationship between the survival rates and toxicant concentrations is determined by regression analyses, and thus, 96h EC50 is calculated for the acute 96h toxicity tests. In the chronic toxicity tests, several parameters are calculated. These include survival rate of parent mysids, total number of juveniles produced, and the first brood releasing time of each concentration. When all these parameters of each treatment are compared with those of the controls, unpaired *t*-test is then applied by *F*-test to compare variances. The toxicity levels are determined according to Sprague, J.B[4]. The discharging level in US, 96hLC50 of SPP above the level of 3×10^4 μ g /L of SPP are used.

2 Results

2.1 Taxonomy, morphology and distribution of *N. awatchensis* and *M. bahia*

Comparisons of the taxonomy, morphology and geographic distributions of *N. awatchensis* and *M. bahia* have been made. Both *N. awatchensis* and *M. bahia* belong to Crustacea, Mysidacea, Mysidae, and inhabit estuaries and oceans. *M. bahia* distributes along the Atlantic coast and the eastern Pacific ocean, mainly in the Gulf of Mexico (Gentile et al., 1982). *N. awatchensis* distributes along the coast of the western Pacific, and mainly in the Yellow Sea and Bohai Sea. *N. awatchensis* adapts to a wide range of temperature and salinity with a short life cycle (Huang, 1994).

The adults of these two species are about 10mm long. The females develop a marsupium to maintain eggs. The juveniles are released after the fertilized eggs are hatched and developed to the juvenile stage in the marsupium (Breteler *et al.*, 1982; Zheng, 1982&1984). The adults of female and male *N. awatchensis* are shown in Fig. 1.

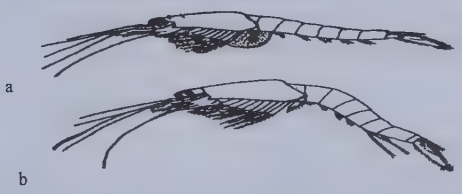

Fig. 1 Female mysid (A) and male mysid (B) of adult *Neomysis awatchensis*

2.2 Sensitivity of *N. awatchensis* to toxicants

The sensitivity of *N. awatschensis* to reference toxins, SDS, $CdCl_2$ and KCl, as compared to that of *M. bahia*, is shown in Table 1. The results indicate that the sensitivity of *N. awatschensis* is similar to that of *M. bahia*, although there are some differences, which may be caused by the differences of experimental conditions, e. g., salinity and temperature, applied in the respective tests.

Tab.1 The sensitivity of *Neomysis awatschensis*, comparing that of *Mysidopsis bahia* to reference toxins, SDS, $CdCl_2$ and KCl

	96hLC50 (mg/L)	
toxicant	*N. awatschensis* (25℃, salinity 30)	*M. bahia* [9]
SDS	11.6	
$CdCl_2$	0.118	0.346 (25℃, salinity 25)
KCl	830	250 (22℃, salinity 25)

Tab. 2 Toxicity evaluations of several drilling fluid products using *N. awatschensis*

No.	Product	SPP 96hLC50 (μg /L)	Toxicity level	Compared with discharging level 30 000(μg /L)
19930725	Drilling fluid	52 000	slight	>
19960525-I	Drilling fluid	308 000	no	>
19960525-II	Drilling fluid	12 000	slight	<
19990513-I	Additives	1 000 000	no	>
19990513-II	Dilution	1 000 000	no	>
19990513-III	Dilution	1 000 000	no	>
20000501	Additives	6 000	moderate	<

2.3 Application of acute toxicity tests using *N. awatschensis*

The acute toxicity method using *N. awatschensis* is applied in toxicity evaluations of drilling fluid and its additives. The results are shown in Table 2. The results demonstrate the usefulness of this species in acute toxicity assessments of this type.

3 Discussion

Postlarvae (stage P3-P4) of *Penaeus chinensis* have been suggested as a standard test organism for toxicity evaluation of drilling fluid. However, there are postlarvae of these stages only in April-May in each year, so they are not available for the test in the whole year. Now *N. awatschensis* has been maintained successfully in our laboratory, so it is convenient for experiment in all the seasons. As the mysid is similar to *M. bahia* in term of taxonomy, morphology, life cycle and sensitivity, it is a good way to compare the results with those of US when the drilling fluid products are exported. Because of the above advantages of the *N. awatschensis*, we suggest that the organism be one of the standard marine organisms for toxicity test in China. It is also a good tool for life-cycle bioassay due to its small size and short life history[10].

For water quality examination, luminescent bacteria have been established as one of the standard organisms and applied in the drilling fluid toxicity test as the toxic substances could inhibit its lighting ability. The method is very easy, convenient and cheap, but it is specific to some pollutants, such as heavy metals. Our method using *N. awatschensis* could more directly reflect the comprehensive influence of drilling fluid and other pollutants on marine organisms.

Because organisms have different structures and physiologically metabolic ways, the toxicities of the same substances to these organisms may vary significantly. Therefore, it is necessary to develop different bioassay methods from different intoxication ways to give more comprehensive toxicity assessment on drilling fluid, in order to avoid or minimize the loss in or damages to the environment caused by discharging.

Although the non-toxic drilling fluid could be allowed for discharging, it does not mean discharging without any control. The amount and time of discharging have to be controlled according to the regulations of the local and national environmental departments.

References

[1] API. (1984) Standard protocol for bioassay test of drilling fluid, collections of API13 (translated by secretariat of the Drilling Fluid Subcommittee, Drilling Standards Committee) [M]. Beijing: Standards Press of China.

[2] ASTM. (1988) Standard Guide for Conducting Life-Cycle Toxicity Tests with Salt-Water Mysids [M]. Annual Book of ASTM, Philadelpia P.A.: American Society for Testing and Materials, 11, 04.

[3] Huang Z. (1994) Species and distribution of marine organisms in China [M]. Beijing: China Ocean Press. 524–526.

[4] Cairns J Jr, Dickson K L. (1973) Biological Methods for the Assessment of Water Quality [M]. Philadelpia P. A.: American Society for Testing and Materials. 6–30.

[5] Gentile S M, Gentile J H, Walker J, Heltshe J F. (1983) Chronic effects of cadmium on two species of mysid shrimp: *Mysidopsis bahia* and *Mysidopsis bigelowi* [J]. Hydrobiologia, 93:195–204.

[6] Zhen Y. (1982) Biology study of *N. awatschensis* I [J], population and reproduction. *Oceanology et Limnology*, **13** (1): 67–77.

[7] Zhen Y., Li M., and Tian F. (1982) Pilled *Artemia* cyst used as foodstuff for *N. awatschensis* [J]. *Marine Science*, 4: 36–39.

[8] Zhen Y. (1984) Biology study of *N. awatschensis* II [J]. Life cycle study. *Oceanology et Limnology*, **15** (4): 288–298.

[9] Weber C I. (1993) Methods for measuring the acute toxicity of effluents and receiving waters to freshwater and marine organisms [M]. United States, Environmental Protection Agency, EPA/600/4–90/027F .

[10] Yan T., Li J., Li Z., Zhou M. (2000) The effect of TPT on *N. awatschensis* [J]. *Oceanology et Limnology*, **31** (5): 485–489.

Effect of salinity on the growth, and agar yield and composition of *Gracilaria tenuistipitata* var *liui* Zhang *et* Xia

He Lihong (贺丽虹)[1], Madeline Wu (吴汪黔生)[2], Shen Songdong (沈颂东)[1], Wang Deli (王得利)[3]
1 *Aquaculture Department, Life Science College, Suzhou University, Suzhou* 215006
2 *Department of Biology, Hongkong University of Science and Technology, Hongkong*
3 *First Institute of Oceanography, SOA, Qingdao* 266003

Abstract *Gracilaria tenuistipitata* var*liui* Zhang *et* Xia is cultivated at two different salinities (21, 33) in the laboratory for 4 weeks. The daily growth rate is determined. The total agar yield and fractional agar composition are analyzed. Results show that algae grow faster in low salinity. The total agar yield is higher under high salinity conditions than under low salinity conditions. Among the eight fractions extracted, the yields of cold water extract and 40% ethanol extract are about the highest. In low salinities the yields of autoclaved extract and 60% ethanol extract are higher, while the yield of cold water extract is lower relative to high salinities.

Keywords *Gracilaria tenuistipitata* var *liui* Zhang*et* Xia, salinity, agar yield, agar fraction

Introduction

In recent years *Gracilaria* species is becoming the principal source of agar worldwide. It is reported that approximately 60% of the agarophytes in the world comes from *Gracilaria* [1]. As a commercially important polysaccharide derived from *Gracilaria,* the heterogeneity of agar has been a subject of investigation for a long period of time. The agar composition of *Gracilaria* species has been reported to be species dependent, and within species to be influenced by morphology, tissue age and growth rate[1-4]; by seasonal variability[5-9] and by culture conditions[10-15]. Nitrogen availability, salinity and temperature have been reported to significantly affect the physical properties of agar gels extracted from *Gracilaria verrucosa* Papenfuss[10-11].

As an important source of agar, *Gracilaria tenuistipitata* var*liui* Zhang *et* Xia is abundant in the tropical and subtropical sea areas in China. Studies have been conducted to evaluate the effect of culture conditions (such as temperature, salinity, nutrient) on the daily growth rate of the algae[16-17]. Yet little has been done to evaluate the effect of environmental conditions on the yield and fractional composition of agar extracted from the seaweed. The present study examines the possible effect of salinity on the yield and composition of agar extracted from *Gracilaria tenuistipitata* v. *liui* Zhang *et* Xia.

Received on September 29, 2001

1 Material and Methods

1.1 Algae cultivation

Healthy thalli of *Gracilaria tenuistipitata* var *liui* are cleaned, hand sorted and pre-cultivated for two weeks prior to the experiment. The algae are cultivated in 6 tanks in the laboratory. Each tank contains approximately 150L culture medium. Exactly 200g algae are introduced to each tank. Two salinity levels are used. The natural seawater with a salinity of 33 is used as the high salinity culture medium, which is referred to in the text as HS. The low salinity culture medium is prepared by adding fresh water to the natural seawater and adjusting the salinity to 21 with a "Hiroba, U-10" water analyzer, which is referred to in the text as LS. The experiment is done in triplicate. During the experimental period the water temperature ranges from 23℃ to 25℃. The wet weight of the seaweeds are determined once after two weeks of cultivation. Algal biomass is cropped back to the initial density after the first weighing. All harvested plants are washed thoroughly with tap water and distilled water, then dried to constant weight in a 60℃ oven.

1.2 Agar extraction

Five grams of dry algae are ground to fine powder with a pestle. The agar is extracted according to the method of Lahaye *et al.*[18]. No acetone treatment is performed prior to the extraction procedure. The algal powders are first suspended in 1L distilled water and shaken at room temperature (~24℃) for 18h. The residues recovered by centrifugation are placed in a plain-bottom flask (1L) fitted with a reflux condenser and extracted with 300ml boiling 99.5% ethanol (~78.5℃) for 2h. Subsequently, the residues are extracted with 300ml boiling 80% (~82℃), 60% (~82.5℃), 40% (~84.5℃), 20% (~92℃) ethanol solutions and distilled water(~100℃) for 2h respectively. The remaining residues are transferred to a flask with 300ml distilled water and autoclaved (~121℃) for 3h. All of the extracted supernatant solutions are recovered by decantation, centrifugation and then pressure filtered. The extracts are referred to in the text as cold water extract (CW), 100% (100), 80% (80), 60% (60), 40% (40), 20% (20) ethanol extracts, distilled water extract (DW) and autoclaved extract (AW) respectively. Carbohydrate content is analyzed using the phenol-sulfuric acid method[19]. The total agar yield is expressed as a percentage of dry algal weight. The yield of each agar fraction is expressed as a percentage of total polymer obtained from the algal sample.

1.3 Growth rate calculation

The daily growth rate is calculated using the formula:$GR = ((\mathrm{Ln}\ Nt - \mathrm{Ln}\ No)/t) \times 100\%$, where GR is the daily growth rate, No is the initial wet weight and Nt the wet weight on day t, t is the interval days.

2 Results and Discussion

2.1 Growth rate

The average daily growth rates of *Gracilaria* cultured in different salinities are shown in Table 1. Plants growing in a low salinity (21) medium has an average growth rate of about 1.68%d^{-1}, which is

58% higher than the average growth rate of plants growing in a high salinity (33) medium. This shows that the salinity of 21 is favorable for the growth of the seaweed. This result is comparable to the earlier study made by Chung-Sing Chen[16], in which the seaweeds gain the maximum growth rate at 20, and the growth rate declines at higher salinity levels (25, 30, 35) and lower salinity levels (5, 10, 15); the rate is approximately one-half that of the best salinity (20) at the two extreme salinities (5, 35). The result in the present study also agrees with the earlier study on the optimum environmental parameters for the growth of this species in pond culture[17].

Tab. 1 The average daily growth rate and agar yield of *Gracilaria* cultured in different salinities

Groups	Growth Rate (±SD)	Agar Yield (±SD)
LS (21)	1.68±0.29	27.04±2.61
HS (33)	1.06±0.44	31.77±2.30

2.2 Agar yield

Higher agar yields are obtained in high salinity conditions (Table 1). The agar yield of algae cultured in high salinities ranges from 29.86% to 34.32%, with an average of 31.77% of algal dry weight; while in low salinities the agar yield ranges from 24.71% to 29.85%, with an average of 27.04% of algal dry weight. This indicates that salinity can affect agar yield.

Daugherty and Bird[10] reported that agar yield was significantly affected by salinity. Previous culture studies with *Gracilaria verrucosa* Strain G-16 found that lower salinities had led to significantly higher agar yields[11]. Bird[11] stressed that under long-term lower salinity conditions, agar deposition between cell walls might provide additional structural support for turgid cells, resulting in an increased agar yield. In the present study higher agar yield at 33 may be due to the similar osmotic acclimation procedure. Results show that *G. tenuistipitata* var*liui* grow optimally at 21, so the normal cytoplasm osmotic pressure of the plants is similar to that of the low salinity (21) seawater. Therefore, under long-term higher salinity (33) conditions the plants also increase agar deposition between cell walls to provide strong support for the cells, which results in an increased agar yield. It may be concluded that increased agar yield at higher or lower salinities may be an indicator of acclimatization of the seaweed to stressed salinity levels.

The results agree with the earlier report of Hurtado-Ponce and Pondevida[12]. It is reported that *Gracilariopsis bailinae* (Zhang *et* Xia) gains the highest agar yield when cultured at 15, medium agar yield when cultured at 35, and the lowest agar yield when cultured at 25. This also shows that the agar yield increases when the seaweed is cultured at lower and higher salinities.

2.3 Fractional Agar Composition

Fractional agar yield as a percentage of total polymers obtained is summarized in Fig.1.

The yields of cold water extract and 40% ethanol extract are highest in the two salinity levels, which is more than 20% of the total carbohydrate obtained. The yields of autoclaved extract and 60% ethanol extract from plants growing at 21 are higher than those growing at 33, while the yield of cold water extract is relatively lower at 21 than at 33. This may suggest that a more stable agar forms or a complete biochemical modification of agar takes place in the optimal salinity (21) conditions, so higher

solubility can be observed at high temperatures. While in high salinity (33) conditions more energy is needed for acclimatization, the agar formed is unstable or an incomplete biochemical modification of agar takes place, which leads to the higher solubility of agar fractions at low temperature. As interpreted by Lahaye*et al.*[18], the temperature at which agar molecules are soluble reflects the degree of polymer association in the network and helical structure of the molecules. High temperature is required to change the conformation from an insoluble helical agarose molecule to soluble random coil. It is also found in the present study that cold water extract has no gel ability, poor gel is formed with 100% ethanol extract, and the gel ability of other extracts is good. The reported high content of sulfate in cold water extract[3,15,18] may lead to the poor gel ability.

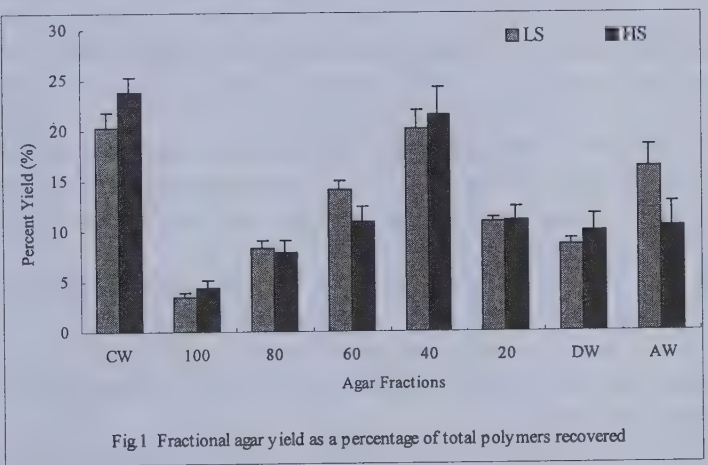

Fig.1 Fractional agar yield as a percentage of total polymers recovered

Results in the present study show that 21 is favorable for the growth and agar synthesis of *Gracilaria tenuistipitata* var*liui* than 33. At 21 the seaweed grows faster and the yield of agar fractions with good gelling ability (especially fractions 60 and AW) is higher than that at 33, though the average agar yield is a little lower. It can be concluded that seaweeds growing under optimum conditions produce lower yield and better quality (high gel strength) of agar, while seaweeds growing under stressed conditions produce higher yield and poor quality (poor gelling ability) of agar. This can be observed in the earlier studies and reports. Studies with *Gracilariopsis bailinae* from Hurtado-Ponce and Pondevida[12] show that the seaweed growing at 25 produces the lowest agar yield, the highest gel strength and the lowest sulfate content (cultured in indoor tanks); on the contrary, higher agar yield, lower gel strength and higher sulfate content (cultured in indoor tanks) are obtained from seaweeds growing at 15 and 35. The results demonstrate that lower and higher salinity may result in an increased agar yield but decreased gel strength, hence decreased agar quality. Daugherty and Bird[10] and Bird[11] als o found less sulfate content and high gel strength at 25, while high sulfate content and poor gel strength at lower salinities. It is suggested that the increase in sulfation in plants growing at low salinities may inhibit the influx of protons from the less saline medium, and the increased sulfate content leads to the poor gel strength[10, 11, 13].

Effect of nitrogen availability on the yield and quality of agar is similar to that of salinity. In

general, lower agar yields and higher gel strengths are correlated with nitrogen enrichment, while higher agar yields and lower gel strengths are obtained under nitrogen deficient conditions[20-22].

It should be noted that culture of seaweeds under optimum conditions is very important to gaining high biomass yield and good agar product quality.

References

[1] Whyte, J. N. C. and J. R. Englar (1980) Chemical composition and quality of agars in the morphotypes of *Gracilaria* from British Columbia. *Bot. Mar.*, **23** (5): 277–283.

[2] Marc Lahaye and Cyrille Rochas (1991) Chemical structure and physico-chemical properties of agar. *Hydrobiologia*, 221:137–148.

[3] Lignell A. and M. Pedersen (1989) Agar composition as a function of morphology and growth rate. Studies on some morphological strains of *Gracilaria secundata* and *Gracilaria verrucosa* (Rhodophyta). *Bot. Mar.*, 32:219–227.

[4] Craigie J.S. and Z. C. Wen (1984) Effects of temperature and tissue age on gel strength and composition of agar from *Gracilaria tikvahiae* (Rhodophyceae). *Can. J. Bot.*, 62:1665-1670.

[5] Bird K. T. and T. L. Hinson (1992) Seasonal variations in agar yields and quality from North Carolina agarophytes. *Bot. Mar.*, 35:291–295.

[6] Freile-Pelegrin and D. Robledo (1997) Effects of season on the agar content and chemical characteristics of *Gracilaria cornea* from Yucatan, Mexico. *Bot. Mar.*, 40:285–290.

[7] Friedlander M., R. Shalev, T. Ganor, S. Strimling, A. Ben-Amotz, H. Klar and Y. Wax (1987) Seasonal fluctuations of growth rate and chemical composition of *Gracilaria* cf. *confertain* outdoor culture in Isreal. *Hydrobiologia*. 151–152 : 501–507.

[8] Shi Sheng-yao and Ji Ming-hou (1980) Agar extracted from *Gracilaria* ∏ Seasonal variation of the production and gel strength of agar. *Transactions of Oceanology and Limnology*, 4:35–37.

[9] Shi Sheng-yao *et al.* (1983) Seasonal variation of the production, physical properties and chemical composition of agar extracted from *Gracilaria*. *Oceanologia et Limnologia Sinica*, **14** (3):272–276.

[10] Daugherty B. K. and K.T. Bird (1988) Salinity and temperature effects on agar production from *Gracilaria verrucosa* Strain G-16. *Aquaculture*, 75: 105–113.

[11] Bird K. T. (1988) Agar production and quality from *Gracilaria* sp. strain G-16: Effects of environmental factors. *Bot. Mar.*, 31: 33–39.

[12] Hurtado-Ponce A. Q. & H. B. Pondevida (1997) The interactive effect of environmental factors on the growth, agar yields and quality of *Gracilariopsis bailinae* (Zhang *et* xia) cultured in tanks . *Bot. Mar.*, 40: 217–223.

[13] Lapointe B. E., D. L. Rice and J. M. Lawrence (1984) Responses of photosynthesis, respiration, growth and cellular constituents to hypo-osmotic shock in the red alga *Gracilaria tikvahiae*. *Com. Biochem. Physiol.*, 77A:127–132.

[14] Christeller J. T. and W. A. laing (1989) The effects of environment on the agar yield and gel characteristics of *Gracilaria sordida* Nelson (Rhodophyta). *Bot. Mar.*, 32:447–455.

[15] Ekman P. and M. Pedersen (1990) The influence of photon irradiance, day length, dark treatment, temperature, and growth rate on the agar composition of *Gracilaria sordida* W. Nelson and *Gracilaria verrucosa* (Hudson) papenfuss (Gigartinales, Rhodophyta). *Bot. Mar.*, 33:483–495.

[16] Chung-Sing Chen (1991) The distribution of *Gracilaria tenuistipitata* var*liue* at the estuary of Tansui river and its casual relation to salinity tolerance and character of substratum. *J. Fish. Soc. Taiwan*, **18** (2): 89–96.

[17] Wu Chaoyuan *et al.* (1994) Study on the optimum environmental parameters for the growth of *Gracilaria tenuistipitata* var *liui* in pond culture. *Oceanologia et Limnologia Sinica*, **25** (1): 60–66.

[18] Lahaye M., C. Rochans & W. Yaphe (1986) A new procedure for determining the heterogeneity of agar polymers in the cell walls of *Gracilaria*spp. (Gracilariaceae, Rhodophyta). *Can. J. Bot.*, 64: 579–585.

[19] Dubois, M. K. A. Gilles, J. H. Hamilton, P.A. Rebers, and F. Smith. (1956) Colorimetric method for determination of sugars and related substances. *Anal. Chem.*, 28: 350–356.

[20] James A. Deboer (1979) Effects of nitrogen enrichment on growth rate and phycocolloid content in *Gracilaria foliifera* and *Neoagardhiella baileyi* (Florideophyceae). *Proc. Int. Seaweed Symp.*, 9:263–273.

[21] Thomas C. Chiles, Kimon T. Bird & Frank E. Koehn (1989) Influence of nitrogen availability on agar-polysaccharides from *Gracilaria verrucosa* strain G-16: structural analysis by NMR spectroscopy. *J. Applied Phycology*, 1: 53–58.

[22] Raul E. Rincones, Shukun Yu & Marianne Pedersen (1993) Effect of dark treatment on the starch degradation and the agar quality of cultivated *Gracilariopsis lemaneiformis* (Rhodophyta, Gracilariales) from Venezuela. *Hydrobiologia*, 260/261: 633–640.

Studies on the Technology for Mass Production of Abalone Breeding

Chen Quanzhen (陈全震), Hu Xigang (胡锡钢), Gao Aigen (高爱根), Yang Junyi (杨俊毅)
Second Institute of Oceanography, SOA, Hangzhou 310012

Abstract Based on the traditional way of abalone breeding, the technological process of industrial abalone breeding suitable for the coastal areas of southern China has been developed. The process is simple and easy to handle, and results in a high yield of young abalones after being applied.

Keywords Abalone, artificial breeding, high-yield technology

Artificial breeding is an important component and link in the development of aquaculture, especially for the abalone, as the natural young of the abalone is far from adequate and the abalone culture relies entirely on artificial breeding. At present, the yield of abalone in China is 3×10^3t less than enough and the producing areas are mainly distributed in Liaoning, Shandong, Hainan, Fujian and Guangdong. As the supply of abalones falls short of demand, they have to be imported from Australia, Thailand, etc. every year. As a result, the abalone culture has undergone major development in the coastal areas of South China in recent years and has become another hot area of mariculture in these regions following the prawn culture and the fish culture in net pen. To make it possible for the abalone culture to develop in a sustained and stable way, it is first of all necessary to carry out industrial artificial breeding and ensure the supply of young abalones.

The paper reports the technological process designed for abalone breeding in Lianjiang of Fujian Province in the past few years by drawing on the working experiences of the predecessors and professionals of the same trade and in the light of the actual local conditions. The results have proved that compared with the traditional way of abalone breeding, this technological process is simple and easy to handle, and can result in a high yield of young abalones, so it is suitable for the mass production of young abalones.

1 Basal Facilities

1.1 Selection of nursery sites

The abalone nursery ground should be set up along the stone reef where the sea area is free from pollution, there are no runoffs nearby, the sea water is clear and the sea water density is normally maintained at 1.019~1.021g/cm^3 all the year round.

1.2 Nursery pond

The nursery pond is rectangular in shape with an area of 800cm×70cm, an average pond height of 100cm and a bottom slope height of about 10cm; The water inlet is set up at the higher end of the pond

Received on December 4, 2001

bottom and the water outlet at the other end; The water flows in from the surface and out from the bottom; The top of the pond is covered with 2~3 layers of black nylon nets to keep out the light, one of which is a movable screen, and the illuminance is controlled at about 1500 lx.

1.3 Water and air supply facilities

The water supply system is composed of the pump room, high-lying water storage tank, sand filtration pond, pipeline and valves. The air supply system consists of air blower, plenum pipe, air tube into the pond, air valve and gas rock. Two gas rocks are placed in each square meter of the pond bottom.

1.4 Bait plate

The bait plate is not only the site where the bait (benthic diatom) attaches and grows, but also the host attached to by the larval abalone. It is made of the non-toxic, colourless transparent or semi-transparent plastics with a size of 40cm×33cm. Each pond uses 640 bait plates.

2 Breeding Technology

2.1 Selection of parent abalones

The abalone is bisexualism with its gonad wrapping up the periphery of the horn-like organs protruding from the visceral mass. The male is yellowish and the female is green, blue or brown. The parent abalones are chosen from the nursery farm and they are required to be healthy, sexually matured ones aged 2~3 years with the shell length exceeding 5cm and the gonad fullness covering over 70% of the periphery of horn-like organs. The parent abalone referred to in this paper is chosen from the filial generation of *Haliotis discus* Reeve(♂) of Japan and *Haliotis discus* Hannai (♀) of northern China.

2.2 Hastening parturition and hatching

Despite the number of female abalones, about 15 male abalones are prepared each night. The parent abalones are cleaned and placed in the brown basin toward evening to be dried in the shade for 1~2 h and then stimulated with the natural seawater flowing through an ultraviolet lamp (The amount is controlled at 1 000mW · h/L); After 1.5h, the male begins to excrete sperms and after 2 h, the female begins to ovulate. The ova are collected about every half an hour and generally about 30×10^4 ova are placed in each bucket. After it is added to by a small amount of diluted sperm, the bucket is filled with water. When the ova have sunk, the upper half part of the water in the bucket is removed and then the bucket is filled with fresh water. This process is repeated about every half an hour so as to wash out the surplus sperm and increase oxygen for the hatching of the zygote. The zygote at the water temperature of 21~23℃ grows and hatches trochophores after 8 h or so.

2.3 Attachment of the young, and cultivation of larval and juvenile abalones

2.3.1 Culture of bait

The bait plates and the nursery pond are disinfected and cleaned following the old routine with bleaching powder and potassium permanganate in advance. 15~20 days before hastening parturition, the bait plate is put into the nursery pond, the sand filteration water is poured into the pond, and the running-water natural culture is carried out. After 2 days, nutrients are added into the water (For each cubic meter of water, 15g urea, 5g potassium dihydrogen-phosphate, 5g sodium silicate, and 1g iron citrate are

added). Subsequently, the nutrients are added in the morning every four days and on the very day when the nutrients are added, the running water culture is not carried out. On the 12th~13th day of culture, the bait plate is reversed so as to ensure the even distribution of the baits on the upper and lower parts of the bait plate in the future attachment of the young.

2.3.2 Planktonic larva and attachment of the young

Generally the young whose parturition is hastened at night can complete its hatching in the next day at 15~16 hours. The hatched young is concentrated and poured into a small pond containing 2 m^3 of water for counting. Then about $37\times10^4/m^3$ planktonic larvae are directly dumped into the attachment pond to allow them to develop by metamorphosis . At a water temperature of 21~23℃, the attachment begins after 3 days. During the attachment, less gas should be filled and the illuminance should be as low as possible (by, for instance, covering the pond with a black cloth), which is favourable for the even attachment of the young. The time of attachment takes about 3~4 days.

2.3.3 Cultivation of larvae

In carrying out running-water culture, the volume of water flow depends on the number of benthic diatoms on the bait plate. When the number of diatoms is small, the water flow should be increased; In a sunny day, illuminance should be adjusted in time to avoid direct irradiance for if the light ray is too stong, the green algae are apt to reproduce, which is harmful to the growth of larval abalones; Once the green algae have grown on the bait plate, it is necessary to reverse the plate in time in order to check the growth of green algae; At dusk when it gets dark, an electric torch should be used to light up the bait plate at the water inlet to see whether there are copepods. Once they occur, they should be killed in time with trichlorfon (with a mass concentration of $2g/m^3$). Going through metamorphosis for many times (veliger larva, enclosing mouth shell larva, upper leg differentiation larva) and culture for about 30 days, when the first spiracle appears in the front of the shell, the larvae turn into the juvenile abalones.

2.3.4 Cultivation of juvenile abalones

With the growth of the individuals, the demand of the young abalones for feeding the bait increases and the benthic diatoms on the bait plate can no longer meet the needs of the growth of young abalones. Therefore, it is necessary to feed the young abalones with artificial baits as supplement. The quality dried laver powder (grain size<180 mesh) may be chosen as artificial bait.The feeding is carried out before dusk, and during the feeding, aeration should be suspended for half an hour not resumed until the laver powder has sunk. The next moring, the water in the pond should be thoroughly changed and the pond bottom washed. The emphasis of management in this stage should be laid on watching out for the change of water temperatre. When the water temperature is high in summer, the water flow should be increased.

2.4 Stripping of the young and the later-stage management

After the young abalone grows to 3~4mm, due to the increase in its feeding amount and the poorer light, the transparent bait plate is no longer suitable for the young abalone to live on. At this time,it is necessary to strip off the young abalones and pour them into a new pond. The bottom of the new pond is covered with imbricate sheets of marble stone for the young abalone to attach to . At dusk every day, the artificial bait is released and the next morning , the pond is cleaned and the water changed thoroughly. As the young abalones grow unevenly, it is necessary to pick out in time the young abalones over 1 cm

for sale or for culture in the cage.

3 Summary and Discussion

3.1 In Northern China, climatic conditions must be taken into consideration in the abalone breeding , while, on the contrary, the black nylon nets used as ceiling are fit for the abalone breeding in the coastal areas of South China. On the one hand, they can regulate light to make it soft and favorable for the growth of benthic diatoms while preventing the bait plate from being irradiated by direct rays, thus checking the propagation of green algae; On the other, they provide better ventilation conditions so as to prevent the water temperature indoor from rising in summer.

3.2 The early way of hastening parturition of abalones is the mixed stimulation by drying in the shade and the running water. This method takes longer time and has little certainty of success; The mixed stimulation by ultraviolet rays and the rising temperature requires the effective does of irradiance of ultraviolet rays on sea water to be 300~800W · h/L and inductive effect by irradiation sea water with ultraviolet rays has improved considerably as compared with that of the original induction by drying in the shade and the rising temperature[2]. On this basis, the method of stimulation by the sea water flowing through the ultraviolet lamp is used. It has been concluded after a number of experiments that the dose should be controlled at 1 000mW · h/L. For the parent abalones stimulated by the sea water having been treated with such a doze, the male would first excrete sperm after about 1.5h and the female ovulates after 2 hours, with an excretion rate of 100% for both the male and the female. The advantage of this way of hastening parturition lies in the fact that it can control the production of ovulation and the time of ovulation.

3.3 The traditional breeding is carried out in such a way that the larvae remain in the hatchery after they have been hatched from the fertilized egg and do not begin their attachment to different ponds until the eyespot of the larva has appeared[2]. Such an operation involves a large amount of work for it is necessary to change water every three hours, which is unfavourable for the large-scale breeding. Besides, in the course of changing water, a large number of larvae would be adsorbed into the bolting silk, thus leading to mechanical damage. The practice of directly pouring the fertilized eggs into the attachment pond after they have been hatched could raise the survival rate of larvae on the one hand and greatly reduce the amount of work on the other, which is suitable for the mass production of the young.

3.4 It is desirable to conduct attachment of the young after the baits have been cultivating for 15~20 days. If the time of cultivation is too long, the baits are liable to aging and the young would fall off along with the baits. The method of cultivating the baits with running water is more convenient and rapid than the traditional method of cultivating the baits by inoculation, so it is fit for the large-scale breeding. According to the traditional amount of attachment, generally the amount of the young released into each pond is 40×10^4, but the young would not be stripped off until they grow to 1cm[2~4]. We have made improvement based on this and release an amount of 150×10^4~200×10^4 of the young into each pond, begin to strip off the young as soon as they have grown to 0.1~0.4cm and feed them with the dried laver powder, which may increase the production of the young by a large margin.

3.5 In South China, the abalones (*Haliotis discus* hannai, *Haliotis discus* Reeve, *Haliotis diversicolor* , etc.) have two stages of sexual maturity, one in spring and the other in autumn. It is generally believed

that the autumn breeding is easier than the spring breeding, which is probably due to the fact that the water temperature gradually rises in spring and the pathogenic organisms also gradually increase. We have carried out research on this in many ways[5-7], but the key problem is how to control the water quality. In the course of spring breeding, the addition of active carbon filtration apart from the sand filtration may have better effect.

References

[1] Chen Quanzhen, Gao Aigen and Hu Xigang (1998) Observation and research on the artificial hatching, and embryonic development and propagation of *Haliotis discus* Reeve [A]. Satellite conference of the third session of the annual youth academic meeting of the China Association for science and technology and concurrently the second session of the youth academic meetion on life science, exploration into and advances in the life science [C]. Hangzhou: Hangzhou University Press, 772-775.

[2] Nie Zongqing (1982) Culture and stock enhancement of abalone [M]. Beijing: Agriculture Press .

[3] Chen Shijie (1977) Preliminary report on the culture and experiment of benthic diatoms---- baits of the young Abalones [J]. *Journal of Zoology of China,* **23** (1): 27-53.

[4] Nie Zongqing and Chen Wenhua (1984) Research on the breeding conditions of *Haliotis discus* hannai, I. Effect of different baits and temperature on the growth of larval and juvenile abalones [J].*Marine Fisheries Research,* (6): 35-40.

[5] Chen Quanzhen and Wu Youlü (1995) Research on the prevention and control of diseases during abalone breeding II. Experiment on the prevention and control of larval abalone diseases by antibiotics [J].*Donghai Marine Science,* **13** (2): 46-51.

[6] Chen Quanzhen, Wu Youlü , Chen Gang *et al.* (1999) Applied research on the prevention and control of bacterial diseases by several new type germicides during the breeding of *Haliotis discus* hannai [A]. *collected papers of conchology of the Chinese Society of malacology* Vol.Ⅷ [C]. Beiging: Xueyuan Press, 161-166.

[7] Chen Quanzhen and He Dehua (2000) Discussion on the harm of dinoflagellates red tide to the abalone culture industry and its prevention and control [J]. *Journal of Fisheries of China,* **24** (2): 151-155.

Effect of Nitrogen Sources on the Growth and Docosahexaenoic Acid Accumulation in *Crypthecodinium cohnii*

Wang Jufang (王菊芳)[1], Wu Haizhen (吴海珍)[1], Liang Shizhong (梁世中)[1], Chen Feng (陈 峰)[2]
1 *College of Food and Bioengineering, South China University of Technology*,Guangzhou 510640
2 *Department of Botany, Hong Kong University*

Abstract The effect of various nitrogen sources on the growth and docosahexaenoic acid (DHA) yield is determined in *Crypthecodinium cohnii* ATCC30556. Single nitrogen tryptone and peptone are suitable to growth, the dry weight biomass is up to 2.78 g/L and 2.70 g/L respectively on medium containing 0.34 g/L nitrogen. Peptone is a favorable nitrogen source for DHA accumulation, DHA yield increases up to 338.56 mg/L. Using peptone and KNO_3 as a multiple nitrogen source, the highest biomass and DHA yield are obtained from media containing 0.34 g/ L nitrogen in which the ratio of peptone–N : NO_3^-–N is 1 : 2, and the biomass and DHA yield are 2.98 g/L(DW) and 527.97mg/L respectively.

Keywords Nitrogen sources, *Crypthecodinium cohnii*, DHA, Biomass

Microalgae have been considered as the most promising source of polyunsaturated fatty acids (PUFAs)[1~3], in which docosahexaenoic acid (DHA) and eicosapentaenoic acid (EPA) have attracted abroad attention in disease prevention and therapy[4], and the industrial production of PUFAs by microalgae has become a very promising commercial field. It has been demonstrated that *Crypthecodinium cohnii* has high ability to accumulate DHA[5]. Our group has obtained a strain *Crypthecodinium cohnii* ATCC30556 with high heterotrophic growth rate and high DHA yield[6]. This study is aimed to explore the effects of nitrogen sources on algal growth and DHA yield, reduce the cost and obtain the optimal nitrogen sources to direct DHA production by culturing *Crypthecidinium cohnii* on a large scale.

1 Materials and Methods

1.1 Microalga and culture conditions

Crypthecodinium cohnii ATCC30556 has been selected by Dr. F. Chen, with the Hong Kong University. Inoculum size is 5%, the culture is maintained in Erlenmeyer flask at 25℃ with orbital shaking at 170 r/ min.

1.2 Composition of medium and nitrogen sources

Porphyridium medium[7] is used as basic medium and its composition is as follows (L^{-1}): artificial water 500ml, distilled water 400ml, soil extraction 100ml, tryptone 1g, yeast extraction 1g, glucose 5g. The single nitrogen source includes tryptone, peptone, potassium nitrate, sodium nitrate, ammonium

Received on January 28, 2001

nitrate and urea. The total nitrogen is 0.34g/L. The pH is adjusted to 6~6.8. Total nitrogen concentration is kept constant, and different C/N ratios are set as peptone and potassium nitrate are multiple nitrogen sources, the ratios of peptone $-N$: NO_3^--N are 3 : 1, 2 : 1, 1 : 1, 1 : 2 and 1 : 3.

1.3 Determination of cell dry weight

100 ml sample is put into a centrifugal tube weighed beforehand, centrifuged for 10 minutes at 4 000 r/min, the precipitation is washed for three times by using distilled water , vacuum dried at 50℃, taken out regularly, cooled in a desiccator and weighed until the constant weight.

1.4 Lipid extraction

Lipid is extracted according to the method previously reported by Bligh and Dyer[8], and we have made some modifications.

1.5 Determination of DHA content

A certain heptadecylic acid is added into the lipid extraction as inner standard. Fatty acid methyl esters are prepared from the lipid extraction by trans-methylation with sodium methanol / methanol. The esters are extracted with hexane for several times, dried by nitrogen and analyzed by Hewlett Packard 5890 capillary gas chromatograph equipped with a thermal-conductivity detector and a DB-5 capillary column (15m×0.35mm). Nitrogen is used as carrier gas and its flow rate is 20 ml/min. Initial column temperature is set at 170℃ and kept for 2 min, then increased at the rate of 8℃/min and the final temperature is 235℃ and kept for 8 min. The injector and detector temperatures are both 265℃.

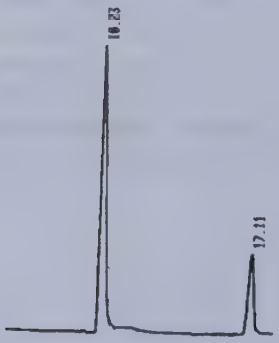

Chromatogram chart of inner standard and DHA

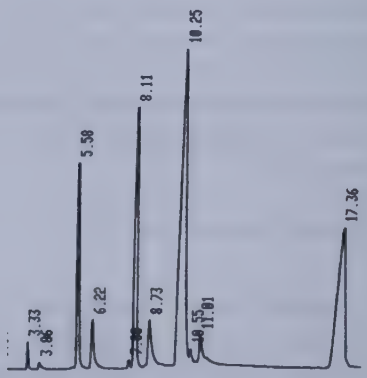

Chromatogram chart of sample

2 Results and Discussion

2.1 The effects of different nitrogen sources on growth and DHA yield by *Crypthecodinium cohnii*

The effects of different nitrogen sources on biomass and DHA yield are plotted in Fig. 1. Both

tryptone and peptone are suitable to algal growth and DHA yield, at the total nitrogen concentration of 0.34g/L, the dry weights of algae are up to 2.78g/L and 2.70g/L respectively. The highest DHA yield is up to 338.56mg/L when peptone is the single nitrogen source. It has been found that NO_3^- has been depleted and the concentration of NH_4^+ maintains the initial level in the broth until harvesting. This is probably due to the absence of enzymes that can absorb and assimilate NH_4^+ in *Crypthecodinium cohnii*, and, apparently, *Crypthecodunium cohnii* ATCC30556 can only use NO_3^- as a nitrogen source.

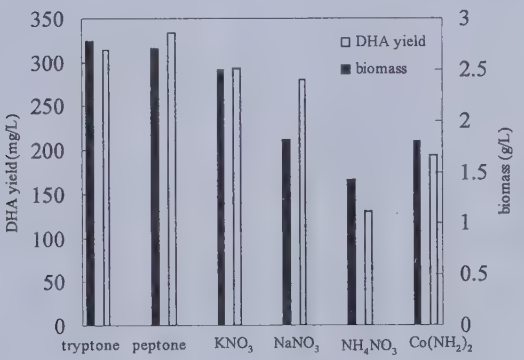

Fig. 1 The effects of various nitrogen sources on growth and DHA yield by *C. cohnii* ATCC 30556

There are differences between lipid and DHA contents in *Crypthecodiium cohnii* when different nitrogen sources are added (Fig. 2). The highest lipid content is 339.58mg/g when the nitrogen source is peptone and the highest DHA content is 153.81mg/g when the nitrogen source is sodium nitrate. The results indicate that organic nitrogen sources are suitable to lipid accumulation in *Crypthecodinium cohnii* ATCC 30556, when tryptone or peptone is the nitrogen source, lipid contents of *Crypthecodinium cohnii* are higher than those when nitrogen sources are inorganic , and organic nitrogen sources are also favorable for DHA accumulation.

In all of the results, biomass and DHA yield are both high when peptone or tryptone is used as single nitrogen source. Furthermore, potassium nitrate is propitious to DHA accumulation and strain growth. Considering the nutritional requirement of this microalga and industrialization in the future, ratios optimization of two nitrogen sources should be carried out to reduce the cost and achieve higher DHA yield.

2.2 The effects of mixed nitrogen sources on growth and DHA accumulation in *Crythecodinium cohnii*

When the ratio of peptone −N : NO_3^-−N is 1 : 2, the highest biomass and DHA yield are 2.98g /L (dry weight) and 527.97mg/L respectively. As for other ratios, the biomass and DHA yield are lower. (Fig. 3)

The highest lipid content is obtained when the organic nitrogen proportion is the highest , the peptone −N : NO_3^-−N = 3 : 1, and the lipid content reaches 361.44 mg /g. When the ratio of NO_3^-−N increases, the lipid content decreases. The highest DHA content in algae is 177.17mg/g (DW) when the

ratio of organic nitrogen : inorganic nitrogen is 1 : 2. Similarly, when the concentration of the organic nitrogen or inorganic nitrogen in mixed nitrogen sources increases, DHA content decreases .(Fig.4)

According to the above trial, the excellent medium for growth and DHA accumulation is the one in which the ratio of peptone −N : NO_3^-−N is 1 : 2 and the total nitrogen concentration is 0.34g/L. In other words, in mixed nitrogen sources, the nitrogen from peptone and that from NO_3^- occupy one third and two thirds of the total nitrogen respectively.

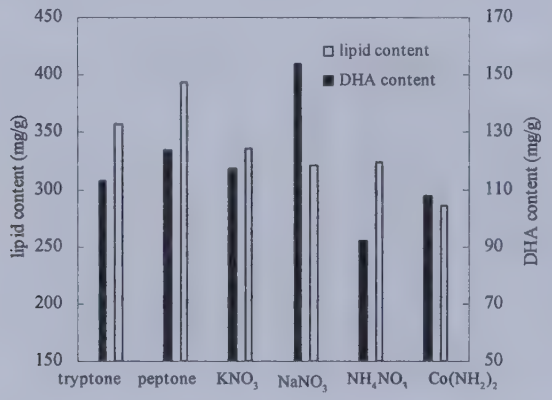

Fig. 2 The effects of various nitrogen sources on DHA and lipid contents by *C. cohnii* ATCC 30556

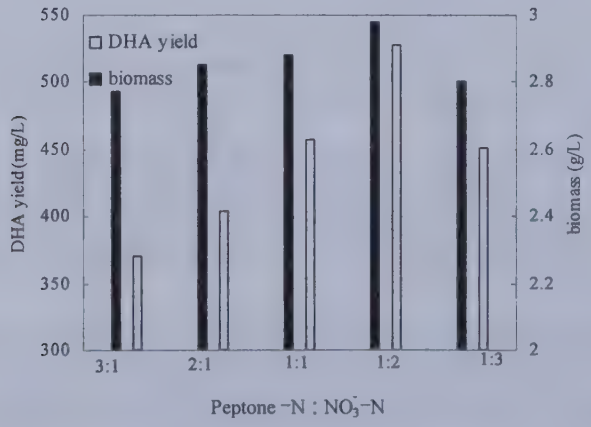

Fig. 3 The effects of mixed nitrogen sources on biomass and DHA yield by *C. cohnii* ATCC 30556

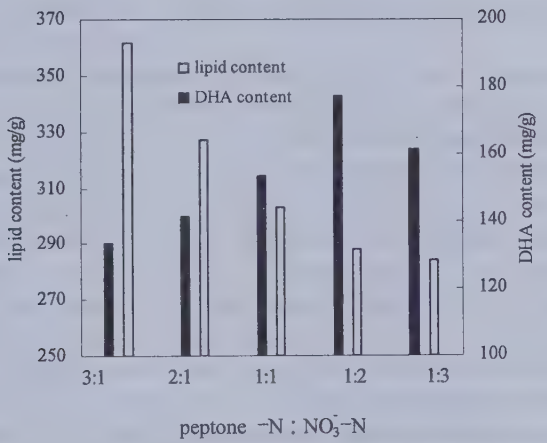

Fig. 4 The effects of mixed nitrogen sources on DHA and lipid contents by *C. cohnii* ATCC 30556

3 Conclusions

Compared to DHA extraction from fish oil, there are many advantages by using microalgae to produce DHA: (1) It can be carried out all the year round, as there is no seasonal or climatic dependence; (2) Environment and nutrition regimes can be easily controlled, allowing the manipulation of the lipid yield and profile; (3) Lipid composition is very simple and there is higher level of the desired acid, thus simplifying the purification. *Crypthecodinium cohnii* ATCC30556 has high DHA productivity, which can be promoted by optimizing the culture condition, and so it can be developed and used in industry.

The natural environment for *Crypthecodinium cohnii* growth is sea water, which is highly nutritionally dependent and prone to use organic nitrogen. Under normal conditions, 1~10% of its cell dry weight is nitrogen, and nitrogen is the main element to constitute the amino acid, aminoglucose, purine and pyrimidin, and it is also significantly correlative to amino acid metabolization, respiration as well as cell growth and product. The combination of lycine hydrochloric acid and histidine hydrochloric acid is used to cultivate the algal *Crypthecodinium Cohnii* by Tuttle[5]. At present, the common algal for use is Porphyridium medium, in which the nitrogen source is tryptone.[7]. Owing to the high price of tryptone, it is very necessary to find a much better and cheaper nitrogen source for mass production.

At the constant total nitrogen of 0.34g/L, nitrogen from peptone occupies one third of the total nitrogen and that from NO_3^- occupies two thirds, which is the best choice for cell growth and DHA yield, and the highest biomass and DHA yield are 2.98g /L(DW) and 527.97mg/L respectively, much higher than those by using tryptone as the single nitrogen source. Thus it also provides useful guidance for reducing the nitrogen cost and for industrialization.

References

[1] Cohen Z. (1994) Production potential of eicosapentanoic acid by monodus subterraneus. JAOCS, **71** (9): 941-945.

[2] Behrens P W, Hoeksema S D, Arnett K L *et al.* (1989) Eicosapentaenoic acid from microglgae. In Demain A L, Somkuti G A, Hunter-Cevers J C *et al.* (eds). Novel Microbial Products for Medicine and Agriculture. Elsevier Science Publishers, Amstedam, 253-259.

[3] Wen Shaohong, Li Xufeng, Ju Bao (2000) Study on polyunsaturated fatty acids in microalgae. *Marine Science Bulletin,* **19** (4) : 86-91.

[4] Gill I , Valivety R. (1997) Polyunsaturated fatty acids, Part I: Occurrence, biological activities and applications, TITECH, 15 : 401-409.

[5] Tuttle R.C, Loeblich A.R. (1975) An optimal growth medium for the dinoflagellate *Crypthecodinium cohnii.* Phycologia, **14** (1): 1-8.

[6] Jiang Y, Chen F, Liang S Z. (1999) Production potential of docosahexaenoic acid by the heterotrophic marine dinoflagellate *Crythecodinium cohnii.* Process Biochemistry, 34: 633-637.

[7] Starr R C, Zeikus J A. (1993) UTEX-the culture collection of algae at the university of Texas Austin. J. Phycol, suppl, 29 : 94.

[8] Bligh E G, Dyer W J. (1959) A rapid method of total lipid extractin and purificaiton. Can. J. Biochem. Physiol. 37: 911-917.

Effects of Lanthanum-Amino Acid Complexes on Egg Hatching and Nauplius Metamorphosis of *Penaeus chinensis**

Xin Fuyan (辛福言), Qu Keming (曲克明)
Yellow Sea Fisheries Research Institute, CAFS, Qingdao 266071

Abstract Studies have been carried out on the effect of lanthanum-amino acid complexes on embryo development and nauplius growth of *Penaeus chinensis*. The experimental results indicate that: (1)The optimum concentrations of lanthanum-proline and Lanthanum-phenylalanine for the development of eggs in monocell and dicell stages are 1.50~ 4.00mg/L and 0.50~3.00 mg/L, respectively, the egg hatching rates being raised by 21.0 ~ 46.0% and 23.0 ~42.8% ($P < 0.05$) respectively. (2)The optimum concentrations of lanthanum- proline complex and Lanthanum-phenylalanine complex for the growth of nauplii are 1.50~4.00 mg/L and 0.50~3.00 mg/L, the metamorphosis rate from nauplius to protozoea being raised by 16.4 ~27.5% and 20.4~26.7% ($P < 0.05$) respectively. (3)The positive effect of lanthanum-amino acid complexes on egg hatching and nauplius metamorphosis of *Penaeus chinensis* is better than that of lanthanum. With regard to the positive effect, lanthanum-proline complex is better than Lanthanum-phenylalanine complex.

Keywords Lanthanum-amino acid complex, *Penaeus chinensis*, Egg hatching, Nauplii

Introduction

Rare earth is the general name for 17 kinds of elements, including lanthanum series, scandium, yttrium, etc. China boasts the largest reserves of rare earth resources in the world. As rare earth elements have special effects on organisms, they have been widely used in agriculture, forestry, livestock husbandry, freshwater aquaculture, herbage and medicine in recent 20 years (Xiong Binghui, 1994), resulting in great economic and social benefits. Studies on the effects of rare earth elements on life process are in the ascendant.

Studies on the effects of rare earth on freshwater organisms related to fish farming (Song Zhengdong, 1994) and algae culture (Chu Zhongxi, 1994) have showed that trace rare earth elements could enhance the growth of freshwater organisms and improve their qualities. However, reports on the effects of rare earth elements on marine organisms have been few so far. The concentration of rare earth elements in natural seawater is only 0.01 μg /L (Elderfield H, 1982). Our previous studies on the effects of single rare earth-lanthanum (Xin Fuyan, 1997), and mixed rare earth (Yuan Youxian, 1999) on egg hatching and nauplius metamorphosis of *Penaeus chinensis*, have showed that rare earths could enhance embryo development and increase hatching rate through being absorbed by eggs. In order to explore the optimum effect of rare earths in seawater aquaculture, further studies have been carried out on the effects of lanthanum-proline complex and Lanthanum-phenylalanine complex on egg hatching and nauplius

Received on February 27, 2002

* Supported by National Natural Science Fund of China (No: 39370548)

metamorphosis of *Penaeus chinensis*.

1 Test Materials and Methods

1.1 Test materials and reagents

Parent prawn *Penaeus chinensis* is caught from natural sea area. The eggs are obtained from the Maidao Fisheries Experimental Station of Yellow Sea Fisheries Research Institute. The experimental seawater is from the coastal area of Maidao Island in Qingdao, with the salinity and pH being 30 ~ 31 and 8.1 respectively. Test seawater is precipitated, filtered through sand, and stored in the polyethene plastic bucker before use. The lanthanum-proline complex and Lanthanum-phenylalanine complex are synthesized and checked out according to the method given by Wang Zemin (1989) and Cao Jinrong (1988). The compositions of lanthanum-proline complex and Lanthanum-phenylalanine complex are La (prol)$Cl_3 \cdot 4H_2O$ and La(phe)$Cl_3 \cdot 5H_2O$. The compositions of proline and phenylalanine are GC purity.

1.2 Test methods

1.2.1 Egg hatching

A group of about 30 ~ 50 eggs are transferred by a suction pipette into 500 ml beakers containing 250 ml seawater. The concentrations of lanthanum-amino acid complexes in the seawater of the beakers are as indicated in Fig.1 and Fig.2 . Each control and trial group has 5 replicates. The temperature is controlled at 18℃ ± 1℃. It takes 40 ~ 50 h for eggs to hatch, then the hatching rate in each beaker is counted. Egg hatching rates are presented as means ± S.D. Differences between control and trial groups are assessed by *t* -test.

1.2.2 Nauplius metamorphosis

A group of about 30 ~ 50 nauplius (N_1) are transferred by a suction pipette into 500 ml beakers containing 250 ml seawater. The concentrations of lanthanum-amino acid complexes in the seawater of the beakers are as indicated in Fig.3 and Fig.4. Each control and trial group has 5 replicates. The temperature is controlled at 20℃ ± 1℃. It took 60 ~ 70 h for nauplius to develop to protozoea, then the metamorphosis rate in each beaker is counted. Metamorphosis rates are presented as means ± S.D. Differences between control and trial groups are assessed by *t*-test.

2 Results and Discussion

2.1 Effects of lanthanum-amino acid complexes on egg hatching

2.1.1 Effect of lanthanum- proline complexes on egg hatching

Fig. 1 shows that the egg hatching rates on the concentrations of 1.50 ~ 4.00 mg/L lanthanum-proline complex are raised by 21.0% ~ 46.0%, significantly higher than that of the control group ($P<0.05$), the optimum concentration being 3.00 mg/L.

2.1.2 Effect of lanthanum-phenylalanine complexes on egg hatching

Fig. 2 shows that the egg hatching rates on the concentrations of 0.50 ~ 3.50 mg/L lanthanum-phenylalanine complex are raised by 23.0% ~ 42.8%, significantly higher than that of control group

($P<0.05$), the optimum concentration being 1.00 mg/L.

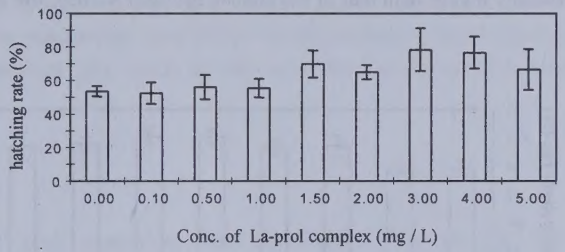

Fig. 1 Effect of Lanthanum-proline complex on egg hatching of *Penaeus chinensis*

Observing the eggs and nauplius under microscope, it is found that the embryos at the optimum concentration develop 5 ~ 6 h faster. Besides, the developed nauplius is more active, and healthy with better phototaxis, compared with the control group. However, when the concentrations of lanthanum-amino acid complexes are higher than the optimum ranges, the hatching rates have no significant difference with the control group.

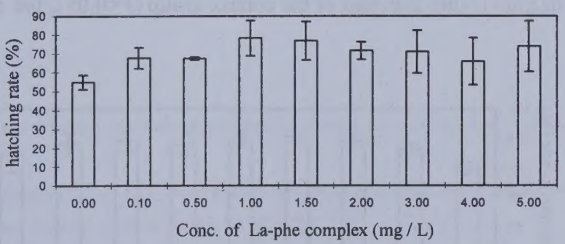

Fig. 2 Effect of Lanthanum-phenylalanine complex on egg hatching of *Penaeus chinensis*

Previous studies (Xin Fuyan, 1997) have indicated that the optimum concentrations of lanthanum for egg hatching are 0.90 ~ 1.80 mg/L, in which egg hatching rates are raised by 17.0% ~ 23.5%. If Lanthanum-proline complex is converted into lanthanum, then the optimum concentrations of the Lanthanum-proline complex would be equal to 0.5 ~ 1.28 mg/L lanthanum, in which egg hatching rates are raised by 21.0% ~ 46.0%. Similarly, the optimum concentrations of the Lanthanum-phenylalanine complex are equal to 0.15 ~ 0.89 mg/L lanthanum, in which egg hatching rates are raised by 23.0% ~ 42.8%. Thus, it could be seen that the positive effects of lanthanum-amino acid complexes on egg hatching are better than that of lanthanum. Comparing the positive effects of Lanthanum-phenylalanine complex with Lanthanum-proline complex, the former is better than the latter. Obviously, the positive effects of lanthanum-amino acid complexes do not result from induction of amino acid (Xin Fuyan, 1998a, b).

2.2 Effects of lanthanum-amino acid complexes on nauplius metamorphosis

2.2.1 Effects of lanthanum-proline complexes on nauplius metamorphosis

Fig. 3 shows that the nauplius (N_1) metamorphosis rates from nauplius (N_1) to protozoea (Z_1) within

the range of the concentrations of 0.50 ~ 4.00 mg/L lanthanum-proline complex are raised by 16.4% ~ 27.5%, significantly higher than that of the control group (P<0.05), the optimum concentration being 2.00 mg/L.

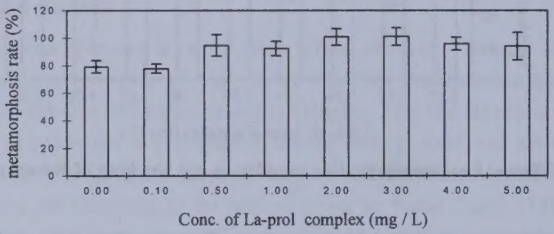

Fig. 3 Effect of Lanthanum-proline complex on naupliar metamorphosis of *Penaeus chinensis*

2.2.2 Effects of lanthanum-phenylalanine complexes on nauplius metamorphosis

Fig. 4 shows that the nauplius (N_1) metamorphosis rates from nauplius (N_1) to protozoea (Z_1) within the range of the concentrations of 0.50 ~ 3.00 mg/L lanthanum-phenylalanine complex are raised by 20.4% ~ 26.7%, significantly higher than that of the control group (P<0.05), the optimum concentration being 1.00 mg/L.

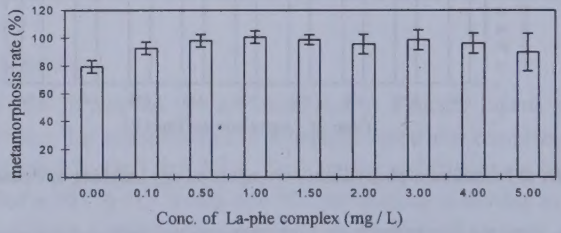

Fig. 4 Effect of Lanthanum-phenylalanine complex on naupliar metamorphosis of *Penaeus chinensis*

Previous studies (Xin Fuyan, 1997) have indicated that the optimum concentrations of lanthanum for naupliar metamorphosis are 0.90 ~ 1.50mg/L, in which the metamorphosis rates are raised by 9.4% ~ 11.7%. If Lanthanum-proline complex is converted into lanthanum, then the optimum concentrations of the Lanthanum-proline complex would be equal to 0.16 ~ 1.28mg/L lanthanum, in which the metamorphosis rates of naupliar are raised by 16.4% ~ 27.5%. Similarly, the optimum concentration of the Lanthanum-phenylalanine complex is equal to 0.15 ~ 0.89mg/L lanthanum, in which the metamorphosis rates of nauplius are raised by 20.4% ~ 26.7%. Thus, it could be seen that the positive effects of lanthanum-amino acid complexes on the metamorphosis rates of nauplius are better than that of lanthanum. Comparing the positive effects of Lanthanum-phenylalanine complex with Lanthanum-proline complex, the former is better than the latter. Obviously, the positive effects of lanthanum-amino acid complexes do not result from the induction of amino acid (Xin Fuyan, 1998a, b).

Observing the larvae under microscope, it is found that the larvae within the range of the optimum concentrations develop 10 ~ 15 h faster , and are more active and healthy, compared with the control group. At the end of the experiment, some larvae on the optimum concentrations have developed from nauplius (N_1) into protozoea (Z_2), while the larvae of the control group have only developed into protozoea (Z_1).

3 Conclusions

Lanthanum-amino acid complexes have significant effects on egg hatching and Nauplius metamorphosis of *Penaeus chinensis*. With regard to the positive effects, lanthanum-amino acid complexes are better than lanthanum, and Lanthanum-phenylalanine complex is better than Lanthanum-proline complex. The enhancement effects of lanthanum-amino acid complexes do not result from the induction of amino acid.

China is rich in rare earth resources, and has fairly large output as well. Shrimp culture is an important fishery industry in China. So, it has important academic significance and practical value to study the effect of rare earths on shrimp growth. As studies on the effect of rare earth elements on marine organisms are underway, further studies are needed to understand the mechanism of enhancement effect of rare earth on the growth of marine organism.

References

[1] Xiong B H (1994) Applied study on biological function compound of rare earth. *Journal of Rare Earth*, **12** (4): 358–365.

[2] Chu Z X, Mu M H, Zhang H P, *et.al.* (1994) Effects of cerous chloride on photosynthesis, pigment and protein syntheses of *spirulina*. *Journal of Rare Earth*, **12** (4): 344–347.

[3] Song Z D, Jiang Z Y, Liu H T, *et. al.* (1992) Effects of rare earth elements on growth and metabolism of *carp*. *Rare earth*, 13:60–62,70.

[4] Xin F Y, Yuan Y X, Qu K M. (1997) Effects of lanthanum on egg hatching and nauplius metamorphosis of *penaeus Chinensis*. *Journal of Rare Earth*, **15** (1):289–292.

[5] Yuan Y X, Qu K M, Xin F Y. (1999) Effects of rare earth on egg hatching and nauplius metamorphosis of *penaeus Chinensis*. *Journal of Fishery Science of China*, **6** (3):111–113.

[6] Elderfield H, Greaves M J (1982) The rare earth elements in seawater. *Nature*, 296:214–219.

[7] Wang Z M, Fu C J, Cao J R. (1989) Synthesis and properties of the coordination compounds of rare earth (III) with L-proline. *Journal of inorganic chemistry*, **5** (4): 59–64.

[8] Cao J R, Wang Z M, Fu C J. (1988) Study on the solid coordination compounds of rare earths with phenylalanine. *Journal of Rare Earth*, **6** (3): 19–22.

[9] Xin F Y, Qu K M, Yuan Y X. (1998a) Effects of lanthanum-amino acid complexes on *Isochrysis galbana*. *Acta oceanologica sinica*, **20** (5): 65–69.

[10] Xin F Y, Yuan Y X, Qu K M. (1998b) Influence of lanthanum-amino acid complexes on *chaetoceros muller*. *Chinese journal of applied ecology*, **9** (2): 206–208.

Marine Science Bulletin

Marine Science Bulletin publishes papers on marine science and technology including physical oceanography, chemical oceanography, marine biology, marine geology, environmental oceanography, estuarine & coastal sciences, marine technology, digital ocean, coastal zone management, ocean engineering, marine economics, etc., and aims to promote international academic exchange.

Editor-in-Chief: Wang Hong（王　宏）
Deputy Editor-in-Chief: Lin Baofa（林宝法） Zhao Xucai（赵绪才）
Yang Ying（杨　鹰）
Executive Editor: Xu Jie（徐　杰） Zhang Deshan（张德山）
Computer typist: Cheng Xiuchun（程秀春）

Marine Science Bulletin **(Vol .4 No.1 May 2002)**

Responsible Institution:
State Oceanic Administration of China
Edited and Published Semi-annually by:
National Marine Data and Information Service
Address: 93 Liuwei Road, Hedong District, Tianjin 300171, China
E-mail: msb@mail.nmdis.gov.cn

ISSN1000-9620
CN12-1271/N

Price: $ 30.00 Per year